

Masters Theses

Dissertations and Theses

December 2020

A Study on Latent Thermal Energy Storage (LTES) using Phase Change Materials (PCMs) 2020

Ritvij Dixit

University of Massachusetts Amherst

Follow this and additional works at: https://scholarworks.umass.edu/masters_theses_2



Part of the [Energy Systems Commons](#), and the [Heat Transfer, Combustion Commons](#)

Recommended Citation

Dixit, Ritvij, "A Study on Latent Thermal Energy Storage (LTES) using Phase Change Materials (PCMs) 2020" (2020). *Masters Theses*. 960.
<https://doi.org/10.7275/18400452> https://scholarworks.umass.edu/masters_theses_2/960

This Open Access Thesis is brought to you for free and open access by the Dissertations and Theses at ScholarWorks@UMass Amherst. It has been accepted for inclusion in Masters Theses by an authorized administrator of ScholarWorks@UMass Amherst. For more information, please contact scholarworks@library.umass.edu.

**TITLE OF THESIS: A STUDY ON LATENT THERMAL ENERGY STORAGE
USING PHASE CHANGE MATERIALS (PCMs) 2020**

A Thesis Presented

by

RITVIJ M. DIXIT

Submitted to the Graduate School of the
University of Massachusetts Amherst in partial fulfillment
of the requirements for the degree of

MASTER OF SCIENCE

September 2020

Department of Mechanical and Industrial Engineering

© Copyright by Ritvij M. Dixit 2020

All Rights Reserved

**TITLE OF THESIS: A STUDY ON LATENT THERMAL ENERGY STORAGE
USING PHASE CHANGE MATERIALS (PCMs) 2020**

A Thesis Presented

by

RITVIJ M. DIXIT

Approved as to style and content by:

Dragoljub (Beka) Kosanovic, Chair

Jon G McGowan, Member

Hari Balasubramanian, Member

Sundar Krishnamurty,
Department Head,
M&I Engineering Department

DEDICATION

To Deva,

For greeting everyone and everything with the warmest of smiles.

ACKNOWLEDGMENTS

I would like to thank Prof. Dr. Dragoljub (Beka) Kosanovic, for his guidance, continuous support, and patience throughout the course of this thesis. This work would not have been possible without his motivation and support. I am forever grateful for the opportunities he has provided, enabling me to learn several things with the Industrial Assessment Center (IAC), while working on challenging problems in diverse industrial settings.

I would like to thank my thesis committee, Prof. Dr. Jon McGowan and Prof. Dr. Hari Balasubramanian, for providing me with their guidance and valuable inputs to improve my thesis.

I would also like to express my gratitude to the IAC staff, Benjamin McDaniel, Lauren Mattison, and Dorothy Kent for helping me throughout my time at the IAC.

I would like to thank my parents Milind and Janhavi for being a constant source of inspiration and guidance, without whom none of this would have been possible. To Khushali, I am forever grateful for her enthusiasm and motivation which has helped me countless of times. Special thanks to my grandparents, Sarita and Vinaykumar Ketkar, and Pradeep and Poonam Korde, Nakul, and Sanjukta for their patience and insights which helped me along the way.

I would also like to thank my friends Srini, Serena, Eric, Avdhoot, Abhishek, Kaushal, and Akshay for all their help. You guys made my time at UMass exciting and in your own ways taught me many important lessons. Cheers to my friends Kedar, Akhil,

Akshay Ambulgekar, Akshay Sadekar, Parth Gandhi, and Ajinkya for being there every single time for me. I am indebted to them, for their invaluable support and insights.

ABSTRACT

TITLE OF THESIS: A STUDY ON LATENT THERMAL ENERGY STORAGE USING PHASE CHANGE MATERIALS (PCMs) 2020

SEPTEMBER 2020

RITVIJ M. DIXIT, B.Tech, VISHWAKARMA INSTITUTE OF TECHNOLOGY

M.S, UNIVERSITY OF MASSACHUSETTS AMHERST

Directed by: Professor Dragoljub (Beka) Kosanovic

The significant increase in energy requirements across the world, provides several opportunities for innovative methods to be developed to facilitate the storage and utilization of energy. The major energy demand is in the form of electrical energy for domestic as well as industrial sectors, a large part of which are the heating and cooling requirements. Appropriate utilization of thermal energy storage can effectively aid in reducing the electrical demand by storage and release of this thermal energy during peak hours.

Thermal Energy Storage using Phase Change Materials (PCMs) is an attractive method of energy storage, with a wide variety of potential applications. Several configurations have been tested by researchers to develop energy storage devices with PCMs. The cycling of melting and solidification of PCMs results in storage and release of heat at a relatively small temperature difference. Design and deployment of these storage systems have certain challenges and considerations associated to them for instance, when used in buildings, PCMs should be non-toxic, non-corrosive, and others.

In this thesis, we aim to provide models for designing Latent Thermal Energy Storage (LTES) devices with PCMs, based on their operating conditions, thermophysical properties of materials, and geometric parameters. The models are developed considering fluid dynamics and heat transfer involved in melting and solidification of PCMs. Parameters like inlet temperature and velocity, and volume of storage container are varied to determine the time taken for melting or solidification. For sizing and predicting performance of the storage devices we aim at presenting an analytical correlation, with time taken for melting as the variable defining the ‘charging/discharging time’ of storage device. Along with this, a transient model is developed to predict amount of PCM melted/solidified, along with rate of latent energy storage in defined time period intervals.

TABLE OF CONTENTS

	Page
ACKNOWLEDGMENTS	v
ABSTRACT	vii
LIST OF TABLES	xi
LIST OF FIGURES.....	xii
CHAPTER	
1. INTRODUCTION	1
1.1 Introduction to Thermal Energy Storage (TES).....	1
1.2 Methods of Thermal Energy Storage (TES).....	3
1.2.1 Sensible Heat Storage	3
1.2.2 Latent Thermal Energy Storage (LTES).....	7
1.3 Objectives	8
1.4 Outline	9
2. REVIEW OF LTES WITH PHASE CHANGE MATERIALS (PCMs)	11
2.1 Research Methodologies	11
2.2 Classification of PCMs.....	12
2.2.1 Hygroscopic Phase Change Materials	13
2.2.2 Organic and Inorganic Materials	13
2.2.3 Solid-Solid Phase Change Materials.....	19
2.3 Selection Criteria of PCMs.....	21
2.3.1 Thermodynamic Criteria	21
2.3.2 Kinetic Criteria	21
i. Supercooling	21
ii. Nucleation.....	22
2.3.3 Technical Criteria	22
2.3.4 Economic Criteria.....	22
3. NUMERICAL SIMULATION AND CASE VALIDATION	23
3.1 Melting in a Vertical Cylindrical Tube	23
3.1.1 Numerical Model.....	24
3.1.2 Simulations with Variation in Mushy Zone Constant	27
3.1.3 Modeling Schemes and Discretization.....	29
3.1.4 Time and Mesh Sensitivity Analysis	31
3.2 Melting in Annular PCM with flow	33
3.2.1 Experimental Model	33
3.2.2 Numerical Model.....	35
3.2.3 Boundary Conditions	37

i. 2-D Case	37
ii. 3-D Case	38
3.2.4 Results and Comparisons	39
4. LTES Storage Design	40
4.1 PCM Selection	40
4.2 Numerical Model	42
4.3 Variations in Inlet Conditions.....	43
4.3.1 Reynold's Number Variations.....	43
4.3.2 Variations in Inlet Temperature.....	44
Results and Comparison.....	44
4.3.3 Solidification	47
4.4 Variations in Diameter of PCM Domain.....	49
4.4.1 Initial Results with 2-D cases	50
4.4.2 Comparison with 3-D cases.....	51
4.4.3 Melting and Solidification with change in Diameter.....	53
5. ANALYTICAL MODEL.....	56
5.1 Further Variations in 'Ti'	56
5.2 Identification of Non-Dimensional Numbers	59
5.3 Dimensional Correlation	61
5.4 Interpolation Model.....	62
5.5 Daily charging and discharging TRNSYS Model.....	64
6. RESULTS AND DISCUSSION.....	67
6.1 Variation in Time taken for Melting and Solidification.....	67
6.2 Correlation Results.....	68
6.3 Interpolation Model Results	72
6.4.1 TRNSYS Model Results.....	74
6.4.2 Results with real-time data	77
7. Future work	82
7.1 Parameters for correlation analysis	82
7.2 Comparison with real time data/cases	82
APPENDICES	
A: Linear Regression Script File with Non-Dimensional Numbers.....	84
B: Interpolation Script File with parameters.....	87
BIBLIOGRAPHY	98

LIST OF TABLES

Table	Page
Table 1: Advantages and Disadvantages of Organic and Inorganic Phase Change Materials	14
Table 2: Classification of PCMs and their Thermophysical Properties.....	15
Table 3: Properties of RT27 (Rubitherm GmBH) used in simulations [18].....	24
Table 4: Properties of RT 35 [20].....	33
Table 5: Properties of HTF.....	34
Table 6: Properties of Erythritol.....	40
Table 7: Properties of HTF.....	41
Table 8: Changes in Inlet Velocity ‘ V_i ’ by variation in Reynold’s Number ‘ Re ’	43
Table 9: Time taken for melting in hours for each combination.....	44
Table 10: Time taken for solidification in hours for each combination	47
Table 11: Inputs for TRNSYS model sample case.....	65
Table 12: Inputs for TRNSYS model case.....	74
Table 13: Results for estimating performance of LTES Device	76
Table 14: Size of LTES system	80

LIST OF FIGURES

Figure	Page
Figure 1: CHP Process Flow Diagram [1]	1
Figure 2: Types of Large-Scale Sensible thermal storage systems [4].....	4
Figure 3: Solar Collectors on top of Apartments and Schematic of the ATES [5]	5
Figure 4: Attenkirchen TES; a. Solar Collector; b. Construction of Concrete Store; c. Schematic of Combined Pit and Borehole Storage [6].....	6
Figure 5: Areas of research in Thermal Energy Storage [7]	11
Figure 6: Classification of energy storage materials [7]	12
Figure 7: Experimental setup for the bulk cycling. (1) Galactitol sample, (2) temperature data logger, (3) hotplate, (4) electric fan, (5) thermocouple (K-type), (6) timer switch (fan), and (7) timer switch (heater) [11]	18
Figure 8: Appearance of three galactitol samples cycled with upper cycle temperature (T_{up}) of 203, 230 and 243 °C per sample [11].....	18
Figure 9: Schematic representation of a Perovskite type SS-PCM [16].....	19
Figure 10: Schematic representation of Polyalcohol type SS-PCMs with crystalline structure changing from (a) sheet like tetrahedral sheet configuration to (b) face centered cubic to (c) disordered amorphous structure [17].....	20
Figure 11: Numerical Model with the PCM and Air interface at $H = 17$ cm [18]	23
Figure 12: Melt Fraction Vs Time (min) for various values of the mushy zone constant for $D = 4$ cm, $H = 17$ cm, and $\Delta T = 10^{\circ}\text{K}$ [18]	27
Figure 13: 2-D mesh for case	28
Figure 14: Melt Fraction Vs Time (min) for $C = 10^5$, 10^6 , and 10^8 , for $D = 4$ cm, $H = 17$ cm, and $\Delta T = 10^{\circ}\text{K}$	30
Figure 15: Mesh and Time sensitivity for $C = 10^6$ from 0.05s to 0.005s	32

Figure 16: Schematic of Experimental Loop and thermocouples with test section [20]	34
Figure 17: 2-D Mesh for the Longeon et al. Case with axisymmetric on X axis.....	35
Figure 18: 3-D Mesh for Longeon et al. case with ‘C-Grid’ blocking	36
Figure 19: 2-D Mesh Zones	37
Figure 20: 3-D Mesh Zones	38
Figure 21: Comparison with Experimental Results for Temperature at Point (K)	39
Figure 22: Variations in time for complete melting with varying Ti and Vi	45
Figure 23: Variations in time for complete solidification with varying Ti and Vi.....	48
Figure 24: Mesh Sensitivity with change in PCM_D	50
Figure 25: Comparison of 2-D and 3-D Melting for 30mm PCM_D	51
Figure 26: Comparison of 2-D and 3-D Melting for 45mm PCM_D	52
Figure 27: Comparison of 2-D and 3-D Melting for 60mm PCM_D	52
Figure 28: Variations in time taken for complete melting and solidification with varying Ti and Vi, for 30mm Diameter.....	53
Figure 29: Variations in time taken for complete melting and solidification with varying Ti and Vi, for 45mm Diameter.....	54
Figure 30: Variations in time taken for complete melting and solidification with varying Ti and Vi, for 60mm Diameter.....	55
Figure 31: 30mm Diameter – Time Taken for Melting with 5°K increment in Ti	56
Figure 32: 45mm Diameter – Time Taken for Melting with 5°K increment in Ti	57
Figure 33: 60mm Diameter – Time Taken for Melting with 5°K increment in Ti	58
Figure 34: Interpolation Methods available in MATLAB [21].....	62

Figure 35: Outline of TRNSYS Model.....	64
Figure 36: TRNSYS model case results – 24 hr charging and discharging.....	66
Figure 37: Comparison of tm and tm-pred Vs Gr	68
Figure 38: Comparison of tm and tm-pred Vs Re	69
Figure 39: Comparison of tm and tm-pred Vs V*.....	70
Figure 40: Predicted Melting Time with Power Law	71
Figure 41: Case A results for solidification or discharging	72
Figure 42: Case B results for melting or charging.....	73
Figure 43: Case C results for solidification or discharging	73
Figure 44: Melt Fraction ‘ γ (%)’ and Latent Energy Storage Rate ‘ q_L (W)’	75
Figure 45: Change in Melt Fraction ‘ $d\gamma$ (%)’ and Change in Latent Energy Storage Rate ‘ dq_L (W)’.....	75
Figure 46: Real-time data for 24 hrs.....	77
Figure 47: Comparisons of Melt Fraction ‘ γ (%)’ for various Volume Sizes (m^3).....	78
Figure 48: Performance of LTES devices with real time data – 145 m^3	79
Figure 49: Change in Melt Fraction ‘ $d\gamma$ (%)’ and Change in Latent Energy Storage Rate ‘ dq_L (W)’ for real time data – 145 m^3	80

CHAPTER 1

INTRODUCTION

1.1 Introduction to Thermal Energy Storage (TES)

Electricity generation can release a large amount of heat that can be stored and utilized further for cooling, heating, and other applications, which would require efficient method of TES. As in case of the Combined Heat and Power (CHP) Plants, the heat released can be extracted using heat recovery units. This process is also known as cogeneration. Heat recovery units are utilized to extract heat from the hot exhaust gases, released from combustion of fuel to run turbines or engines. This heat can then be used for heating or cooling purposes in buildings or facilities. The CHP process flow can be seen in [Figure 1](#) below,

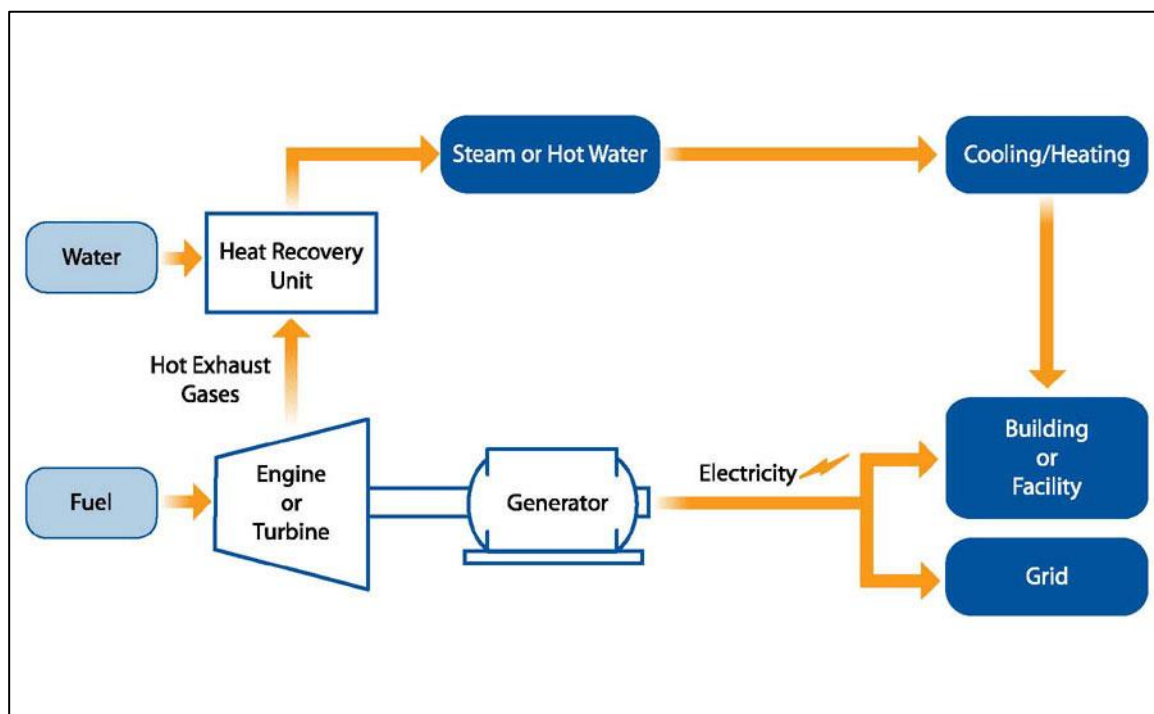


Figure 1: CHP Process Flow Diagram [1]

The heat released from the cogeneration process can be stored using various modes or methods of Thermal Energy Storage (TES). The principle of all TES applications is the same, i.e. thermal energy is supplied to storage media for periodic usage and heat extraction. The main difference arises in the scale and method of storage media [2].

TES refers to storage of energy for certain period and its subsequent usage. Applications for this technology can be found in diverse disciplines like cogeneration, Solar Power, HVAC systems, and others. With the appropriate TES system, diurnal or seasonal storage and utilization of energy is possible. This means that, in areas where heating in winter or cooling in summer is required, it is possible to store heat during the summer and utilize it in the winter, and vice-versa for cooling in summer. This method would be targeted at a large time scale across months. Similar TES methods can be used for daily heating requirements at a smaller scale. TES provides several advantages like,

- Application in active and passive systems (allowing usage of waste energy)
- Peak load shifting strategies
- Rational use of thermal energy
- Increase overall efficiency and better reliability
- Reduction in investment and running costs
- Reduction in CO₂ emissions and pollution of the environment [3]

The various methods and types of TES systems are discussed in the following section.

1.2 Methods of Thermal Energy Storage (TES)

Thermal energy can be stored using several media which focus on various methods of storage. TES is mainly classified into sensible, latent, and chemical energy storage, some of which have been discussed here.

1.2.1 Sensible Heat Storage

Sensible Heat is the energy released by a material as its temperature is reduced, or absorbed by a material as its temperature is increased, and this method of TES is called the Sensible Heat Storage. The effectiveness of Sensible Heat Storage depends on the specific heat of the storage material and, if volume is important, on its density. Sensible storage systems commonly use materials like rocks, ground, or water as the storage medium, and the thermal energy is stored by increasing the storage-medium temperature [2]. Following are certain examples of Sensible Heat Storage,

- The four main types of large-scale Sensible Storage systems are Aquifer thermal energy storages (ATES), Borehole thermal energy storages (BTES), Tank thermal energy storages (TTES), and Pit thermal energy storages (PTES), as shown in Figure 1.2. Each storage concept has different capabilities with respect to storage capacity, storage efficiency, possible capacity rates for charging and discharging, requirements on local ground conditions and on system boundary conditions (e.g. temperature levels), building costs, and others [4].

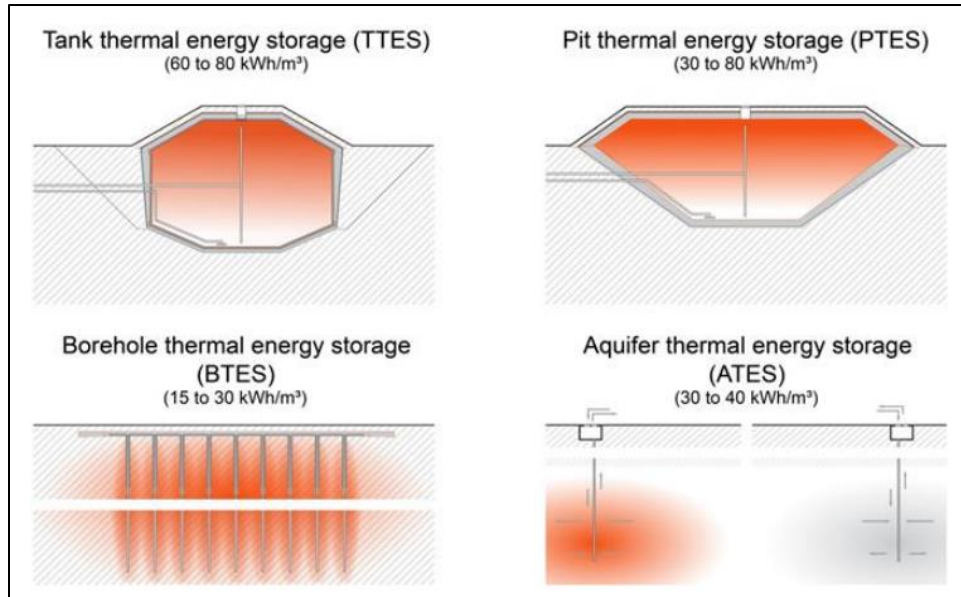


Figure 2: Types of Large-Scale Sensible thermal storage systems [4]

- **Aquifer Thermal Energy Storage (ATES) in Rostock, Germany**

The first Central Solar Heating plant with Aquifer Thermal Energy Storage (ATES) went into operation in 2000, in Rostock, Germany. The system supplies a multifamily house with a heated area of 7000 m² in 108 apartments with heat for space heating and domestic hot water preparation. On the roof of the building 980 m² of solar collectors are mounted. The ATES operates with one doublet of wells and is located below the building. The storage works as a seasonal heat storage to overcome the gap between high amount of solar energy in summer and highest heat demand of residential buildings in winter. The solar system was designed to cover half of the yearly heat demand for space heating and domestic hot water preparation by solar energy [5].

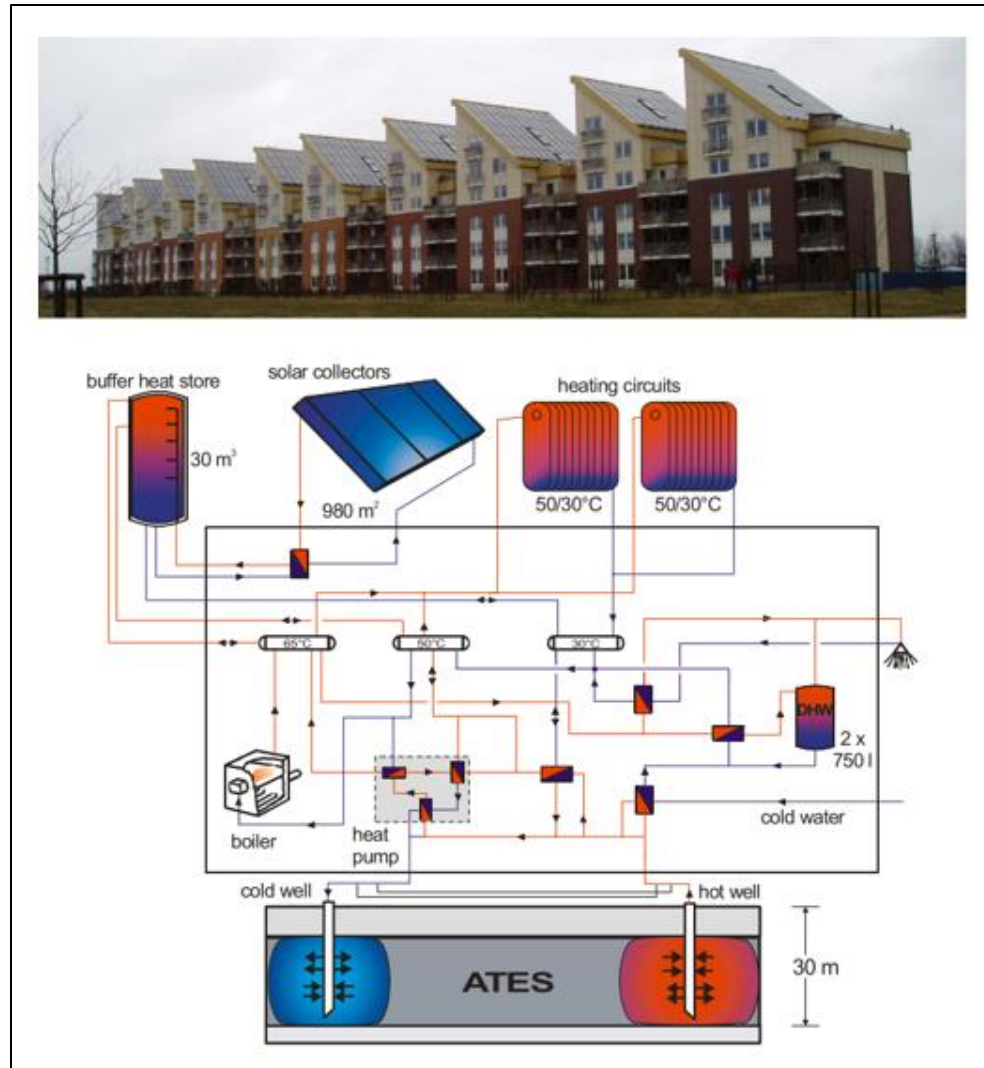


Figure 3: Solar Collectors on top of Apartments and Schematic of the ATES [5]

- **Combined Pit and Borehole Thermal Energy Storage in Attenkirchen, Germany**

In Attenkirchen, a small community near Freising north of Munich, Germany, a combination of Pit and Borehole TES was installed for a developing area of 30 homes. A solar collector roof with an effective area of 836 m², has a copper absorber with a selective surface for achieving good thermal performance. The combined storage system consists of central prestressed concrete, serving as a short-term or buffer storage, while surrounding borehole field represents the long-term storage. The pit measures 9.00 m in diameter and 8.50 m in depth with a total volume of 500 m³. This combination allows a simpler and cheaper construction of the water store. In Attenkirchen, 90 borehole heat exchangers of 30 m deep were installed in three rings surrounding water store which gives a volume of 10,500 m³. The average volumetric heat capacity of the underground measure at this location is 2.7 MJ/m³/K. Thus, the borehole storage volumes correspond to 6,800 m³ water equivalent and both together 7,300 m³ [6].

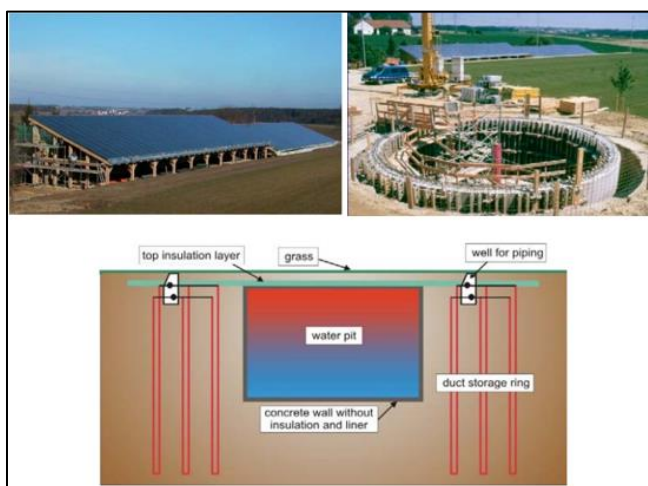


Figure 4: Attenkirchen TES; a. Solar Collector; b. Construction of Concrete Store; c. Schematic of Combined Pit and Borehole Storage [6]

1.2.2 Latent Thermal Energy Storage (LTES)

Storage by phase change (the transition from solid to liquid or liquid to vapor with no change in temperature) is a mode of TES known as *latent heat storage*. These systems store energy in PCMs, with the thermal energy stored when the material changes phase, usually from solid to liquid. The specific heat of solidification/fusion or vaporization and the temperature at which phase change occurs are of design importance. Both sensible and latent heat TES also may occur in the same storage material [2].

Several configurations have been considered for utilizing PCMs as storage media. Usually they are stored in specialized containers like shells, tubes, shallow panels, and others.

PCMs or Latent Thermal Energy Storage (LTES), provides certain advantages over Sensible Energy Storage, as listed below,

- Higher Thermal Storage capacities
- Relatively constant temperatures during charging and discharging
- Chemical and Thermal Stability [2]

Several configurations have been tested by researchers across the world to develop LTES devices, some of which have been discussed in [Chapter 2](#).

1.3 Objectives

- Analyzing melting and solidification of Phase Change Materials (PCMs) with variations in operating conditions and geometric parameters
- Designing Latent Thermal Energy Storage (LTES) devices using PCMs with mean melting temperature in the range (373.15 to 473.15°K), which is the temperature at which the by-product heat is released in CHPs
- We aim at validating Finite Volume simulations against experimental results, using CFD software Fluent 18.2, to understand the significance of variations in parameters, the dynamics of phase change behavior, and heat transfer involved in the phase change process
- To predict performance of LTES device, we aim at developing a correlation incorporating key parameters like melting time and melt fraction
- Along with this, we aim at developing a method to predict performance of LTES devices over defined time periods, by developing models with MATLAB interpolation techniques and commercial transient simulation software TRNSYS

1.4 Outline

In the following chapters several topics have been discussed in detail relevant to methods of designing an effective LTES device. The second chapter includes a detailed review of PCMs with their melting temperatures in the range of $100 - 200^\circ\text{C}$ ($373.15^\circ\text{K} - 473.15^\circ\text{K}$), from respective sources. These materials have been classified based on their properties to provide guidelines for selecting the right material based on the application requirements. Certain experimental studies have also been discussed in brief, which utilize PCMs for energy storage.

In [Chapter 3](#), the numerical models have been described in detail for validation of existing experimental and numerical investigation of utilizing PCMs in LTES devices. The chapter also includes discretization of the computational domain. The first model consists of a domain with an Air-PCM interface and the melting in PCM is due to variation in wall temperature. The second model investigates the melting of PCM in vertical annulus with a hot fluid flowing through the inner tube. This helps in further understanding of the convection phenomenon involved in energy storage with Phase Change.

In [Chapter 4](#), considerations to design a LTES device are explored. The three parameters changed for obtaining the time taken for melting were the inlet temperature and velocity of the HTF domain, and the outer diameter of the PCM domain. This provides a comparison of the different combinations with changes in computational domain in terms of the important parameter, which in the scope of this study is the time taken for melting or solidification.

The results obtained with these comparisons are further utilized to develop a correlation as discussed in [Chapter 5](#), which can be utilized for sizing a LTES system. In this chapter, the interpolation and TENSYS models utilized to predict the performance of the LTES Device have also been discussed.

The results for the correlation and their significance, have been discussed in [Chapter 6](#). Along with this, case results for the interpolation and TRNSYS models developed have also been included in this chapter.

CHAPTER 2

REVIEW OF LTES WITH PHASE CHANGE MATERIALS (PCMS)

2.1 Research Methodologies

The Thermal Energy Storage (TES) research in the past 20 years has focused on two main aspects, as described by Zalba et al. [7], which have been discussed below. Materials Research includes experimentation with the thermal storage of material, compatibility, thermophysical properties of material for energy storage, long and short-term behavior, and others. The second main aspect is the development of Heat Exchangers, which includes sizing and selection of the exchanger type and parameters, design and simulation of conditions for thermal analysis, prototyping for use based on applications, testing on the field, cost analysis, and others. A flowchart with details of the research aspects can be seen below.

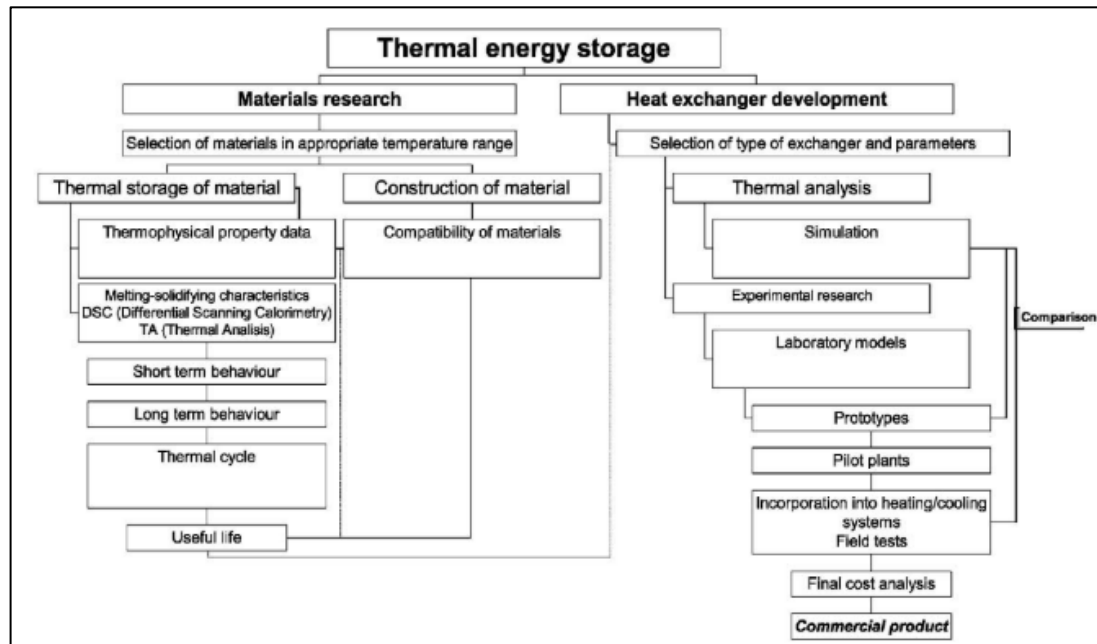


Figure 5: Areas of research in Thermal Energy Storage [7]

2.2 Classification of PCMs

PCMs are classified based on several criterion, including type of phase change, thermophysical properties, chemical properties, and others. The energy storage with PCMs, occurs from solid-solid, liquid-solid, solid-liquid, solid-gas, and liquid-gas phase changes. Even though liquid-gas phase changes have a higher heat of transformation than their solid-liquid counterparts, they prove to be impractical for thermal storage since, large volumes or high pressure are required to store materials in their gas phase. Solid-solid phase changes have relatively low heat of transformation and are slow processes. Thus, solid-liquid and liquid-solid are more practical for TES. A flowchart below shows the classification of materials as provided by Zalba et al. [7].

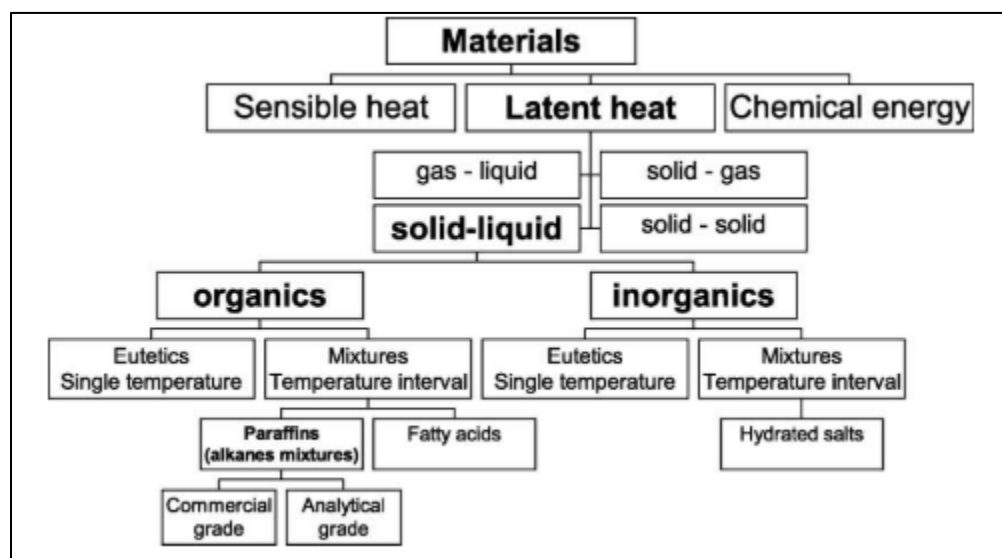


Figure 6: Classification of energy storage materials [7]

2.2.1 Hygroscopic Phase Change Materials

Hygroscopic Materials can absorb and release water with change in temperature.

Several construction materials are naturally hygroscopic such as, clay, wool insulation, and others. The water evaporates when phase transformation occurs from liquid to gaseous state. This process releases a limited amount of heat, but when considered over large surfaces in buildings, the heat transfer can be significant and can reduce temperatures. The process can be segregated as,

- Condensation (gas to liquid): $\Delta H < 0$; enthalpy decreases
- Evaporation (liquid to gas): $\Delta H > 0$; enthalpy increases [2]

2.2.2 Organic and Inorganic Materials

Organic materials are typically derived from bio-based compounds, Paraffin waxes (C_nH_{2n+2}), carbohydrates, lipid derived compounds, and others. A significant number of authors have based their work on organic materials such as alkanes, waxes, or paraffins. Within organic materials, there is a class called MCPAM (Phase change materials made up of molecular alloys), formed by alkane-based alloys which have the advantage of being thermo-adjustable, which means they allow alterations to the phase change temperature through their composition.

Inorganic materials primarily consist of salt hydrates and eutectic mixtures. These materials are noted for their multiple applications in Solar Energy Storage. Following are some of the advantages and disadvantages of Organic and Inorganic materials.

Table 1: Advantages and Disadvantages of Organic and Inorganic Phase Change**Materials**

Types	Advantages	Disadvantages
Organics	Large PC Temp Range	Low thermal conductivity
	High L Heat of fusion	Relatively large volume changes
	No super-cooling	Flammability
	Chemically Stable and Reliable	
	Good compatibility with other materials	
Inorganics-Salt Hydrates	High volumetric LH Storage Capacity	Incongruous melting and phase separation
	Availability & Low Cost	High change of volume
	Sharp Melting Point	Corrosive
	High Thermal Conductivity	Super-cooling
	High LH of fusion	Often become inoperative after repeated cycling
Inorganic Eutectics	Non-Flammable	
	Sharp melting point	Reduced thermal performance upon cycling, corrosive, high volume change and super-cooling
	Slightly higher Volume storage density than organic PCMs	Sharp crystal formation
	Dissolving anhydrous salts can prevent phase change degradation, allowing gel formation by melting	Limited data on thermophysical properties

For the purpose of this project, literature with PCMs having melting temperatures or temperature intervals between 100 to 210°C (212 to 410°F), has been reviewed. This is due to the considered application of storing by-product heat at moderate temperatures, i.e. (100 to 200°C), produced during power generation by CHPs. Following table includes a list of these materials with their thermophysical properties. References [8] to [14] are included in Table 2.

Table 2: Classification of PCMs and their Thermophysical Properties

(continued on the next few pages)

PCM Name & Type	Melting Temperature		Specific Heat Capacity ($\frac{J}{kgK}$)		Thermal Conductivity ($\frac{W}{mK}$)	Latent Heat ($\frac{kJ}{kg}$)	Density ($\frac{kg}{m^3}$)	References
	°C	°F	T	Cp				
Organic								
1. Sugar Alcohols					0.1 - 0.75			
Xylitol	93 - 94	199.4 - 201.2	T _s	1,330	0.2865	258 - 270	1,500	[8]
			T _l	2,360	0.1035			
Arabinitol	90	194				230		
Lactitol (monohydrate)	94 - 105	201.2 - 221						
Sorbitol	96 – 101	204.8 - 213.8				196 - 217		
Ribitol	100	212				250		
Erythritol	116.75 - 118.75	242.15 - 245.75	T _s	1,240	0.733 - 0.326	339	1,480	[9]
			T _l	2,480				
Maltitol	145 - 152	293 - 305.6			approx. 0.2	159.7 - 173	1,620	
Lactitol	146 - 152	294.8 - 305.6			approx. 0.3	142	1,690	
D-Mannitol	166	330.8	T _s	1,310	0.279	326	1,520	[10]
			T _l	2,360	0.307		1,450	
Galactitol/ Dulcitol	187.1 - 190.1	368.6 - 374.18		239.5 ($\frac{J}{(mol \cdot K)}$)		330- 373.3	1,470	[11]
Pentaerythritol	186 - 187	366.8 - 368.6			0.236	287- 298	1,400	[10]

2. DiCarboxylic and other Acids					0.11 - 0.2			
Adipic Acid	150 - 152	302 - 305.6	T _s	1,870	0.162	213- 260	1,360	
			T _l	2,720			1,093	[12]
Succinic Acid	187	368.6			0.164	279		
Inorganic Salts and Alkalies			approx. 2,000					
KNO ₃ + LiNO ₃ (wt: 73/27)	165	329						
NaOH + KOH (wt: 50/50)	169 - 171	336.2 - 339.8				202- 213		
Aluminum chloride	180 - 192	356 - 377.6				85-260	2,480	[10]
NaOH + LiOH (wt 70/30)	185 - 216	365 - 420.8				185- 216		
Sugars and Similar Compounds								
Melezitose	153 - 160	307.4 - 320				140	1,810	
Arabinose	153 - 164	307.4 - 327.2				260	1,510	
Glucuronic acid	156	312.8				280	2,000	
Turanose	157	314.6				150	1,900	
Sorbose	159 - 161	318.2 - 321.8				250	1,700	
Galactose	167 - 188	332.6 - 370.4	($\frac{J}{(mol \cdot K)}$)	0.239		188- 352	1,800	
Inulin	178	352.4				40		
Aromatic Hydrocarbons/ Arenes								
4 - Methylacetanilide	146 - 151	294.8 - 303.8	T _s	204.6 ($\frac{J}{(mol \cdot K)}$)	approx. 0.147	180	1,100	[13]
			T _l	267.5 ($\frac{J}{(mol \cdot K)}$)				
Anthranilic Acid	147	296.6				148	1,400	[14]

4 - Nitroaniline	147	296.6				152		[14]
3 - Chlorobenzoic Acid	154	309.2				152-164		[14]
Benzaldehyde phenylhydrazone	155	311				135	1,100	[13]
Salicylic Acid	157 - 159	314.6 - 318.2			approx. 0.217	199	approx. 1,500	[13]
Benzanilide	161	321.8	Ts	236.4 $\left(\frac{J}{mol-K} \right)$		162	approx. 1,200	[13]
			Tl	328.5 $\left(\frac{J}{mol-K} \right)$				
Hexamethylbenzene	166	330.8			approx. 0.116	127	1,065	[14]
1,4 - Dinitrobenzene	171	339.8				157	approx. 1,600	
Hydroquinone	172 - 173	341.6 - 343.4	Ts	1,590	approx. 0.163	192-258	approx. 1,400	[13]
			Tl	1,640				
p -Toluic Acid	180	356				167	approx. 1,300	[14]
4 - Aminobenzoic acid	187 - 188	368.6 - 370.4				153	approx. 1,400	[13]

Several experiments have been carried out by researchers across the world to select the appropriate materials by testing their thermophysical properties appropriate for TES. In 2015, at the Nelson Mandela Institution of Science and Technology, John G. et al. [11] conducted bulk thermal cycling tests with Galactitol, a phase change material, with melting temperature 187°C (368.6 °F). Galactitol was identified as a possible PCM for medium temperature latent heat storage of solar cookers [11]. The PCM samples were repeatedly heated and cooled in an experimental setup. The effects of changing the upper temperature T_{up} , for the hotplate used to heat the samples kept in a closed container, defined as the average of cycle temperatures with the standard deviations for each cycle, were observed and documented. It was concluded that Galactitol is thermally stable at temperatures up to 200°C. Also, the upper cycle temperature of bulk galactitol with

repeated heating and cooling cycles has a great influence on the rate of structural change.

Figures 7 and 8 depict the experimental setup and influence of varying upper cycle temperatures on galactitol.

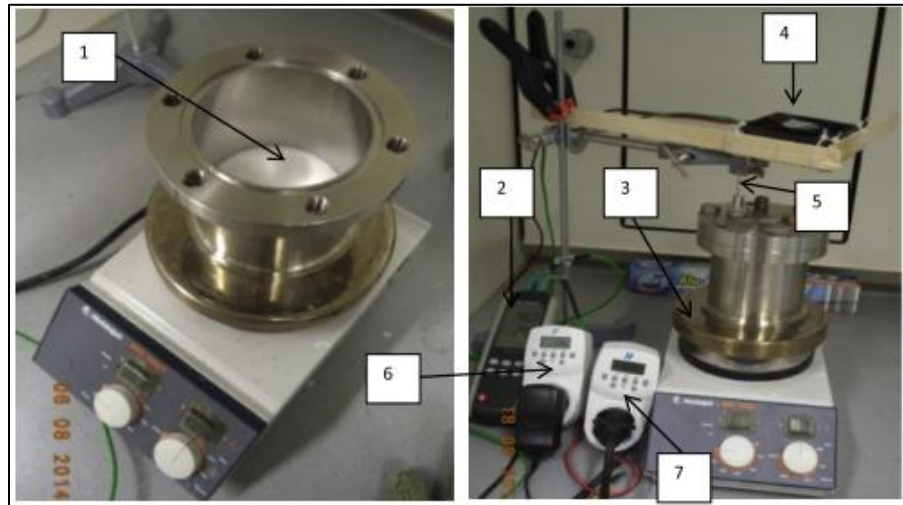


Figure 7: Experimental setup for the bulk cycling. (1) Galactitol sample, (2) temperature data logger, (3) hotplate, (4) electric fan, (5) thermocouple (K-type), (6) timer switch (fan), and (7) timer switch (heater) [11]

T_{up} (°C)	Number of cycles	0	20	40	60	80	180	220
203								
230								
243								

Figure 8: Appearance of three galactitol samples cycled with upper cycle temperature (T_{up}) of 203, 230 and 243 °C per sample [11]

2.2.3 Solid-Solid Phase Change Materials

Solid-solid PCMs (SSPCMs) absorb and release heat by reversible phase transitions between a (solid) crystalline or semi-crystalline phase, and another (solid) amorphous, semi-crystalline, or crystalline phase. Different from solid-liquid-PCMs, SSPCMs retain their bulk solid properties within certain temperature ranges and are therefore also referred to as “solid-state” PCMs [15]. Following schematic shows change in crystalline structure of a Perovskite type SSPCM [16]. The SSPCMs can change crystalline structure from one lattice to another with change in temperature. These materials have comparable latent heat capacity to the solid-liquid PCMs. Problems associated with handling liquids like containment, potential leaks, and others, are not applicable to the SSPCMs.

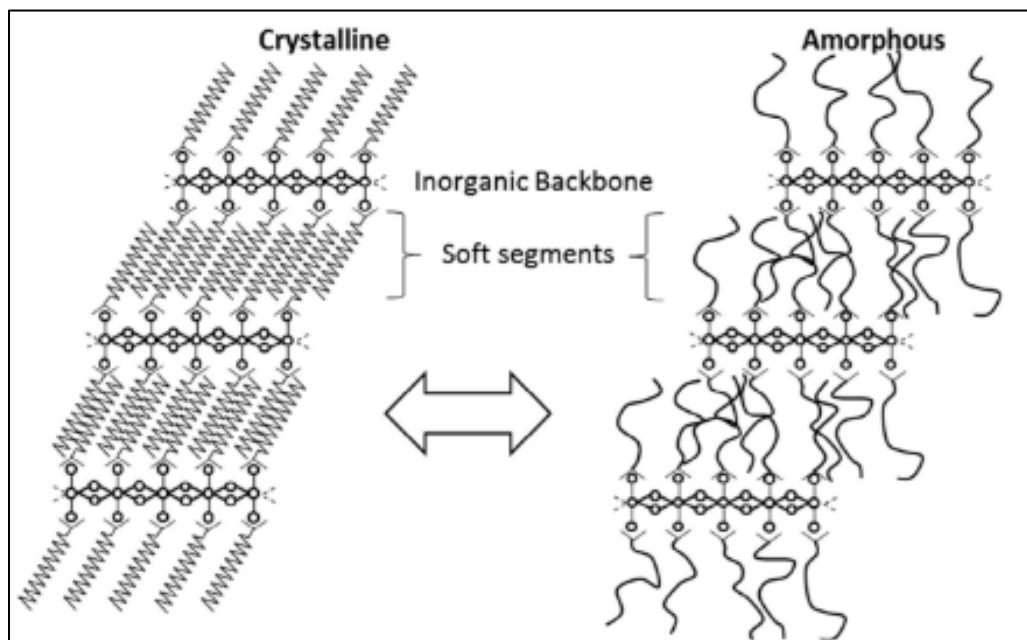


Figure 9: Schematic representation of a Perovskite type SS-PCM [16]

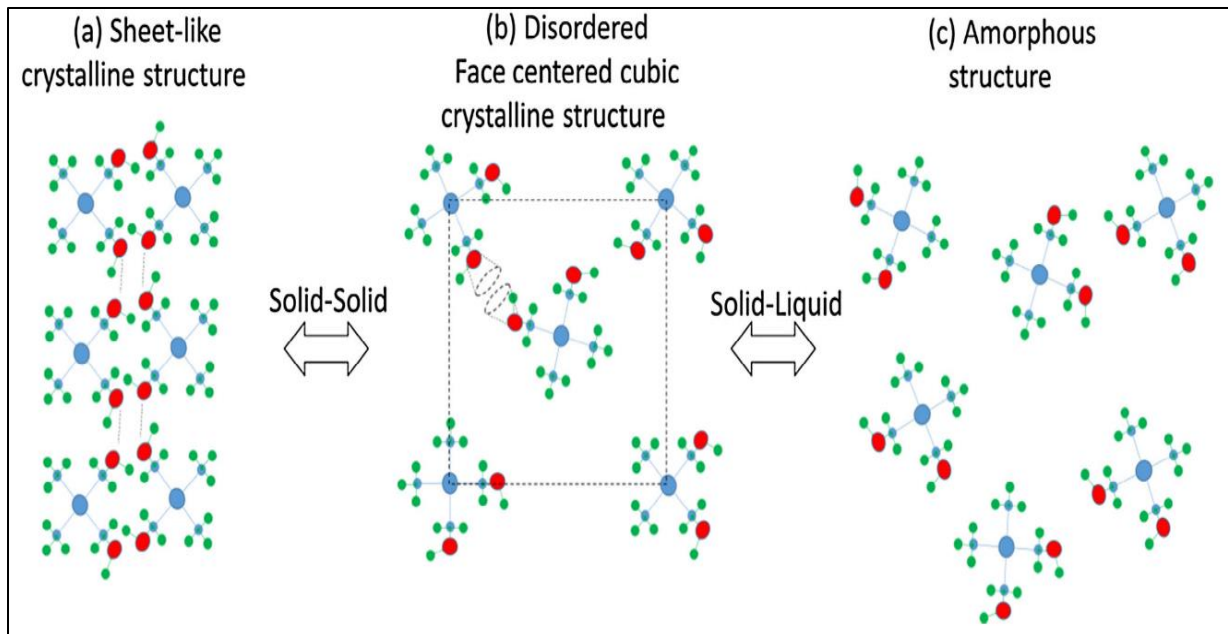


Figure 10: Schematic representation of Polyalcohol type SS-PCMs with crystalline structure changing from (a) sheet like tetrahedral sheet configuration to (b) face centered cubic to (c) disordered amorphous structure [17]

2.3 Selection Criteria of PCMs

Several organic and inorganic PCMs melt with a high heat of fusion in the moderate melting temperature range of (100 to 200°C). For their utilization as effective LTES materials, PCMs must possess certain desirable thermodynamic, kinetic, chemical, technical, and economic characteristics [2]. Following are some of the criteria considered in evaluating PCMs for LTES.

2.3.1 Thermodynamic Criteria

- Melting Temperature in the desired operating temperature range
- High Latent Heat of Fusion per unit volume
- High Specific heat capacity, so that significant sensible TES can occur
- High Density, so that less volume is occupied by the material
- High Thermal Conductivity, so that small temperature differences are needed for charging and discharging the storage
- Small Volume changes on phase transformation, so that a simple containment and heat exchanger can be used

2.3.2 Kinetic Criteria

i. Supercooling

A major problem associated with salt hydrates as PCMs is the fact that they tend to supercool considerably. The reason for the high degree of supercooling is the rate of nucleation (of crystals from the melt) or the rate of growth of nuclei (or both) is very slow, which reduces the advantage of the material for heat storage. Thus, little or no supercooling is desirable, i.e. the melt should crystallize at its freezing point [2].

ii. Nucleation

Supercooling can often be mitigated by adding nucleating materials. Some success has been attained by using additives with a crystal structure like that of the PCM. The nucleating agents should have certain characteristics like insoluble in water at all temperatures, have a melting point higher than the highest temperature reached by the energy storage material in the storage cycle, not form solid solutions with the salt hydrate, not chemically react with the hydrate, and others.

2.3.3 Technical Criteria

Certain technical criteria should be observed for effective storage of PCMs like compactness, compatibility, viability, reliability, design simplicity, and others.

2.3.4 Economic Criteria

Economic Criteria like commercial availability and low cost are important for the PCMs. These prove to be important considerations for development of storage devices, since the scale of energy storage would depend on the respective application. When carefully evaluated, PCMs have the potential to significantly reduce electric demand and expenditure.

CHAPTER 3

NUMERICAL SIMULATION AND CASE VALIDATION

3.1 Melting in a Vertical Cylindrical Tube

In 2010, Shmueli H. et al. [18] conducted numerical and experimental analysis of a PCM in a vertical cylindrical tube. They also investigated effect of mushy zone constant ‘C’, on melting in a vertical cylindrical tube, using the solidification/melting model of the commercial CFD software Fluent. Vertical cylindrical tubes of 3 cm and 4 cm in diameter, with the wall temperatures of 10 and 30°C above mean melting temperature of the PCM, were considered for their experimental and numerical investigation. Following figure shows the interface of PCM exposed to air at 17 cm from the base, the total height of the tube being 20 cm.

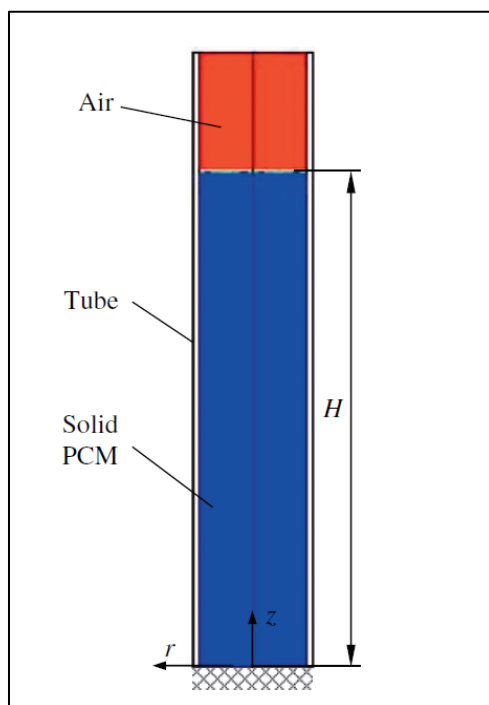


Figure 11: Numerical Model with the PCM and Air interface at $H = 17$ cm [18]

3.1.1 Numerical Model

For the numerical model, properties of PCM are based on a commercially available PCM, Rubitherm GmbH (RT27), with a melting temperature interval of 299.15 – 301.15°K (26-28°C), with the entire system being at an initial temperature of 295.15 °K (22°C). It is assumed that both solid and liquid phases are homogeneous and isotropic, and the melting process is axisymmetric. The molten PCM and the air are incompressible Newtonian fluids, and laminar flow is assumed in both. A temperature dependent expression is used to describe the density of air given as,

$$\rho = 1.2 \times 10^{-5}T^2 - 0.001134T + 3.4978 \quad (3.1)$$

The properties of the PCM can be seen in the table below,

Table 3: Properties of RT27 (Rubitherm GmbH) used in simulations [18]

Dynamic Viscosity, μ ($\frac{\text{kg}}{\text{ms}}$)		Specific Heat Capacity, C_p ($\frac{\text{J}}{\text{kg}^\circ\text{K}}$)	Thermal Conductivity, k ($\frac{\text{W}}{\text{m}^\circ\text{K}}$)	Density, ρ ($\frac{\text{kg}}{\text{m}^3}$)	Latent heat, L ($\frac{\text{kJ}}{\text{kg}}$)
Solid	-	2,500	0.24 (0.2)	870	179
Liquid	$-1.137439 \times 10^{-8}T^3$ $+ 1.178188 \times 10^{-5}T^2$ $- 0.004111388T$ $+ 0.4857203$	2,500	0.15 (0.2)	870 @ 299°K	
				781.5 @ 301°K	
				750 @ 343°K	

The interface in the PCM-air system is described, with a moving internal interface without inter-penetration of the two media, using the volume-of-fluid (VOF) model in Fluent. If the q^{th} fluid's volume fraction in the cell is denoted as α_q , then following conditions are possible,

- $\alpha_q = 0$; The cell is empty (of the q^{th} fluid).
- $\alpha_q = 1$; The cell is full (of the q^{th} fluid).
- $0 < \alpha_q < 1$; The cell contains interface between the q^{th} fluid and one or more other fluids.

The variables and properties in any given cell are either purely representative of one of the media, or representative of a mixture of the media, depending upon the volume fraction values.

To model the phase change of the material, the enthalpy-porosity approach is utilized as described in the melting and solidification model in Fluent User Guide [19]. The governing equations used for the PCM-air are,

- Continuity

$$\frac{D\alpha_n}{Dt} = 0 \quad (3.2)$$

- Momentum

$$\rho \frac{DV^\rightarrow}{Dt} = -\nabla p + \mu \nabla^2 V^\rightarrow + \rho g^\rightarrow + S^\rightarrow \quad (3.3)$$

- Energy

$$\rho \frac{Dh}{Dt} = k \nabla^2 T \quad (3.4)$$

where ρ is the density, k is the thermal conductivity, μ is the dynamic viscosity, S^\rightarrow is the momentum source term, V^\rightarrow is the velocity vector, T is the temperature, and h is the specific enthalpy . The specific enthalpy is defined as a sum of the sensible enthalpy, $h_s = h_{ref} + \int_{T_{ref}}^T C_p dT$, and the enthalpy change due to phase change γL , where, h_{ref} is the reference enthalpy at the reference temperature T_{ref} , C_p is the specific heat, L is the specific enthalpy of melting (latent heat of the material), and γ is the liquid fraction during the phase change which occur over a range of temperatures $T_s < T < T_l$, where ‘ T_s ’ and ‘ T_l ’ are the ‘solidus’ and ‘liquidus’ temperatures respectively, defined by the following relations,

$$\gamma = \begin{cases} 0 & \text{if } T < T_s \\ 1 & \text{if } T > T_l \\ \left(\frac{T - T_s}{T_l - T_s} \right) & \text{if } T_s < T < T_l \end{cases}$$

The source term S^\rightarrow in the momentum equation is given by,

$$S^\rightarrow = -A(\gamma)V^\rightarrow \quad (3.5)$$

where $A(\gamma)$ is the “porosity function”, which makes the momentum equation mimic Carman-Kozeny equations for flow in porous media,

$$A(\gamma) = \frac{C(1 - \gamma^2)}{\gamma^3 + \epsilon} \quad (3.6)$$

where $\epsilon = 0.001$ is a small computational constant used to avoid division by zero, and C is the mushy zone constant [18]. The Fluent manual describes the mushy zone constant as the measure of amplitude of damping, the higher this value, the steeper the transition of the velocity of the material to zero as it solidifies. Very large values may cause the solution to oscillate.

3.1.2 Simulations with Variation in Mushy Zone Constant

The results for the model configuration with tube diameter of 4 cm, height of phase change material in the tube being 17 cm, and the wall temperature 10°K above the mean melting temperature of the PCM, have been studied for the purpose of this project. The effect of varying ‘C’ on the melting of PCM, between 10^5 and 10^{10} , was investigated by Shmueli et al. [18] to obtain comparable results to the experimental results, as can be seen in the figure below,

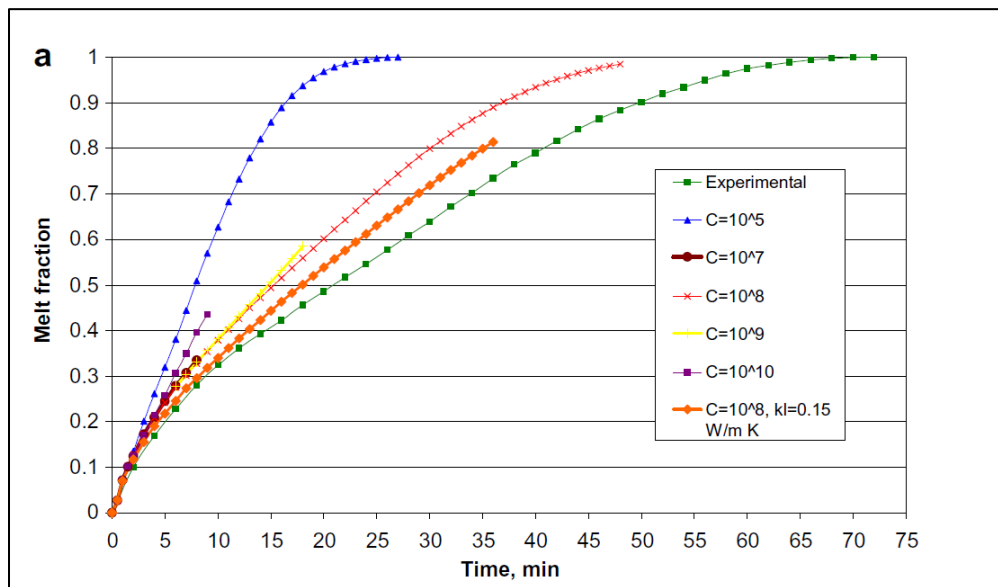


Figure 12: Melt Fraction Vs Time (min) for various values of the mushy zone constant for D = 4 cm, H = 17 cm, and $\Delta T = 10^\circ\text{K}$ [18]

In the present study, the values of C ranging from 10^5 to 10^8 are explored. The grid was built utilizing ICEM software. The sizing was considered keeping in mind the CFL condition. [Figure 13](#) shows the initial grid utilized for simulations, with approx. 10.5k nodes. Fluent defines axisymmetric 2-D space, as the domain axisymmetric to the X axis. Thus, gravity is defined along the -X direction in the solver. For this reason, grid is created with the consideration that axis of symmetry is the X axis. The element size in

the +X direction is 1.15 mm, and a growth ratio of 1.077 is utilized for the nodes in the +Y direction with Bi-geometric mesh criteria. This concentrates the nodes near the wall and axis, aiding in effective modeling of the heat transfer.

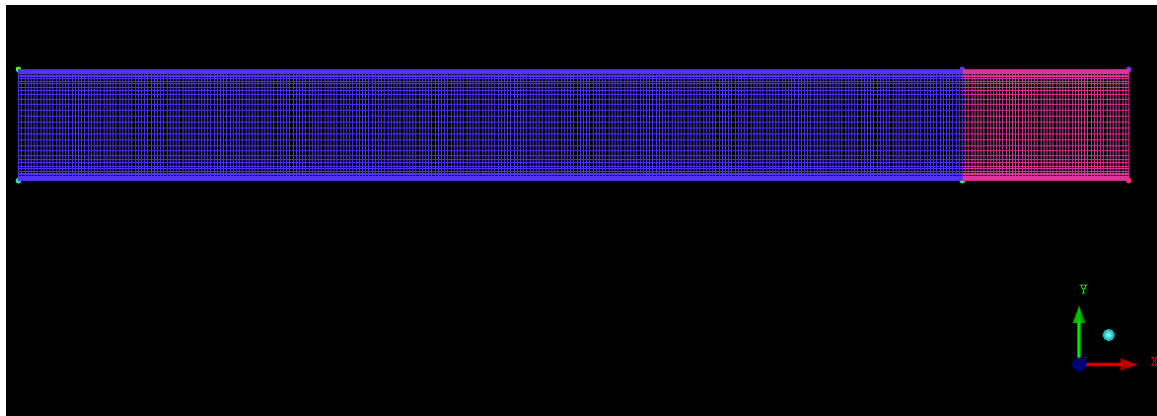


Figure 13: 2-D mesh for case

3.1.3 Modeling Schemes and Discretization

Three models are available for Multiphase modeling in Fluent for pressure-based solvers namely, Volume of Fluid (VOF), Mixture, and Eulerian models. The VOF model uses an Eulerian approach to model multi-phase flows.

The boundary conditions for the momentum equation are no-slip and no penetration at all solid boundaries [18]. A pressure-outlet boundary condition is used at the upper boundary, which is open to the atmosphere, with the ambient temperature of 300.15°K at this boundary. At the PCM-air interface, the interior boundary condition is used. The outer tube wall is maintained at a constant temperature of 10°K above the mean melting temperature of the PCM. An adiabatic wall condition is used for the bottom wall of the tube. The edges parallel to the X axis are assigned the axis boundary conditions.

Comparing with the experimental results, the value of ($C = 10^6$), yields the most accurate results, as shown below.

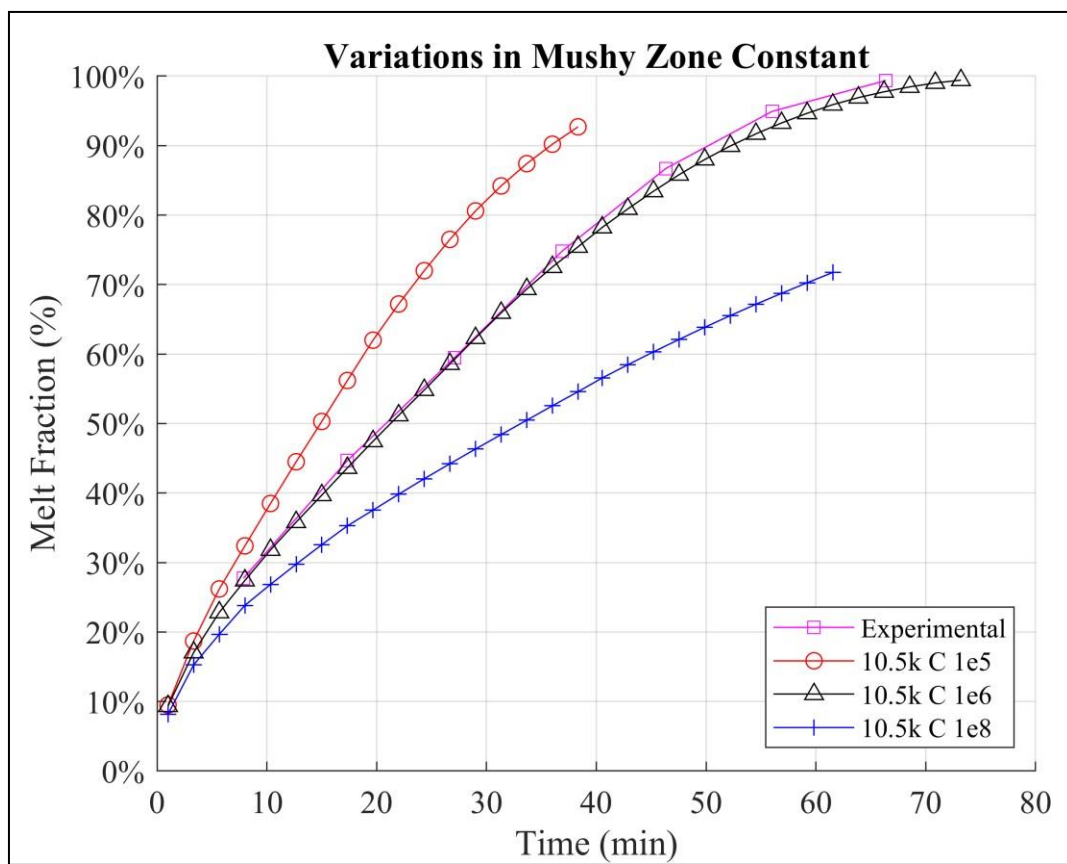


Figure 14: Melt Fraction Vs Time (min) for $C = 10^5, 10^6$, and 10^8 , for $D = 4$ cm, $H = 17$ cm, and $\Delta T = 10^\circ\text{K}$

3.1.4 Time and Mesh Sensitivity Analysis

Implicit volume fraction formulation was used for the VOF modeling. The implicit formulation is iterative and can be used with either the Steady or Transient solver. It is well-suited to steady-state applications as the solution information propagates much faster compared to the explicit formulation. However, with a transient case where results are dependent upon initial flow conditions, a larger time-step size is more suitable which is available with Implicit formulation. The time step sizing was done based on the Courant-Friedrichs-Lowy (CFL) condition. For a case with ‘n’ dimensions, the general CFL condition is given by the equation,

$$C = \Delta t \sum_{i=1}^n \frac{u_{x_i}}{\Delta x_i} \leq C_{\max} \quad (3.7)$$

where, Δx_i is the length of the first node of each spatial variable for which ($i = 1, 2, \dots, n$) (dimension being length), u_x is the magnitude of velocity (dimension being length/time), Δt is the time step (dimension being time), and C is the dimensionless Courant number for which ($C_{\max} \geq 1$).

The time step sizes chosen for time sensitivity analysis range from 0.005s to 0.05s. Along with this, spatial length variations were also considered in the X direction for mesh refinement. The results for the time and mesh sensitivity can be seen in [Figure 15](#). Case proves to be insensitive to time and mesh variations, with small variations in total time taken for melting, when compared to the experimental results provided by Shmueli et al [18].

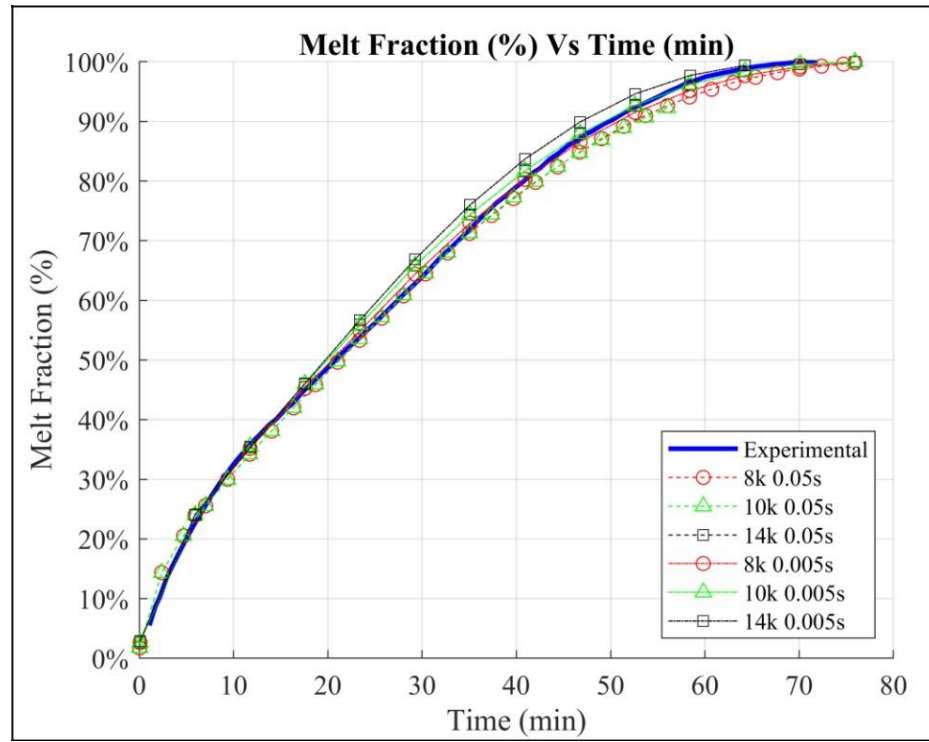


Figure 15: Mesh and Time sensitivity for $C = 10^6$ from 0.05s to 0.005s

3.2 Melting in Annular PCM with flow

3.2.1 Experimental Model

Another configuration which considers the melting of PCM in a vertical cylinder was experimentally and numerically investigated by Longeon et al. [20], for the melting of paraffin RT35 with a melting temperature of 308.15°K (35°C) provided by Rubitherm. The experimental setup is composed of a test-section, several instrumentation devices and a Heat Transfer Fluid (HTF) Control Loop. The configuration explored injection of a Heat Transfer Fluid (HTF) in an inner tube. The experimental loop and thermocouple positions, along with test section can be seen in the [Figure 16](#). The physical and numerical properties of RT35 can be found in the table below.

Table 4: Properties of RT 35 [20]

Property	Value	Variation with Temp		Unit
Density (ρ)	880	-	-	$\frac{\text{kg}}{\text{m}^3}$
Thermal Expansion Coefficient (β)	0.001	-	-	1/K
Latent Heat Capacity (L)	157,000	-	-	J/kg
Melting Temperature (T_m)	308.15	-	-	K
Specific Heat Capacity (C_p)		306.15 K	1,800	$\frac{\text{J}}{\text{kgK}}$
		308.15 K	2,400	
Thermal Conductivity (k)	0.2	-	-	$\frac{\text{W}}{\text{mK}}$
Kinematic Viscosity (ν)	3.3×10^{-6}	-	-	$\frac{\text{m}^2}{\text{s}}$

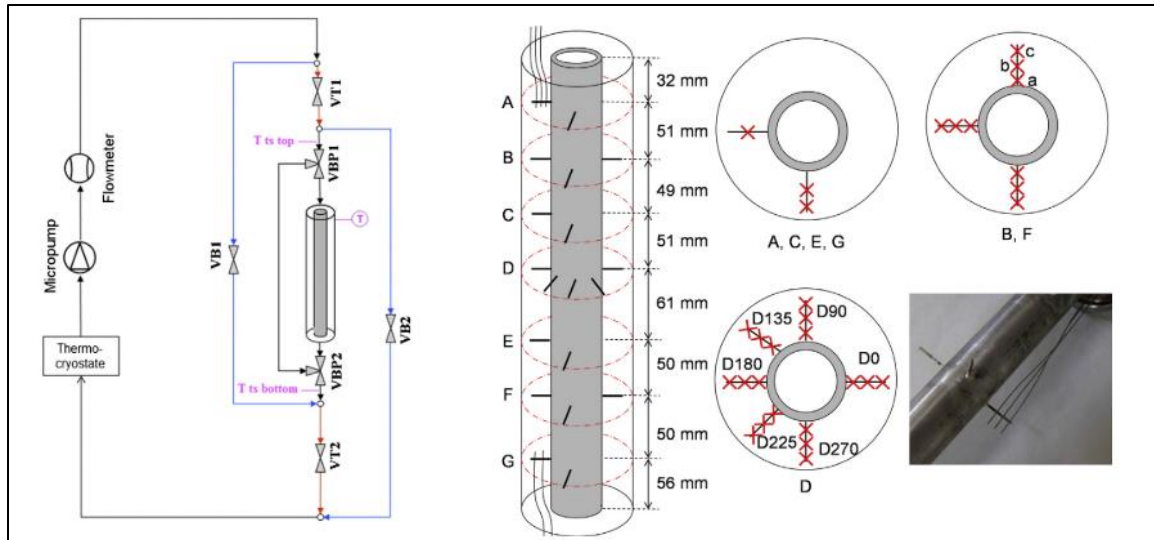


Figure 16: Schematic of Experimental Loop and thermocouples with test section

[20]

The PCM storage system is composed of two concentric cylinders, with an inner diameter of 44 mm is made of Plexiglass, enabling visualization of the contents, and the other has an inner diameter of 15 mm made of stainless steel and has a thickness of 2.5 mm, with 400 mm being total length of the whole system. The HTF flows in the inner tube, and 480 g of PCM fills up the annular space, so that regenerator can store 120 kJ (from 28°C to 46°C) [20]. Properties of the HTF can be seen in the table given below.

Table 5: Properties of HTF

Property	Value	Unit
Density (ρ)	998.2	$\frac{\text{kg}}{\text{m}^3}$
Specific Heat Capacity (C_p)	4,182	$\frac{\text{J}}{\text{kg}^\circ\text{K}}$
Thermal Conductivity (k)	0.6	$\frac{\text{W}}{\text{m}^\circ\text{K}}$
Dynamic Viscosity (μ)	0.001003	$\frac{\text{kg}}{\text{ms}}$

3.2.2 Numerical Model

Transient simulations of the melting process were conducted using the commercial CFD software Fluent. The experimental setup was modeled with a 2-D axisymmetric geometry and a 3-D symmetric geometry. In both cases the flow is in +X direction for the HTF in the inner tube of annular geometry, the outer annulus containing the PCM. Also, gravity is defined along -X direction in the solver.

Both the meshes were created using ANSYS ICEM CFD software. Multi Block-Grid was created for both types of meshes. For the 2-D mesh the bottom wall parallel to X-axis is chosen as the axis of symmetry as can be seen in [Figure 17](#). A mesh with 5k nodes for 2-D case was utilized, with element size

For the 3-D mesh a partial ‘O-Grid’ or ‘C-Grid’ blocking strategy was implemented for individual zones as can be seen in [Figure 18](#). Both the meshes have same number of nodes along the axis of the annulus and the diameter. This enables a direct comparison between the two cases to check for any changes in the solution associated with the mesh type.

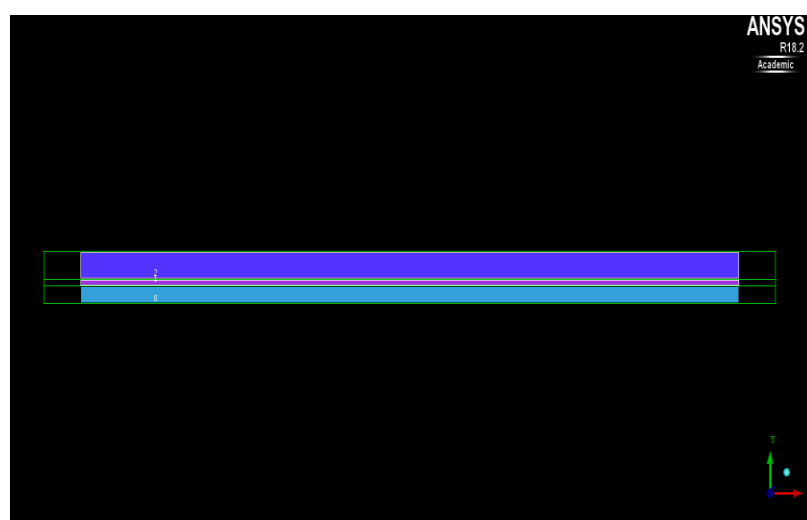


Figure 17: 2-D Mesh for the Longeon et al. Case with axisymmetric on X axis

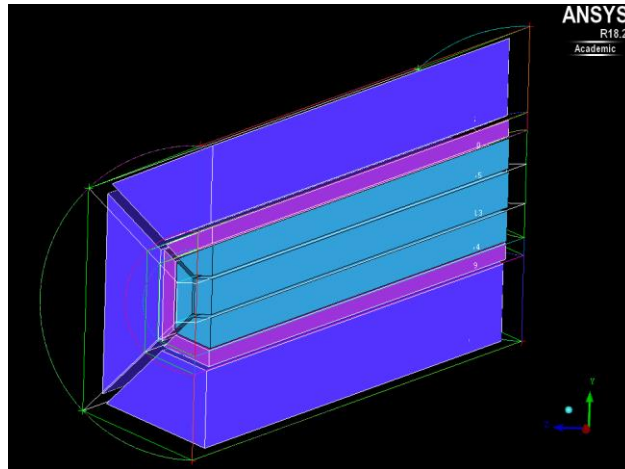


Figure 18: 3-D Mesh for Longeon et al. case with ‘C-Grid’ blocking

Natural Convection is taken into consideration, by utilizing the Boussinesq approximation for the density of material RT35. The model incorporating Boussinesq approximation as described in Fluent User’s Guide [19], treats the density as a constant value in all solved equations, except the buoyancy term in the momentum equation, given by,

$$(\rho - \rho_0)g \approx -\rho\beta(T - T_0)g \quad (3.8)$$

where, ρ_0 is the constant density, T_0 is the operating temperature, and β is the thermal expansion coefficient. The Boussinesq approximation is used for eliminating ρ from the buoyancy term as given below,

$$\rho = \rho_0(1 - \beta\Delta T) \quad (3.9)$$

The approximation is valid if the changes in actual density are small, specifically, the Boussinesq approximation is valid when,

$$\beta(T - T_0) \ll 1 \quad (3.10)$$

3.2.3 Boundary Conditions

i. 2-D Case

The 2-D Case was modeled using certain specific boundary conditions for the different zones in the geometry. The inlet zone is defined with velocity-inlet boundary condition with 0.01m/s and 326.15°K, whereas the outlet is defined with a pressure-outlet boundary condition, with a backflow temperature of 308.15°K. The bottom HTF wall parallel to X-axis is defined with the axis boundary condition. The inner and outer surfaces of the HTF-Tube are defined with coupled-wall boundary condition. The PCM side and outer walls are defined with adiabatic wall conditions. [Figure 19](#) below shows some of the various zones of the 2-D mesh.

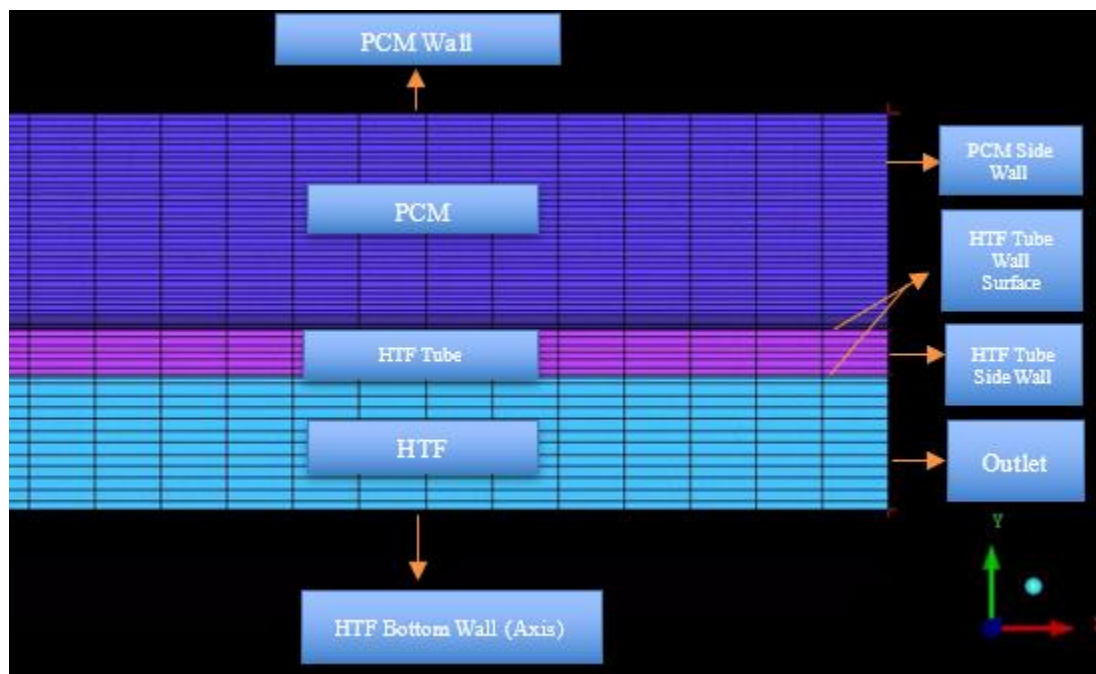


Figure 19: 2-D Mesh Zones

ii. 3-D Case

The 3-D Case was defined with same boundary conditions for the inlet and outlet zones, as that of the respective zones in the 2-D case. The symmetric walls of each domain, i.e. HTF, HTF-Tube, and PCM domains, are defined as symmetric walls. The inner and outer surfaces of the HTF-Tube are defined with coupled-wall boundary condition. The side walls of HTF-Tube and PCM domains, along with the outer wall of the PCM domain, are defined with adiabatic wall boundary conditions. [Figure 20](#) below shows the various zones of the 3-D mesh.

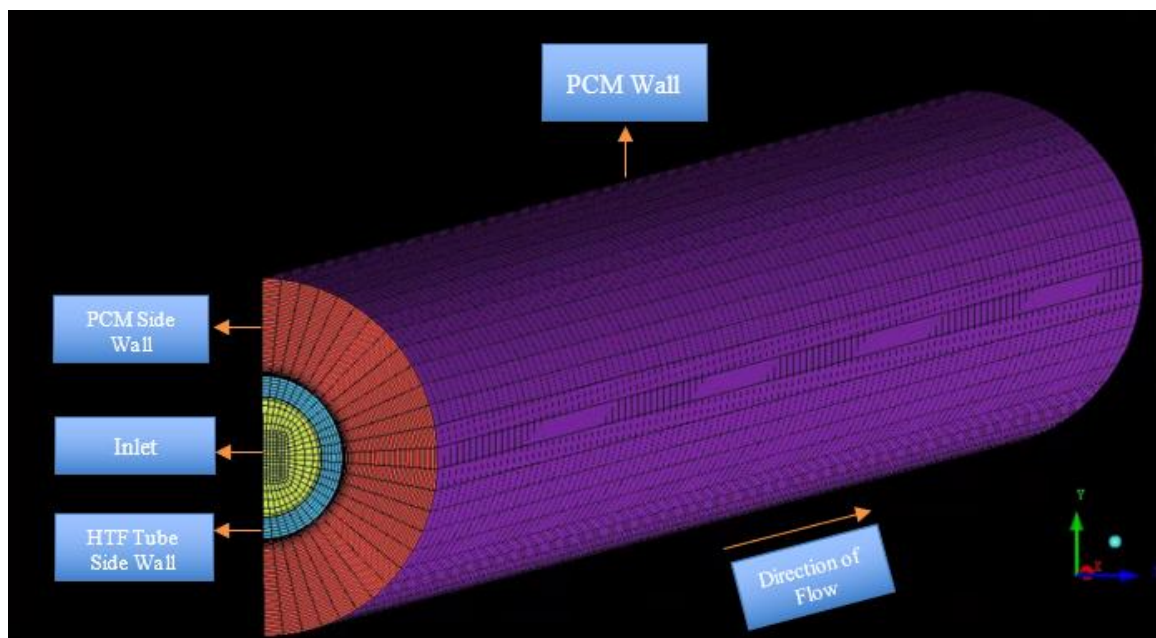


Figure 20: 3-D Mesh Zones

3.2.4 Results and Comparisons

The temperature at various angles and radial positions was measured with the help of thermocouples by Longeon et al [20]. The temperature output of thermocouple at radial position 6.6 mm and 0° angular position in ‘D’ as shown in [Figure 21](#), is chosen for comparison of the simulation results of both cases with the experimental results.

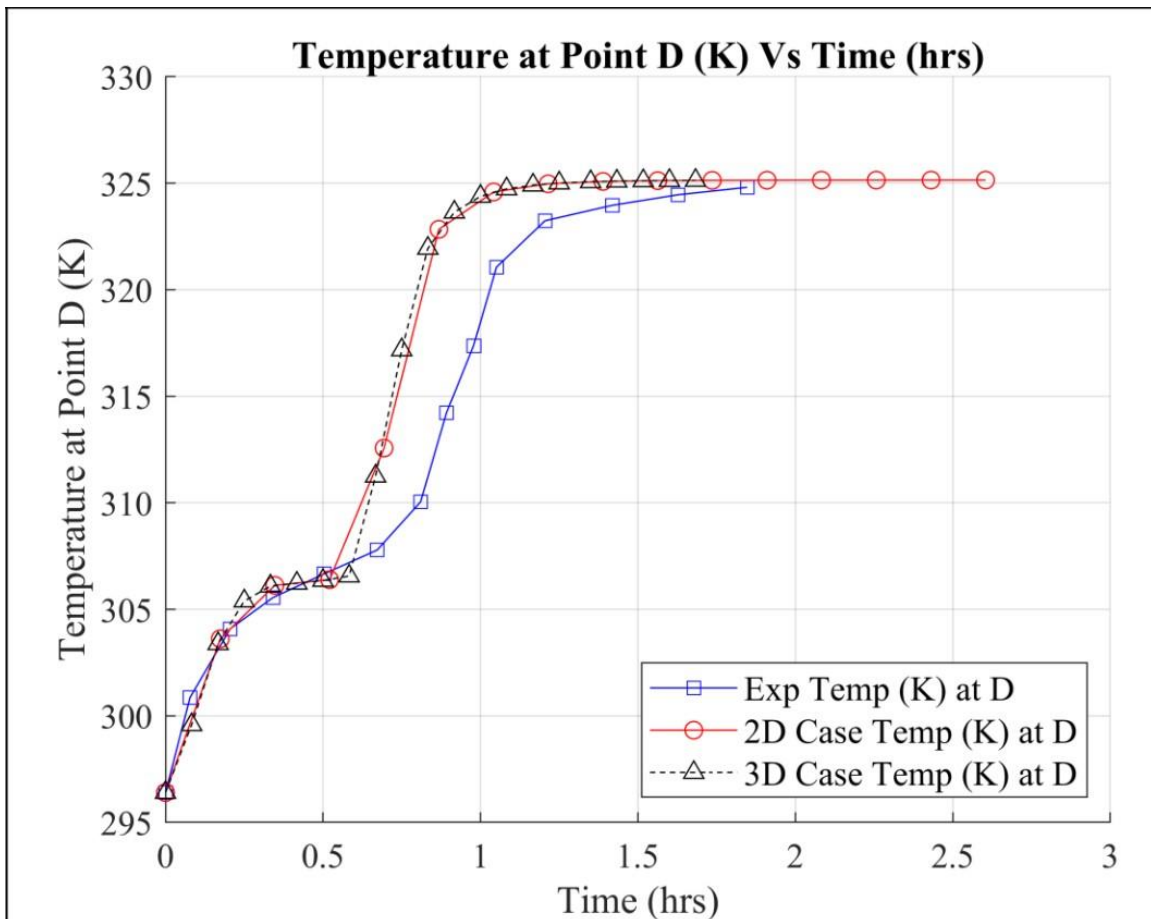


Figure 21: Comparison with Experimental Results for Temperature at Point (K)

CHAPTER 4

LTES STORAGE DESIGN

4.1 PCM Selection

To simulate the conditions of heat storage/transfer, for the moderate temperature 100 to 210°C (212 to 410°F) by-product heat produced by CHPs, the organic sugar-based alcohol Erythritol is chosen as the PCM. The properties of erythritol are given in [Table 6](#). The respective changes in specific heat capacity and thermal conductivity of the PCM with changes in temperature can be seen below.

Table 6: Properties of Erythritol

Property	Value	Variation with Temp		Unit
Density (ρ)	1,480	-	-	kg/m ³
Thermal Expansion Coefficient (β)	0.001014	-	-	1/ ^o K
Latent Heat Capacity (L)	339,800	-	-	J/kg
Temperature Solidus (T _s)	389.85	-	-	^o K
Temperature Liquidus (T _L)	391.85	-	-	^o K
Specific Heat Capacity (C _p)		293.15 ^o K	1,380	$\frac{J}{kg\cdot K}$
		391.85 ^o K	2,760	
Thermal Conductivity (k)		293.15 ^o K	0.733	$\frac{W}{m\cdot K}$
		391.85 ^o K	0.326	
Dynamic Viscosity (μ)	0.01	-	-	$\frac{kg}{ms}$

The HTF chosen for the new design is a dow-corning 550 fluid. Properties for both these fluids were specified by Parry et al [9]. An experimental setup created to

model TES with a Shell-and-Tube Heat Exchanger using erythritol, was also numerically validated by Parry et al [9]. This is chosen due to the considerations for its common availability as an industry supply fluid and relatively low cost. The properties of the HTF can be seen in the Table 7 below.

Table 7: Properties of HTF

Property	Value	Unit
Density (ρ)	1,065	$\frac{\text{kg}}{\text{m}^3}$
Specific Heat Capacity (C_p)	396	$\frac{\text{J}}{\text{kg}^\circ\text{K}}$
Thermal Conductivity (k)	0.1465	$\frac{\text{W}}{\text{m}^\circ\text{K}}$
Dynamic Viscosity (μ)	0.133125	$\frac{\text{kg}}{\text{ms}}$

4.2 Numerical Model

For both, i.e. 2-D and 3-D cases, the same modeling schemes are used as described in [Chapter 3](#). The HTF and PCM domains are modeled separately, where effect of variations in parameters are observed on the melting and time taken for complete melting in the PCM domain. Commercial CFD software Fluent is utilized to simulate the flow conditions and heat transfer.

Mesh domains were developed using the ANSYS ICEM CFD software for both the cases as discussed in [Section 3.2.2](#). Axisymmetric meshes for the 2-D cases and symmetric meshes for their 3-D counterparts were created with the same number of nodes and growth ratios for the simulations. For the initial simulations, to study the effect of inlet conditions on the time taken for complete melting, cases with 2-D axisymmetric mesh was developed as mentioned above. (Refer [section 3.2.2](#))

Along with the inlet conditions, the effect of change in amount of PCM was also studied by carrying out simulations in 2-D and are compared with 3-D simulations with same mesh size and conditions.

4.3 Variations in Inlet Conditions

4.3.1 Reynold's Number Variations

For the purpose of this project, melting in PCM due to laminar flow in the HTF domain is studied. This is due to complexity of turbulent heat transfer and difficulty in coupling the models available in Fluent for the same. Keeping the geometry of the computational domain the same, as that of the experimental model by Longeon et al. [20], melting in the PCM domain was studied.

The Reynold's Number 'Re', for the HTF Domain is defined as,

$$Re = \frac{\rho_{HTF} \times v_i \times D_{i,HTF}}{\mu} \quad (4.1)$$

where, ' ρ_{HTF} ' is the density of HTF in ($\frac{kg}{m^3}$), v_i is the inlet velocity in ($\frac{m}{s}$), ' $D_{i,HTF}$ ' is the inner diameter of the HTF tube in (m), and ' μ ' is the viscosity of the HTF in ($\frac{m^2}{s}$).

All the properties can be found in [Table 7](#).

To maintain laminar flow in the HTF zone, inlet velocity was varied first, in order to regulate the Reynold's Number below 2,300 (Re < 2,300 for laminar flow). The inner diameter of the HTF domain is 15mm and the thermal properties of the HTF can be found in Table 4.2. The values determined for the inlet velocities, according to change in the respective Reynold's Number can be seen in the [Table 8](#) below.

Table 8: Changes in Inlet Velocity 'Vi' by variation in Reynold's Number 'Re'

Re	vi (m/s)
1,020	8.5
1,530	12.75
2,040	17

4.3.2 Variations in Inlet Temperature

The variations in inlet temperature ‘ T_i ’, were also studied along with variation in V_i . Since, the melting interval of PCM is 116.7 to 118.7°C (389.85 to 391.85°K), three values for T_i were considered in the increment of approx. 10°K from 403.15°K, as shown in [Table 9](#). This facilitates a comparative study of the inlet temperatures above the mean melting temperature of the PCM. In turn, this comparison gives us 9 combinations of T_i and V_i , which aides in further understanding of the significance of inlet conditions on the TES with PCM.

The boundary conditions for the solver are the same as discussed in [section 3.2.3](#).

Results and Comparison

Results for the time taken for complete melting can be seen in [Figure 22](#). From the distribution it is evident that the time taken for melting decreases with increase in T_i . Comparatively, the time taken for melting does not increase as significantly with increase in velocity. The time for completing melting for each combination can be seen in [Table 9](#). The maximum time taken was observed for lowest T_i and V_i values i.e. 403.15°K and 8.5 m/s, whereas the minimum time taken for complete melting was for the highest values of T_i and V_i i.e. 423.15°K and 17 m/s.

Table 9: Time taken for melting in hours for each combination

T_i/V_i	8.5 m/s	12.75 m/s	17 m/s
403.15°K	3.51	3.45	3.30
413.15°K	2.10	1.97	1.90
423.15°K	1.55	1.47	1.42

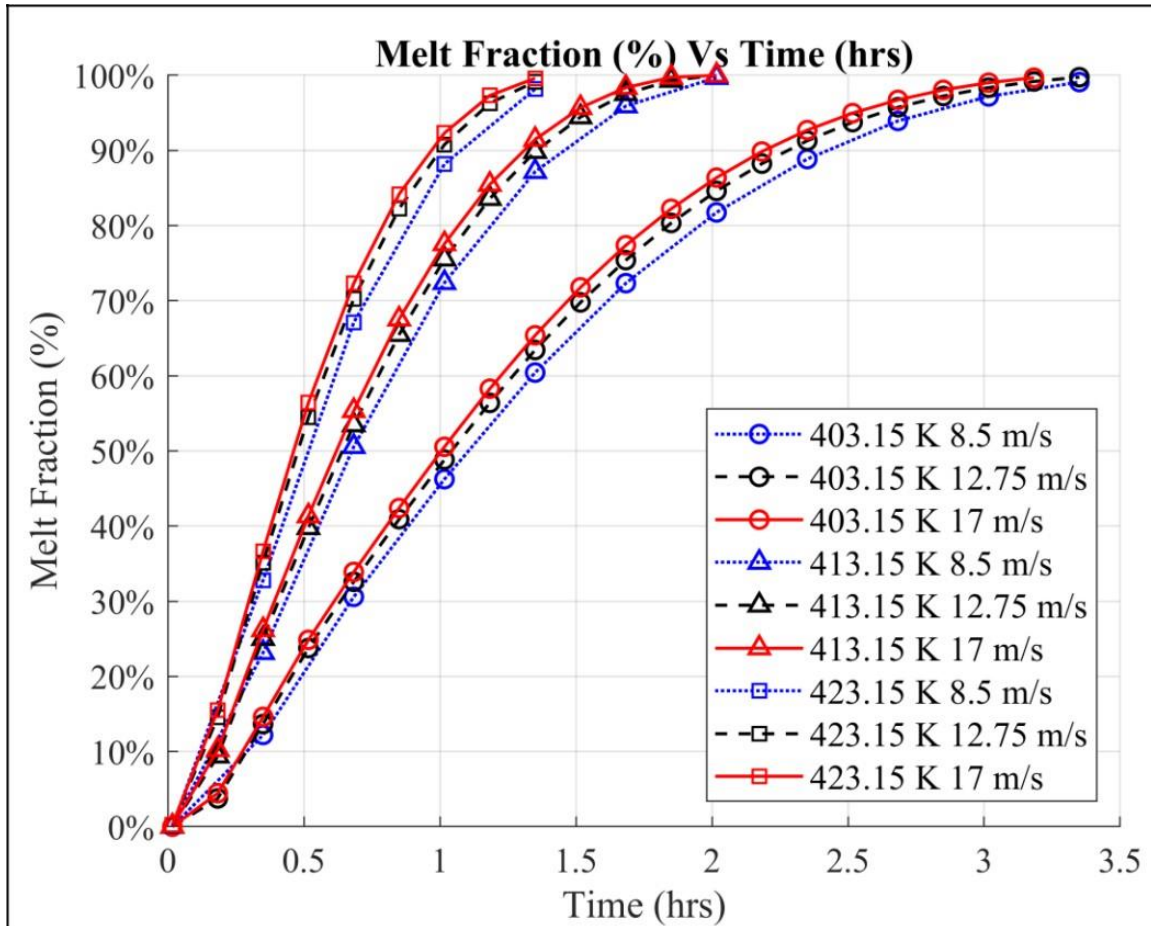


Figure 22: Variations in time for complete melting with varying Ti and Vi

For further analysis, the combination of 423.15°K and 17 m/s is selected. The total amount of PCM can be changed by change in the outer cylindrical diameter of the PCM domain (PCM_D). For this purpose, three diameter sizes were chosen at an increment of 15 mm, i.e. 30, 45, and 60 mm.

From Figure 22, it is evident that with increase in ‘Ti’ the time taken for melting reduces significantly, as compared to the melting time with increase in ‘Vi’. This can be attributed to the increased rate of heat being transferred across the hot fluid tube wall. Also, it can be inferred that, melting progresses linearly from approx. (10% to 80%), even with variations in input parameters.

As can be seen in Figure 22, the variations in ‘Ti’ are displayed with different symbols, while the variations in ‘Vi’ are displayed with different types of lines. The same convention has been followed for the figures displaying results in this report.

4.3.3 Solidification

The discharging process of the LTES device is considered by the solidification of PCM, as heat is extracted from the completely melted PCM in the container by passing a colder fluid through the inner tube. To have consistency with the melting process, variations in Vi were limited by the Re in order to have laminar flow in the inner tube ($Re < 2,300$). The variations in Ti were considered below the mean melting temperature, which along with the variations in Vi , which provide nine more combinations as shown in [Table 10](#) below. It was observed that with decrease in Ti the time taken for solidification decreases proportionally. Also, the time taken for solidification decreases with increase in Vi , due to heat being carried away by the colder fluid faster at higher Vi . In order to obtain comparative results, the cases were initialized with 423.15°K as the initial temperature for HTF Tube and PCM domains.

Table 10: Time taken for solidification in hours for each combination

Ti/Vi	8.5 m/s	12.75 m/s	17 m/s
358.55°K	1.78	1.75	1.67
368.55°K	2.73	2.67	2.52
378.55°K	5.18	4.97	4.70

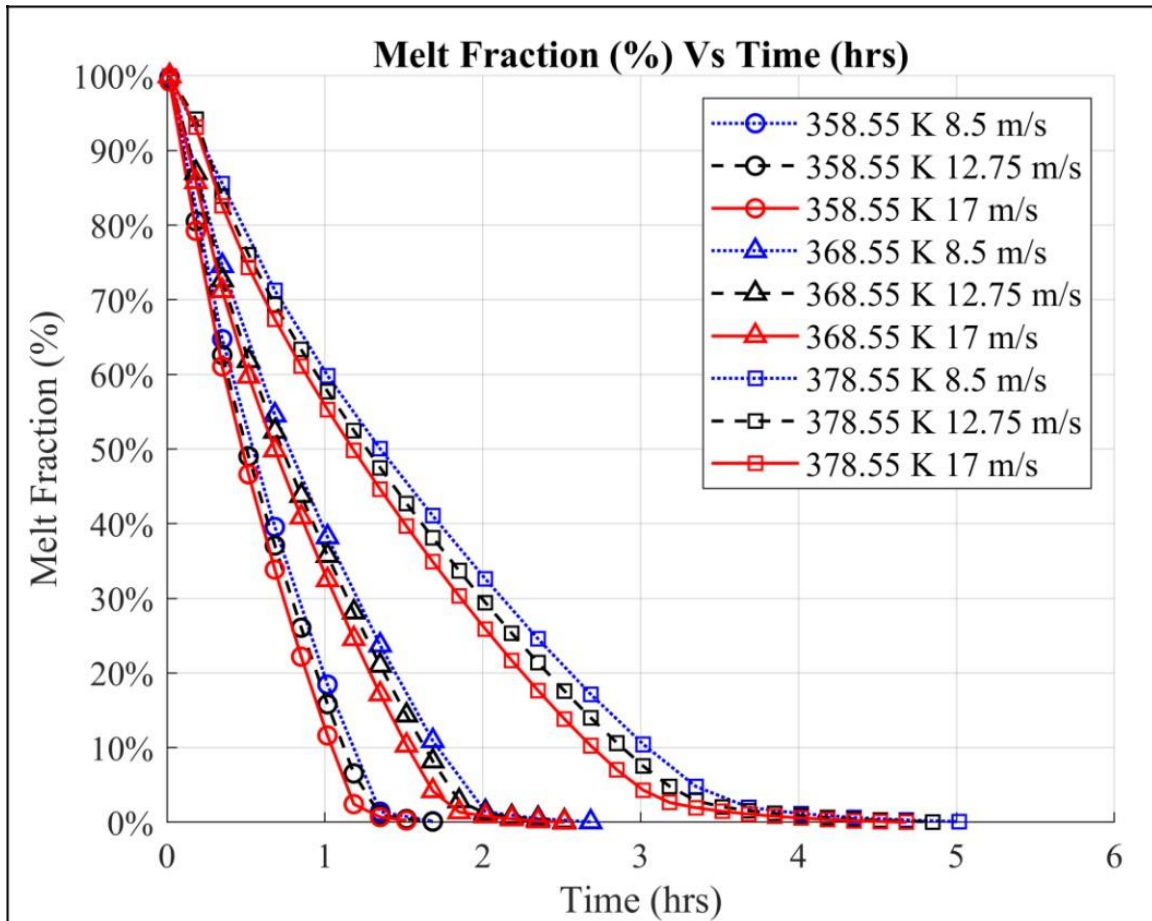


Figure 23: Variations in time for complete solidification with varying Ti and Vi

4.4 Variations in Diameter of PCM Domain

The effect of change in PCM_D is an important parameter for designing a LTES Device. The amount of PCM stored changes proportionally to the change in diameter of the storage container. The 2-D and 3-D cases follow the considerations described previously (Refer [section 3.2.3](#)).

4.4.1 Initial Results with 2-D cases

Initial simulations were conducted with 2-D axisymmetric mesh for all three diameter sizes. Significant changes in time required for complete melting in the PCM domain were observed. With increase in diameter the time required for melting increases. Grid sensitivity analysis was done with two grids of 5k and 10k nodes for the new meshes with all three diameters, as increase in size of the device could affect the spatial discretization. Since, no significant change was observed in the final melting time for grids with more nodes, cases prove to be grid independent, as can be seen in [Figure 24](#). The maximum time taken for complete melting is for the 60 mm diameter case which is 3.15 hours.

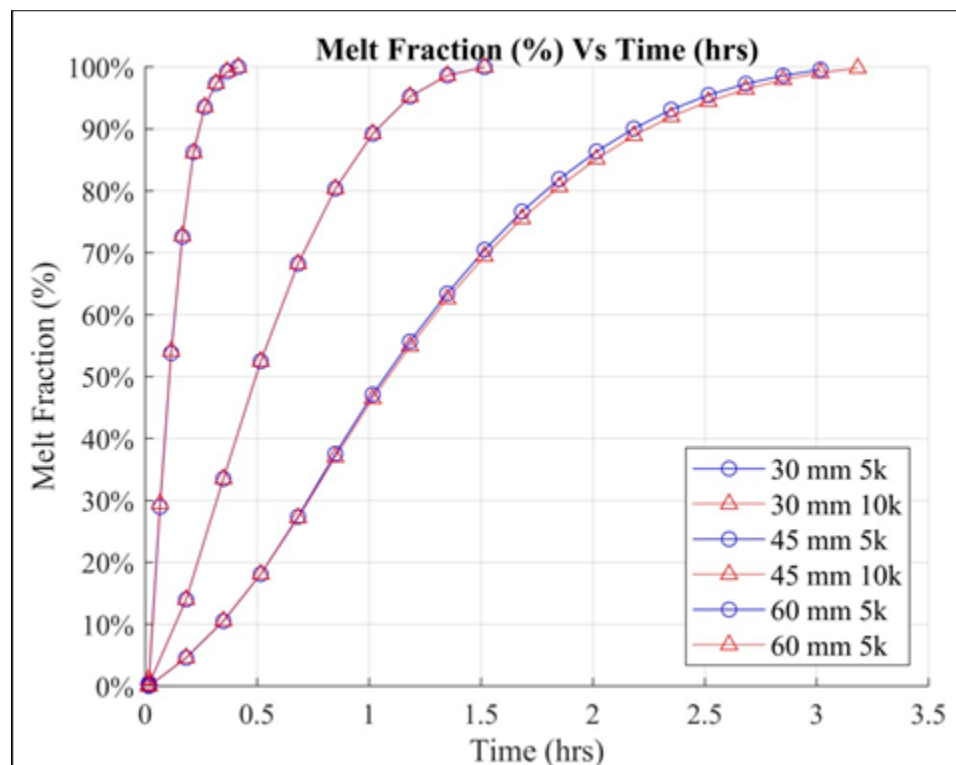


Figure 24: Mesh Sensitivity with change in PCM_D

4.4.2 Comparison with 3-D cases

The results from 2-D cases were compared with 3-D cases, which were developed with the same mesh sizing along axial and radial directions. The smaller mesh size of 5k for 2-D cases were chosen as guideline for their 3-D counterparts.

The comparisons in between the average melt fraction for each diameter case with 3-D cases can be seen in Figures [25](#), [26](#), and [27](#). The comparisons indicate no significant change in the time taken for complete melting for all diameter variations.

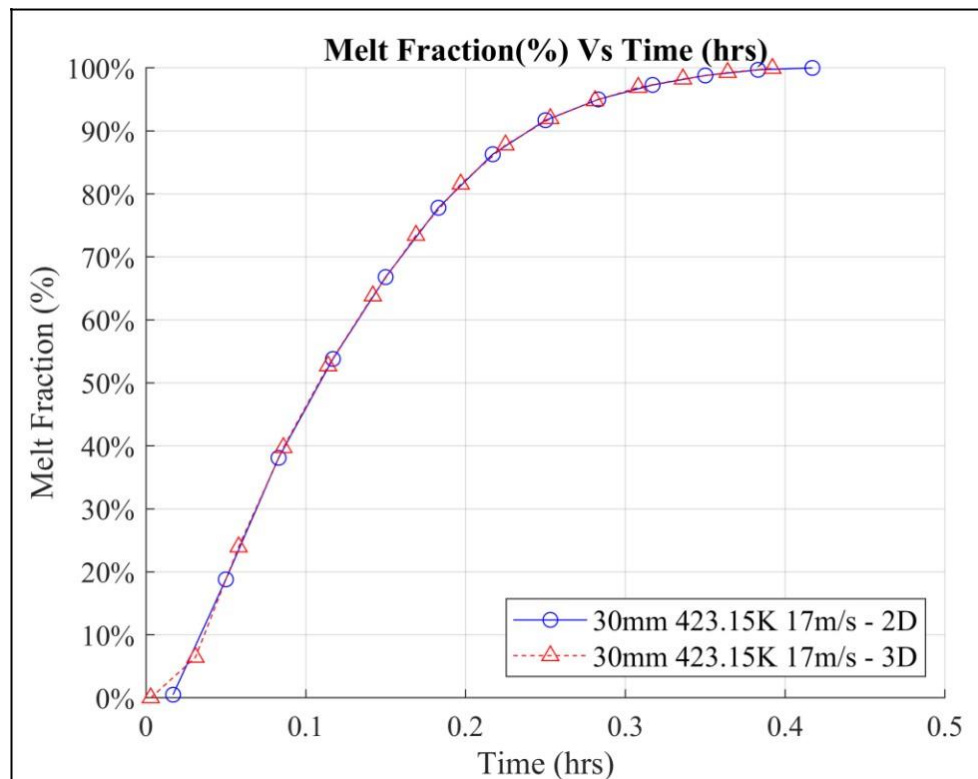


Figure 25: Comparison of 2-D and 3-D Melting for 30mm PCM_D

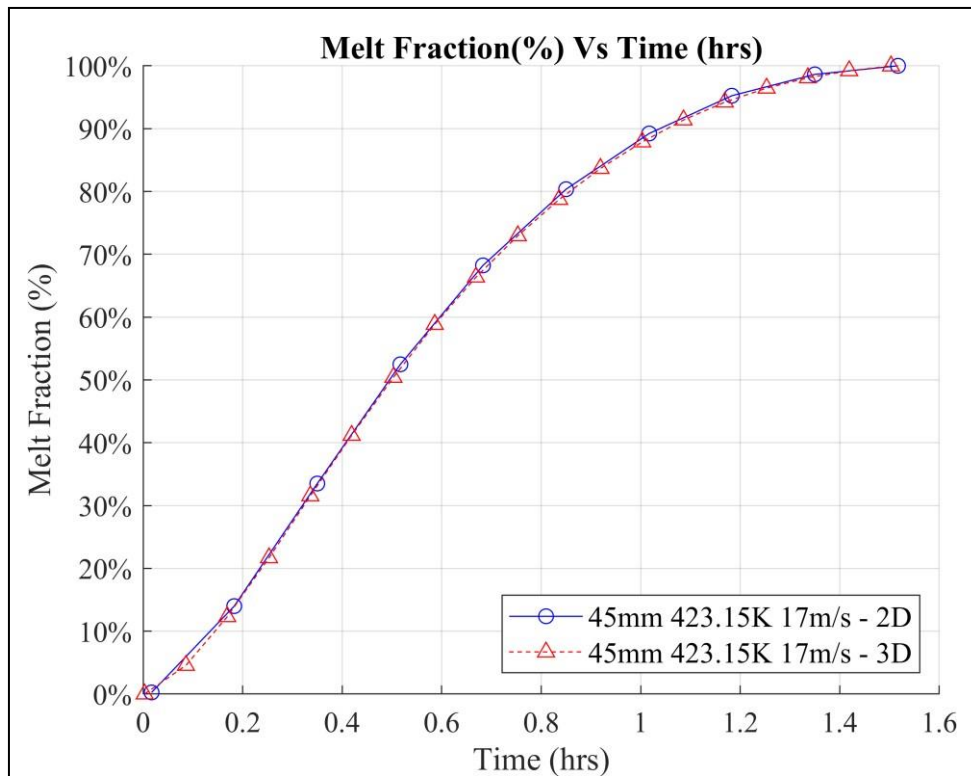


Figure 26: Comparison of 2-D and 3-D Melting for 45mm PCM_D

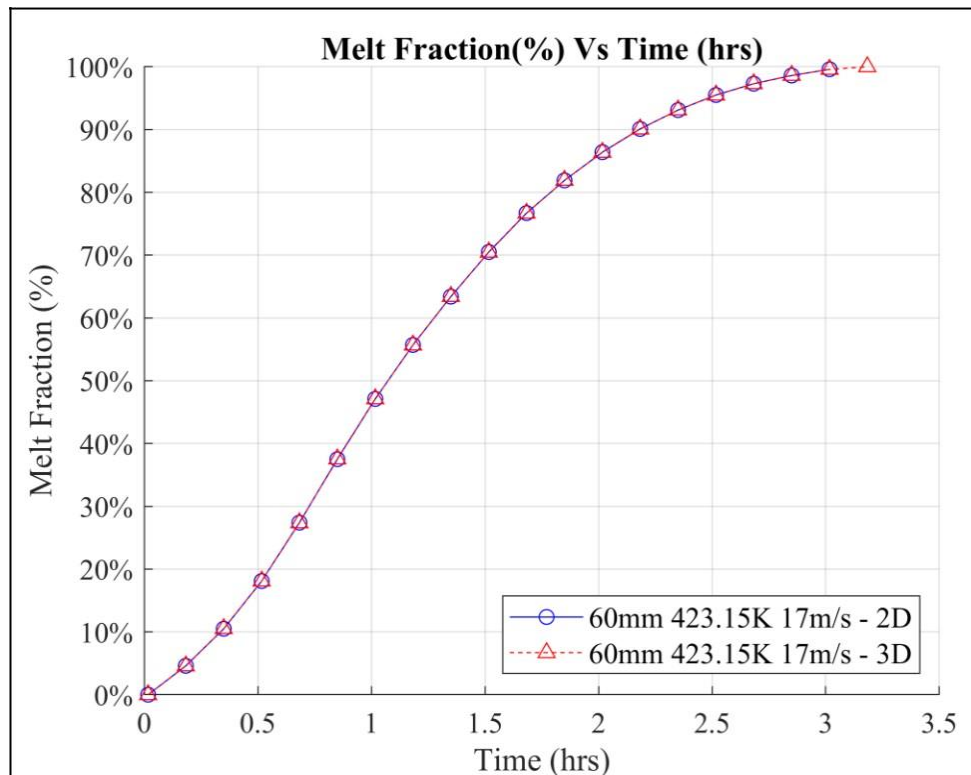


Figure 27: Comparison of 2-D and 3-D Melting for 60mm PCM_D

4.4.3 Melting and Solidification with change in Diameter

Since the comparisons with 3-D simulations revealed negligible errors, 2-D cases were chosen for further analysis. Along with changes in diameter, simulations were carried out with variations in inlet temperature and velocity considering the values as described in Sections [4.3.1](#) and [4.3.2](#). This provides a complete set of results for all 3 diameters as can be seen in Figures below.

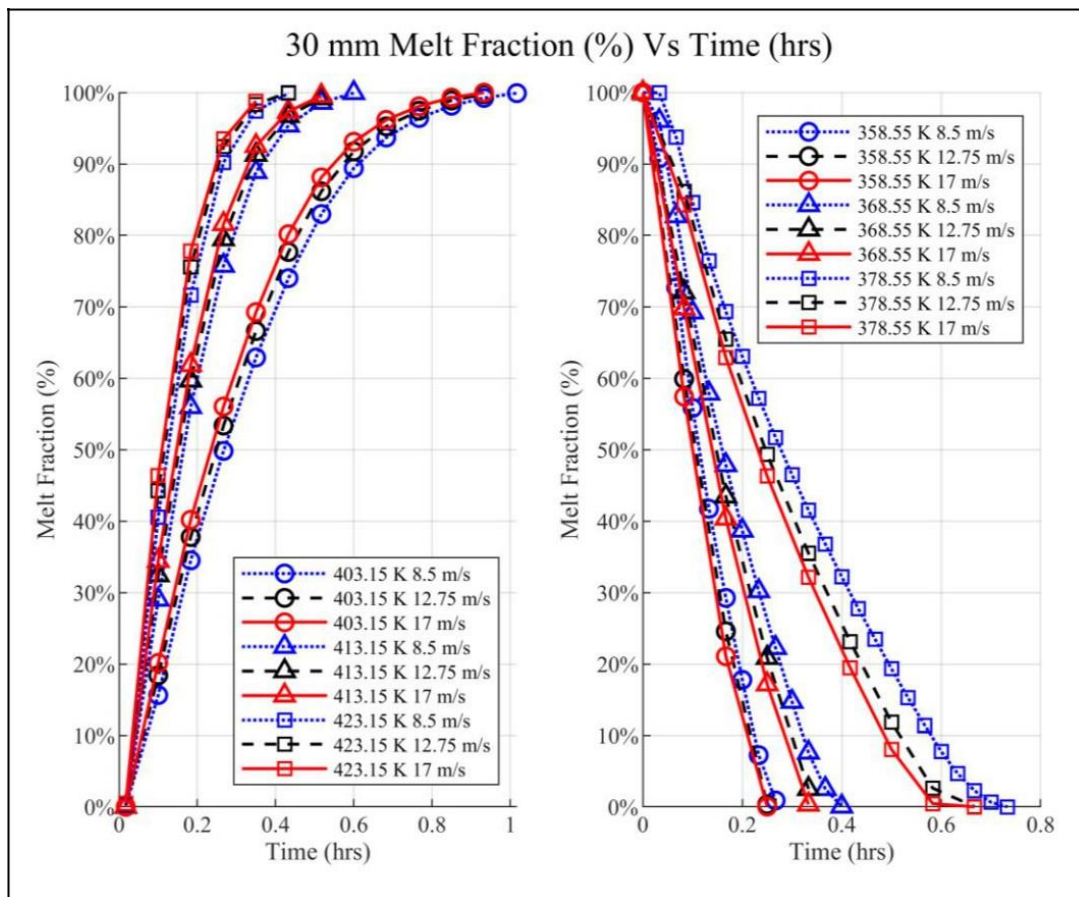


Figure 28: Variations in time taken for complete melting and solidification with varying T_i and V_i , for 30mm Diameter

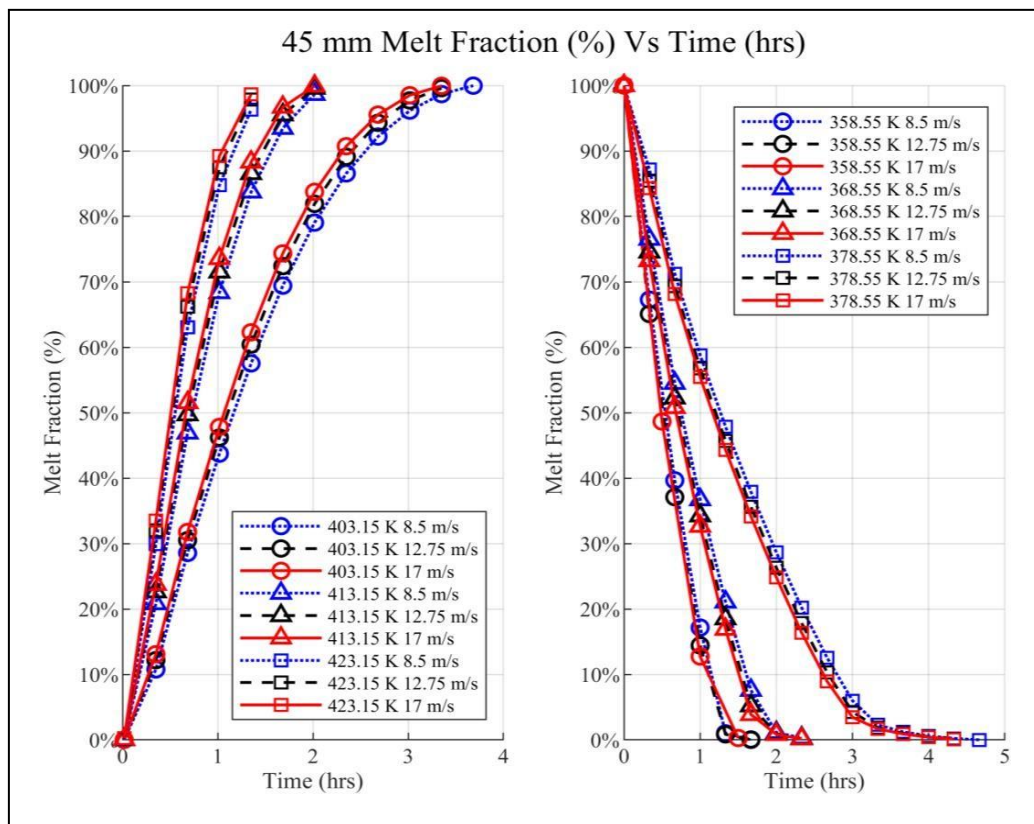


Figure 29: Variations in time taken for complete melting and solidification with varying Ti and Vi, for 45mm Diameter

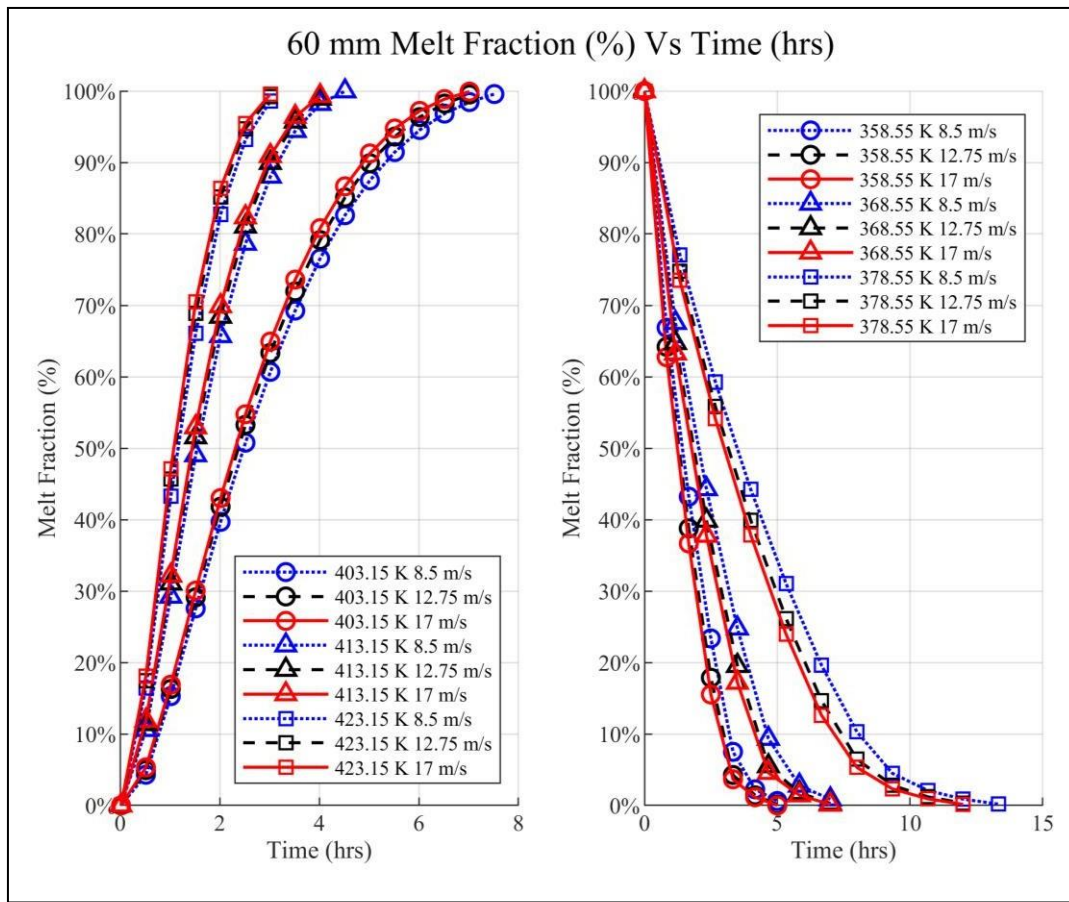


Figure 30: Variations in time taken for complete melting and solidification with varying Ti and Vi, for 60mm Diameter

CHAPTER 5

ANALYTICAL MODEL

5.1 Further Variations in ‘Ti’

Since the ‘Ti’ was varied with an increment of 10°K from 403.15°K , we obtained a total of 27 cases considering the simultaneous change in velocities and diameters. To obtain an analytical correlation the inlet temperature was varied further within this range with increments of 5°K , in order to obtain a more inclusive dataset to determine the variations in time taken for melting, as can be seen in the Figures 31, 32, and 33.

To develop an analytical correlation, the time taken for melting ‘tm’ is considered as the variable representing complete melting of the PCM in the storage device. This can also be termed as the total charging time of the device.

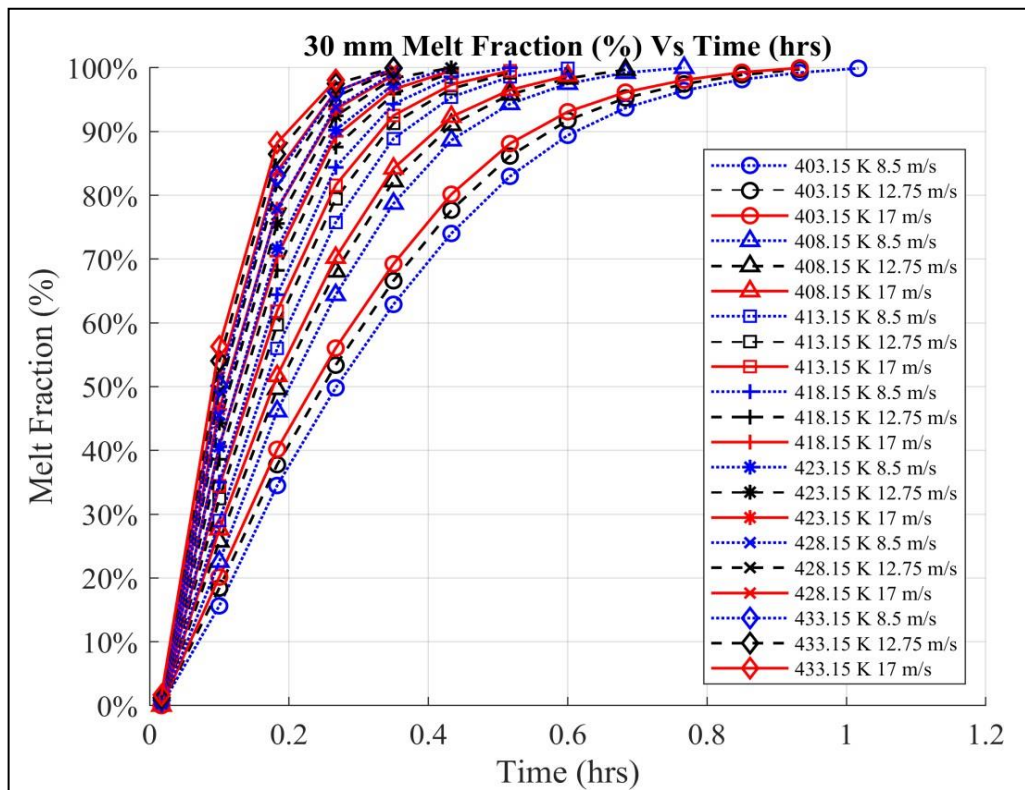


Figure 31: 30mm Diameter – Time Taken for Melting with 5°K increment in Ti

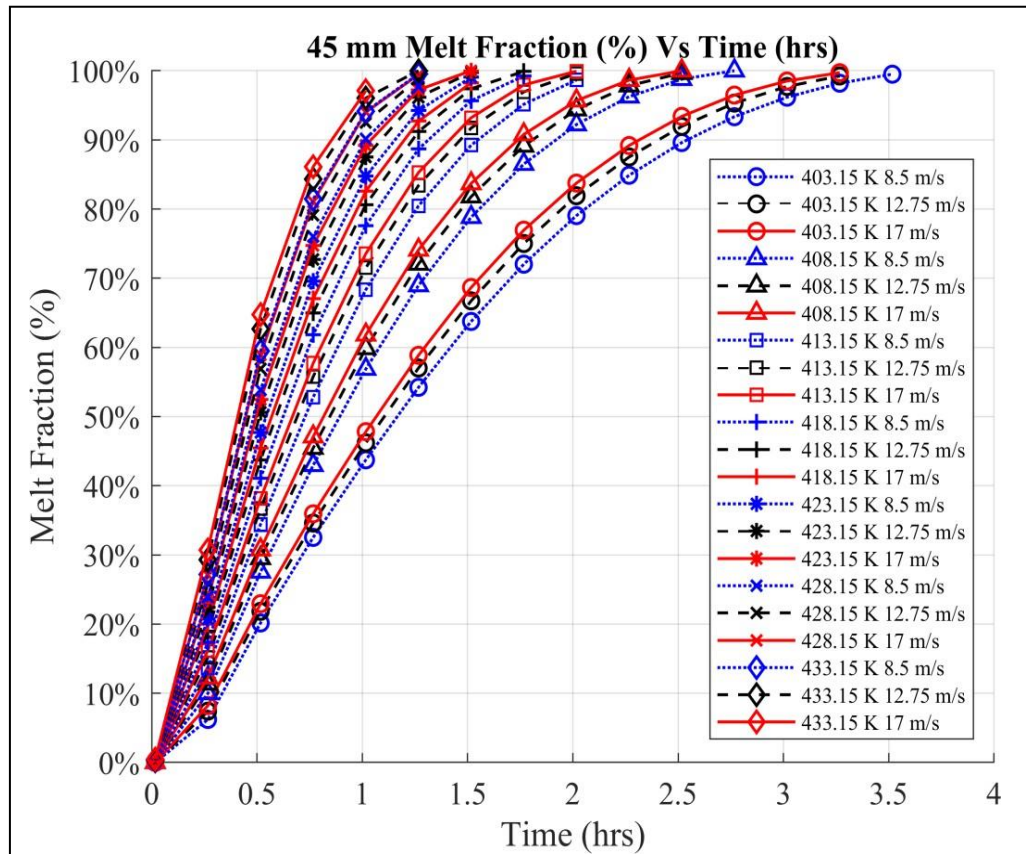


Figure 32: 45mm Diameter – Time Taken for Melting with 5°K increment in Ti

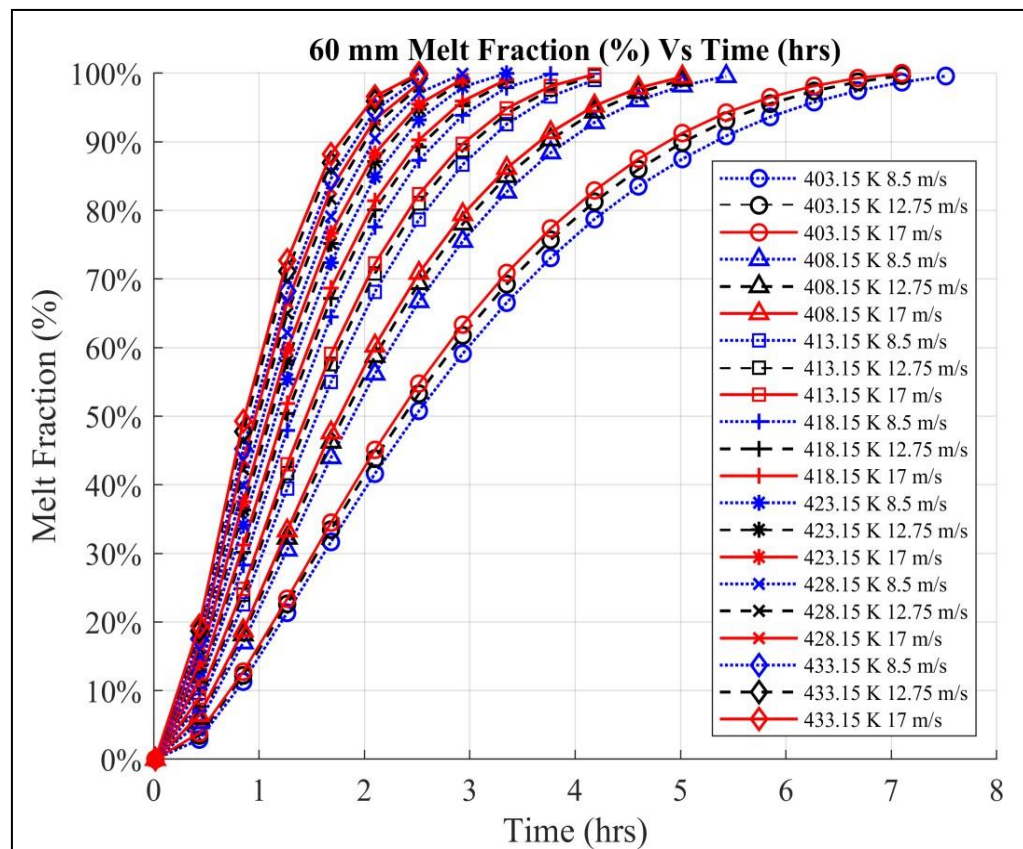


Figure 33: 60mm Diameter – Time Taken for Melting with 5°K increment in Ti

5.2 Identification of Non-Dimensional Numbers

The variations in Reynold's number (Re) were previously discussed in [Section 4.3.1](#). These were considered to check the effect of varying the inlet velocity 'Vi' on the time taken for melting, with the limiting Re considerations of (Re < 2,300), to have laminar flow in the HTF domain.

With variations in temperature, we can consider the Grashof number to approximate the ratio of buoyancy to viscous force over a length, which is analogous to the Reynold's number in natural convection heat transfer. The Grashof Number (Gr) can thus be defined as,

$$Gr = \frac{g \times \beta \times (D_o - D_i)^3_{pcm} \times (T_i - T_{melt})}{v^2} \quad (5.1)$$

where,

Gr = Grashof Number

g = Acceleration due to gravity, $9.81 \frac{\text{m}}{\text{s}^2}$

β = Thermal Expansion Coefficient, $0.001014 \frac{1}{\text{K}}$

$(D_o)_{pcm}$ = Diameter of PCM Domain, (varies from 30 mm to 60 mm)

$(D_i)_{pcm}$ = Inner Diameter of PCM Domain, 20 mm

T_i = Inlet Temperature of the HTF Fluid, (varies from 403.15°K to 433.15°K)

T_{melt} = Melting Temperature of the PCM, 391.85°K

v = Kinematic Viscosity of PCM, $4.565 \times e^{-11} \frac{\text{m}^2}{\text{s}}$

Along with this, the geometric variations can be defined by a Volumetric Ratio (V^*), as the ratio of the volumes of PCM and HTF-tube domains. This can be defined as follows,

$$V^* = \frac{(D_o^2 - D_i^2)_{PCM}}{(D_o^2 - D_i^2)_{HTF-tube}} \quad (5.2)$$

where,

V^* = Volumetric Ratio

$(D_o)_{PCM}$ = Outer Diameter of PCM Domain, (varies from 30 mm to 60 mm)

$(D_i)_{PCM}$ = Inner Diameter of PCM Domain, 20 mm

$(D_o)_{HTF-tube}$ = Outer Diameter of HTF-tube Domain, 20 mm

$(D_i)_{HTF-tube}$ = Inner Diameter of HTF-tube Domain, 15 mm

5.3 Dimensional Correlation

A dimensional correlation for the time taken for melting can be developed using the power law equation with the variations in dimensionless numbers and can be expressed as follows,

$$t_m = f(Gr, Re, V^*) \quad (5.3a)$$

$$t_m = a \times Gr^b \times Re^c \times V^{*d} \quad (5.3b)$$

Considering log on both sides of the equation,

$$\log t_m = \log a + b \log Gr + c \log Re + d \log V^* \quad (5.4)$$

The Multiple Linear Regression model is developed for the correlation using MATLAB 2019a. The independent variable is termed ‘Y’, which is a matrix of log values of the time taken for melting in hours for each of the cases considered as shown in Figures [31](#), [32](#), and [33](#). The model incorporates multiple independent variables and solves them in matrix form to determine the individual coefficients or exponents for the best fit. The model has been described below,

$$\begin{aligned} [Y] &= [\phi][X] \\ [\phi] &= [X' \times X]^{-1} \times [X'] \times [Y] \\ Y &= \phi_1 + \phi_2 X_2 + \phi_3 X_3 + \phi_4 X_4 \end{aligned} \quad (5.5)$$

From the model we obtain a correlation for the time taken for melting represented here as ‘ t_{m-pred} ’ (predicted time taken for melting), and is given as follows,

$$t_{m-pred} = 55.59 \times Gr^{-0.79} \times Re^{-0.12} \times V^{*2.8} \quad (5.6)$$

The script file with linear regression code is included in [Appendix A](#).

5.4 Interpolation Model

An interpolation model is developed to determine the charging and discharging time required for the LTES devices based on variations in ‘Ti’, ‘Vi’, and ‘(Do)pcm’. For this MATLAB 2019a, specifies various interpolation methods which can be utilized based on the availability of data. For the ‘interp1’ function in MATLAB 2019a, there are multiple interpolation methods available as can be seen in Figure 34 below.

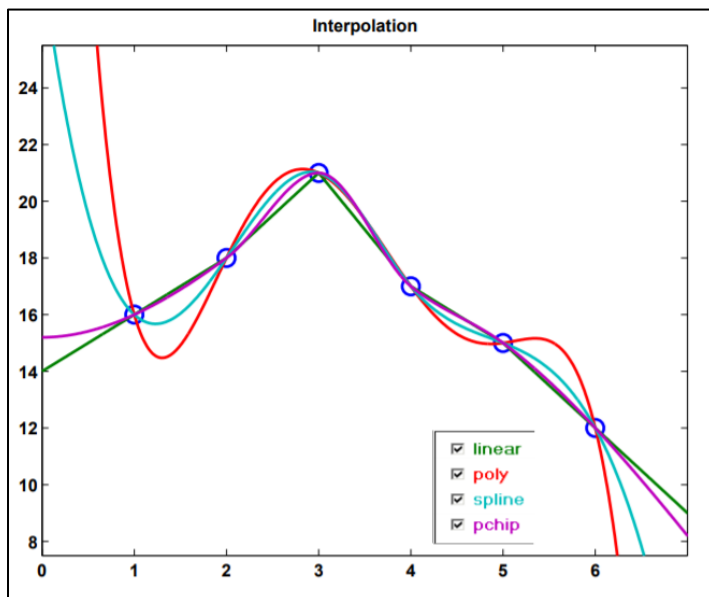


Figure 34: Interpolation Methods available in MATLAB [21]

The linear interpolation method is utilized for the model to predict the performance of LTES Device. The individual parameters with melt fraction values are utilized as the existing dataset. This is done to have multiple parameters as inputs to the model for which the melting or solidification can be predicted using the interpolation method. The equation described for the model is given below,

$$v = v_1 + \left(\frac{(v_2 - v_1)(x - v)}{x_2 - x_1} \right) \quad (5.7)$$

The syntax for the ‘interp1’ function is described as,

vq = interp1(x, v, xq)

Where,

x = Array of sample points in the dataset

v = Array of values corresponding to the sample points in the dataset

xq = Query points

vq = Corresponding interpolated values to the query points.

Various values in between the dataset for the three variables were considered to obtain the solidification and melting values with interpolation. The results for sample cases have been shown in [section 6.3](#). The script file with interpolation model is included in [Appendix B](#).

5.5 Daily charging and discharging TRNSYS Model

Metrics for daily charging and discharging of LTES devices can be obtained with the commercial transient analysis software TRNSYS 17. A model was developed utilizing the existing interpolation model, to analyze daily charging and discharging based on existing dataset and variations in parameters. The Matlab Type 155 in TRNSYS 17 is utilized to read the script file with interpolation model. Along with this, TRNSYS includes several components which have been utilized to specify the inputs and parameters varying over time, to simulate and analyze daily charging and discharging. The Forcing Function (Type 14h) is used to specify various ‘Ti’ values at different timesteps to vary the melting and solidification. Other inputs are ‘Vi’, and ‘ $(D_o)_{pcm}$ ’, which can interact with the Matlab Type 155, and compute amount of PCM melted/solidified (Melt Fraction in % of volume melted), based on existing data. The results are plotted with the Type 65c ‘Plotter’ component. The outline of the model can be seen in the Figure 35 below.

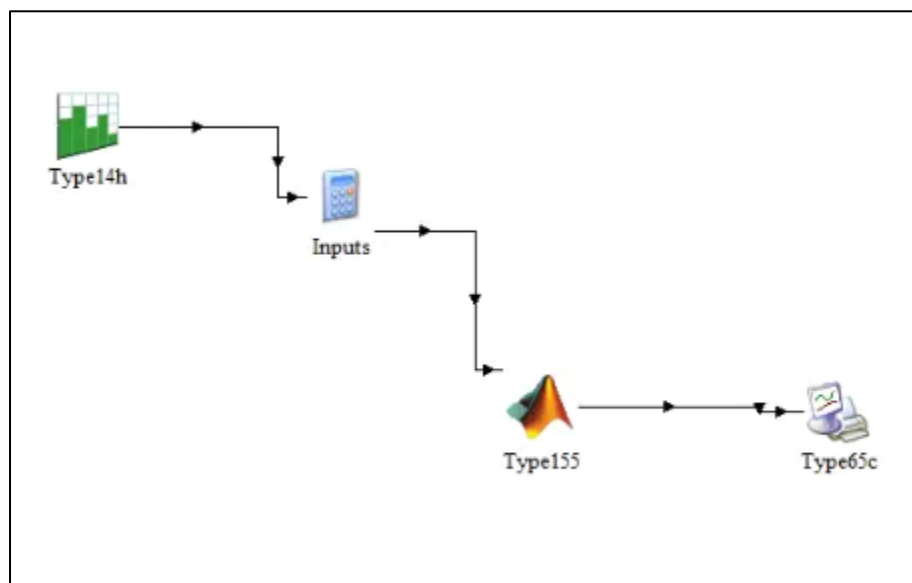


Figure 35: Outline of TRNSYS Model

Along with the melt fraction, the latent energy storage rate ‘ q_L ’ is also computed by the model, the expression for which is given below.

$$q_L = M \times \left(\frac{\delta\gamma}{\delta t} \right) \times L = \rho_{pcm} \times V_{pcm} \times \left(\frac{\delta\gamma}{\delta t} \right) \times L \quad (5.8)$$

Where,

q_L = Latent Energy Storage Rate, W

M_{pcm} = Mass of PCM in the container, kg

γ = Melt Fraction, (%)

L = Latent heat capacity of the PCM, $339,800 \frac{J}{kg}$

ρ_{pcm} = Density of PCM, $1,480 \frac{kg}{m^3}$

V_{pcm} = Volume of PCM Container, m³

A sample case was analyzed to determine ‘ γ ’ and ‘ q_L ’. The case inputs are specified as given in Table 11 below.

Table 11: Inputs for TRNSYS model sample case

Case Input	Time (hr)	Value	Unit
$(D_o)_{pcm}$	-	60	mm
T_i	0.017	403.15	K
	8.017	378.55	K
	22.017	403.15	K
V_i	-	8.5	m/s

The results from the model with given inputs can be seen in the Figure 36 below,

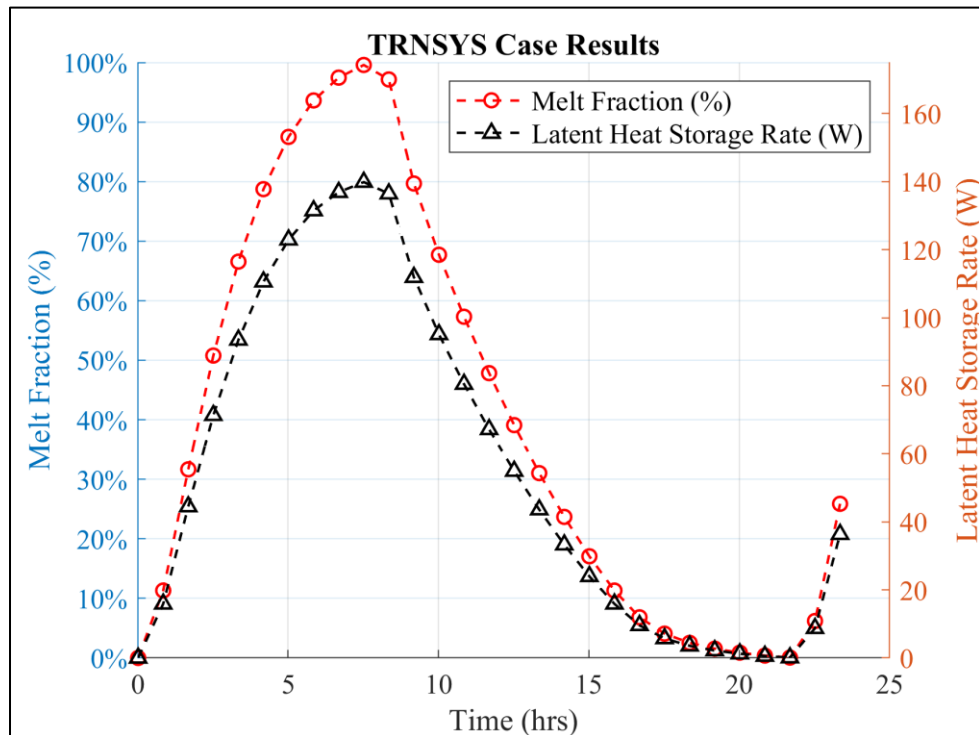


Figure 36: TRNSYS model case results – 24 hr charging and discharging

CHAPTER 6

RESULTS AND DISCUSSION

6.1 Variation in Time taken for Melting and Solidification

1. The time taken for melting decreases with increase in ‘Ti’, since more heat is available for storage due to higher temperature difference in the initial temperature of HTF and the initial temperature of PCM. This holds true for time taken for solidification as well, i.e. the time taken for solidification decreases for lower ‘Ti’ values.
2. The time taken for melting or solidification decreases with increase in ‘Vi’, since the heat transfer is accelerated with increase in inlet velocity. During solidification, heat rejected by the PCM is accelerated with increase in inlet velocity.
3. The time take for melting and solidification increases significantly with increase in diameter for the same set of inlet conditions. The volume of PCM stored increases proportionally to the square of the diameter which requires more time for melting or solidification.
4. The difference in 3-D and 2-D simulations was observed to be negligible, for the axisymmetric model considerations, which effectively indicates that 2-D cases are adequate to model the melting and solidification processes for vertical annular cylinders.

6.2 Correlation Results

1. The correlation holds valid for the laminar natural convection, defined over the range of ($10^5 < \text{Gr} < 10^8$). For our case, the Grashof number varies from (2,462 to 575,918) with variation in ‘ T_i ’ from (403.15°K to 433.15°K), and variation in ‘ $D_{o\text{-PCM}}$ ’ from (30 mm to 60 mm). The comparisons for ‘ tm ’ and ‘ $tm\text{-pred}$ ’ are shown below as they vary over the range of ‘ Gr ’.

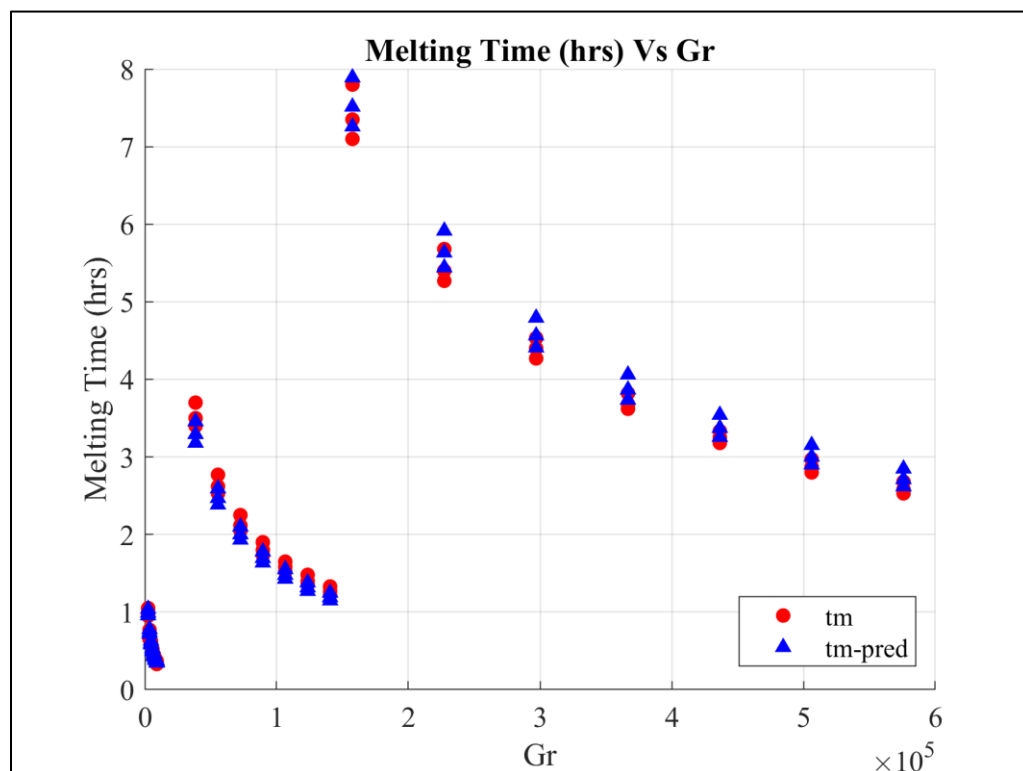


Figure 37: Comparison of tm and $tm\text{-pred}$ Vs Gr

2. For the Reynold's number variation in laminar flow regime, the correlation is valid, as considered over the range from 1,020 to 2,040. This ensures laminar flow in the HTF domain. The comparison can be seen below.

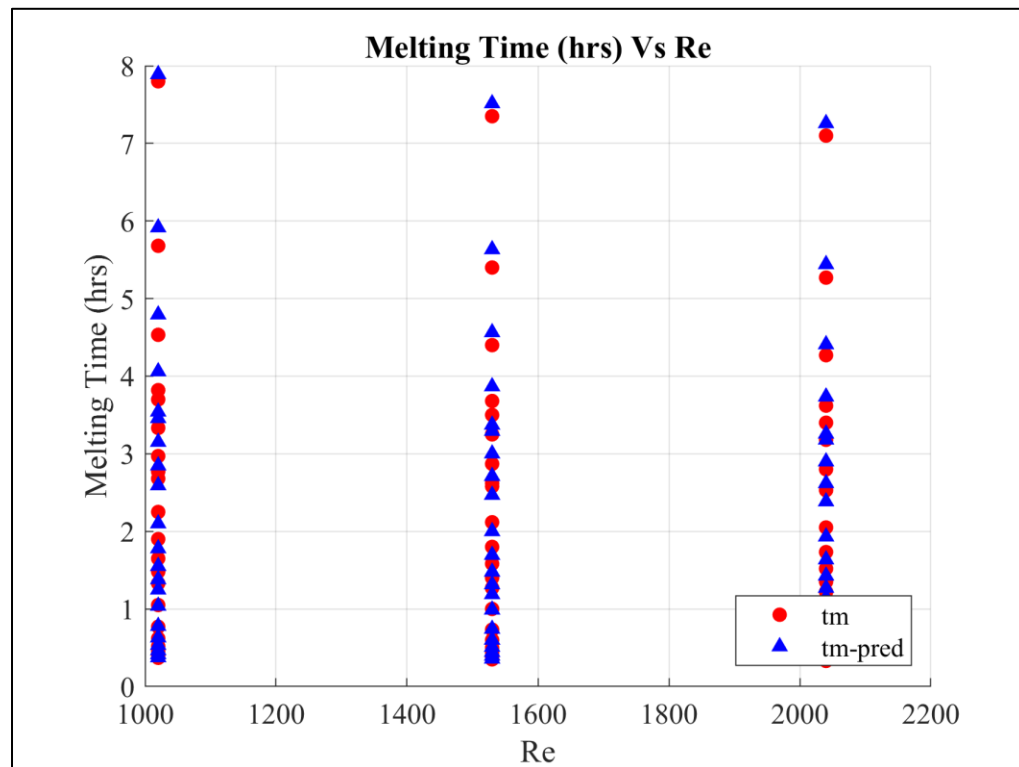


Figure 38: Comparison of tm and tm-pred Vs Re

3. The comparisons for the results over the change in diameter, considered with a proposed Volumetric ratio ‘ V^* ’, prove that the correlation holds valid for this range as can be seen below,

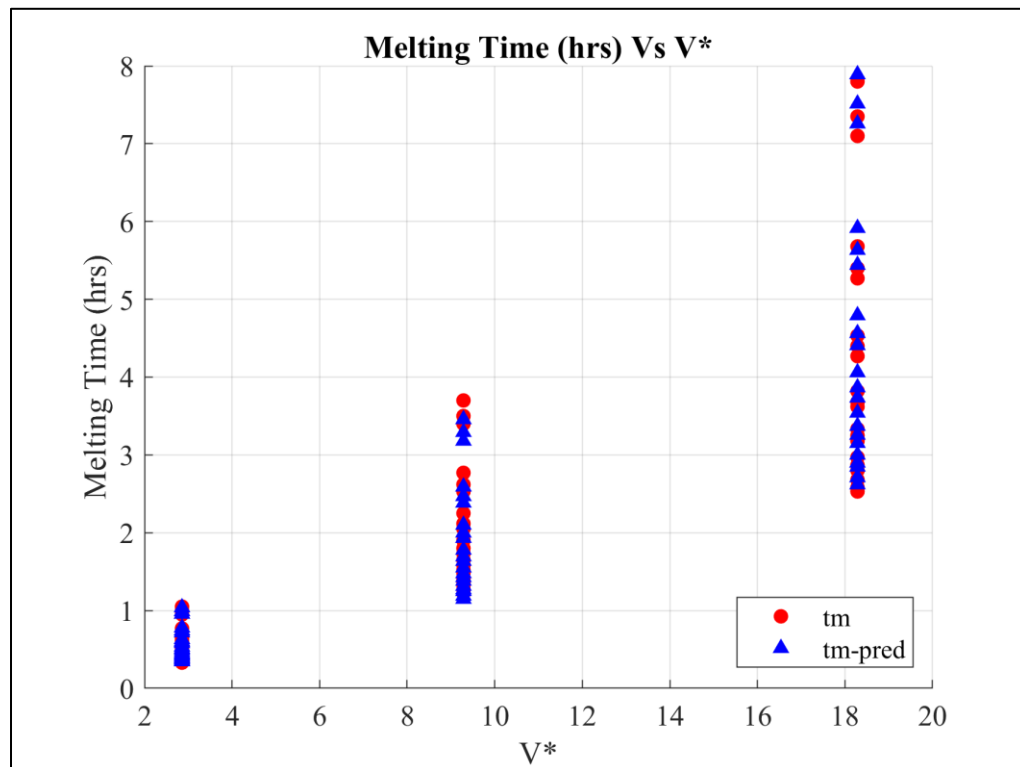


Figure 39: Comparison of tm and tm-pred Vs V^*

4. The error in correlation can be considered with the mean R-squared value, which for the entire dataset is 0.997. The correlation results can be seen below as plotted in 5% prediction bounds. As evident from the plot, the power law correlation provides an effective way of determining the time taken for melting.

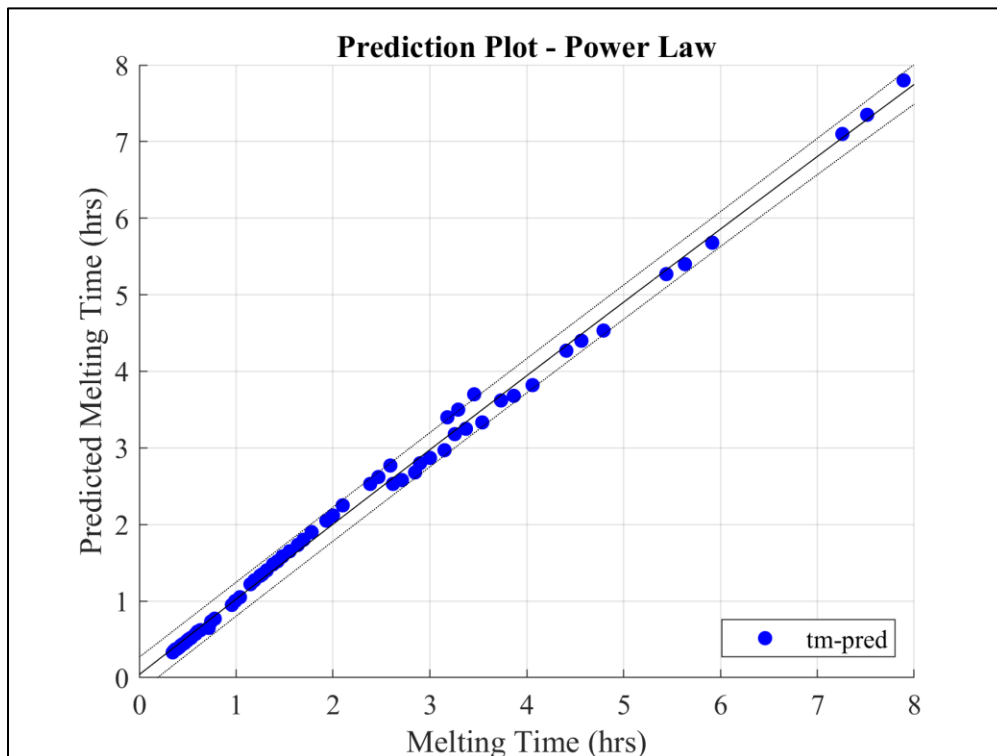


Figure 40: Predicted Melting Time with Power Law

6.3 Interpolation Model Results

Different cases were considered to determine values of melt fraction, or the amount of PCM melted, with variations in ' $(D_o)_{pcm}$ ', 'Ti', and 'Vi'. The model can predict amount of time required for charging or discharging, with variations in any of the parameters. Some of the cases tested have been shown in the figures below.

1. Case A: ($(D_o)_{pcm} = 30$ mm), ($T_i = 360.55^{\circ}\text{K}$), and ($V_i = 17$ m/s)

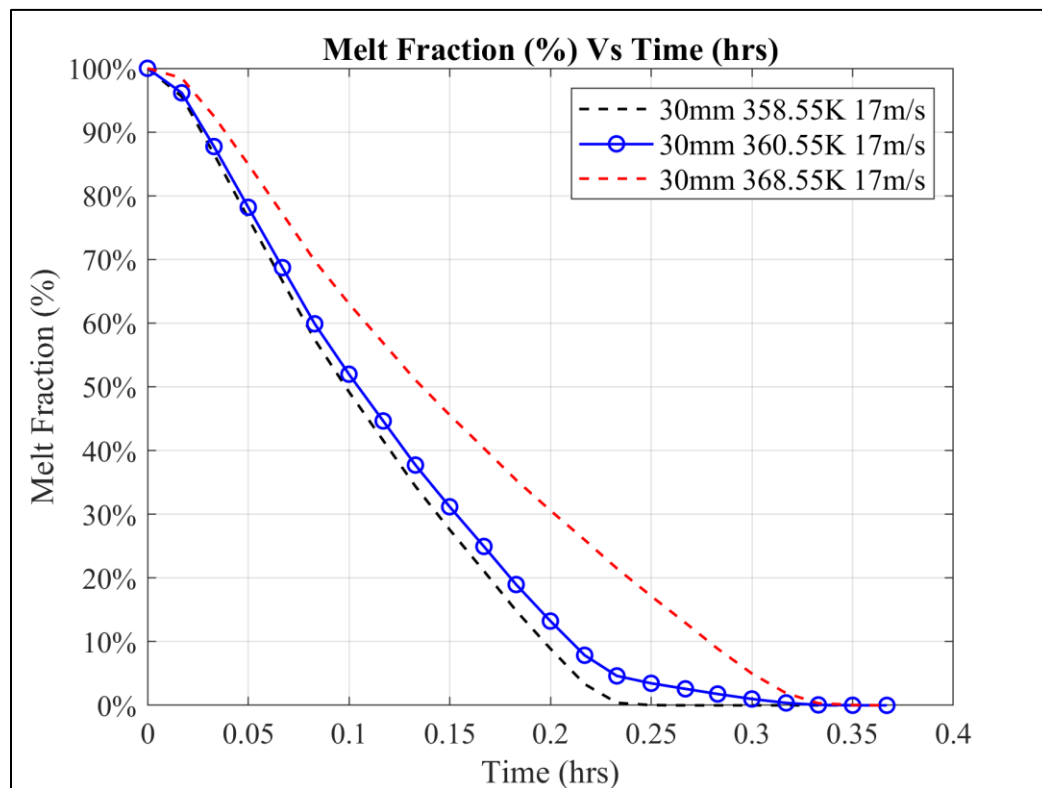


Figure 41: Case A results for solidification or discharging

2. Case B: $((D_o)_{pcm} = 55 \text{ mm})$, $(T_i = 425.15^\circ\text{K})$, and $(V_i = 15 \text{ m/s})$

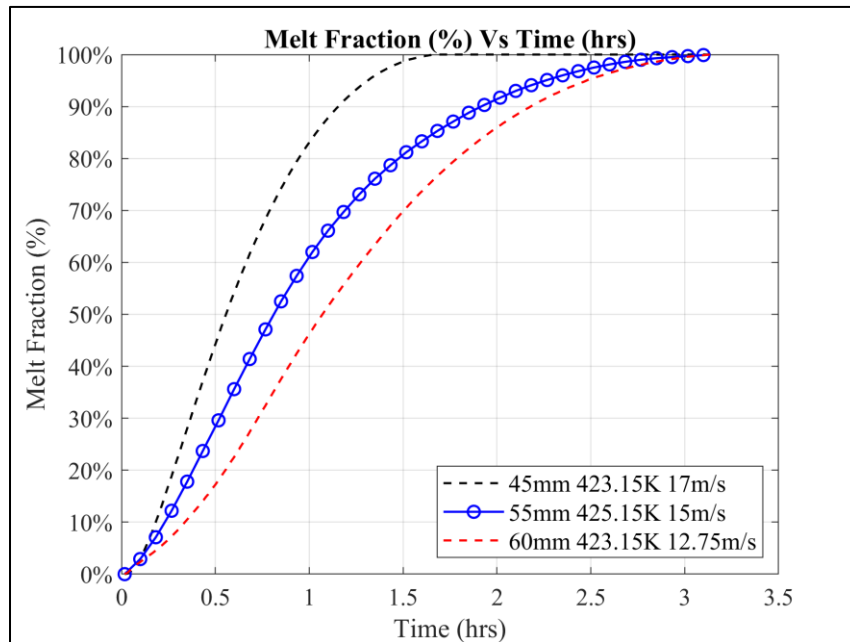


Figure 42: Case B results for melting or charging

3. Case C: $((D_o)_{pcm} = 60 \text{ mm})$, $(T_i = 375.55^\circ\text{K})$, and $(V_i = 10 \text{ m/s})$

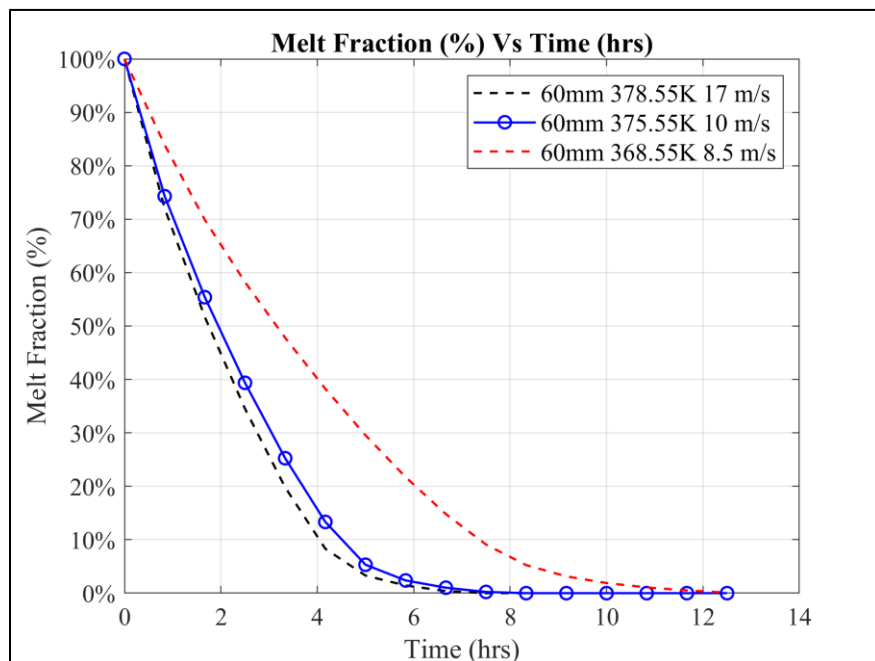


Figure 43: Case C results for solidification or discharging

6.4.1 TRNSYS Model Results

The TRNSYS Model developed, as described in Section 5.5, is utilized for obtaining metrics for amount of PCM melted/solidified, and the rate of latent energy storage, in daily cycles. For this ‘ T_i ’ is the key variable, since ‘ $T_i > T_{melt}$ ’ (T_{melt} is the mean melting temperature of the PCM 390.85°K) indicates charging of the LTES device whereas, ‘ $T_i < T_{melt}$ ’ indicates discharging. The Latent Energy Storage Rate ‘ q_L ’ is determined based on equation 5.8. For switching between charging and discharging, T_i is varied across 24 hours to determine the two variables, i.e. Melt Fraction, ‘ γ (%)’ and Latent Energy Storage Rate ‘ q_L (W)’. A case was built with these considerations, inputs for which can be seen in the table below.

Table 12: Inputs for TRNSYS model case

Case Input	Time (hr)	Value	Unit
$(D_o)_{pcm}$	-	60	mm
T_i	0.017	403.15	K
	5.017	378.55	K
	15.017	403.15	K
	19.017	378.55	
V_i	-	8.5	m/s

The results for this case can be seen in Figures 44 and 45, as seen below. Figure 44 displays the variables ‘ γ (%)’ and ‘ q_L (W)’. Figure 45 displays the change in these variables, termed as ‘ $d\gamma$ ’ and ‘ dq_L ’ respectively. The solidification and melting cycles after the initial melting cycle, continue from the respective values from the previous timesteps, i.e. at 5.00 hrs ($\gamma = 87.36\%$) and is taken as the first value when ‘ T_i ’ changes at 5.017 hrs, marking the start of solidification/discharging cycle.

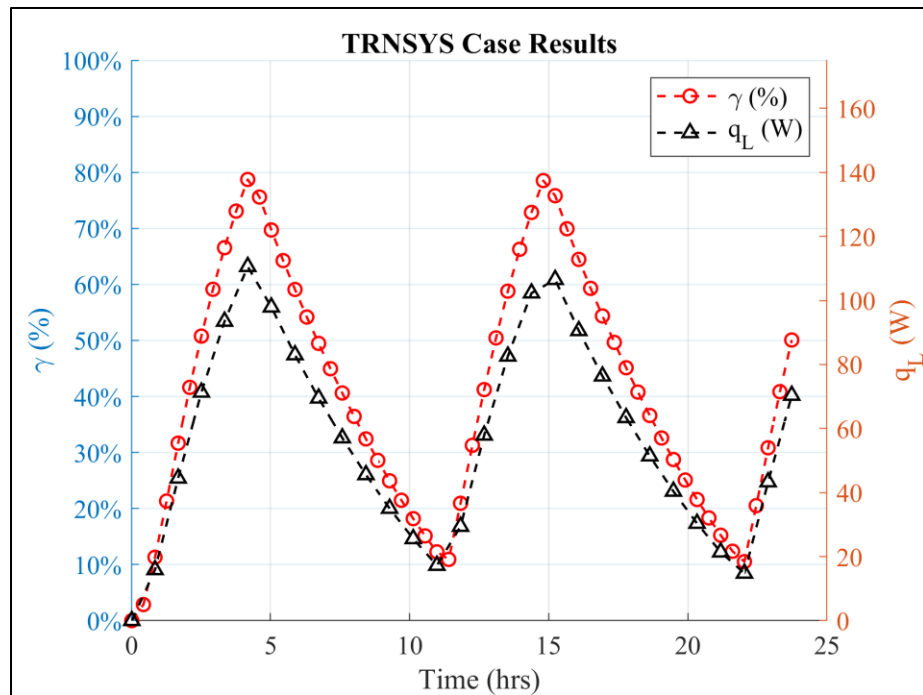


Figure 44: Melt Fraction ‘ γ (%)’ and Latent Energy Storage Rate ‘ q_L (W)’

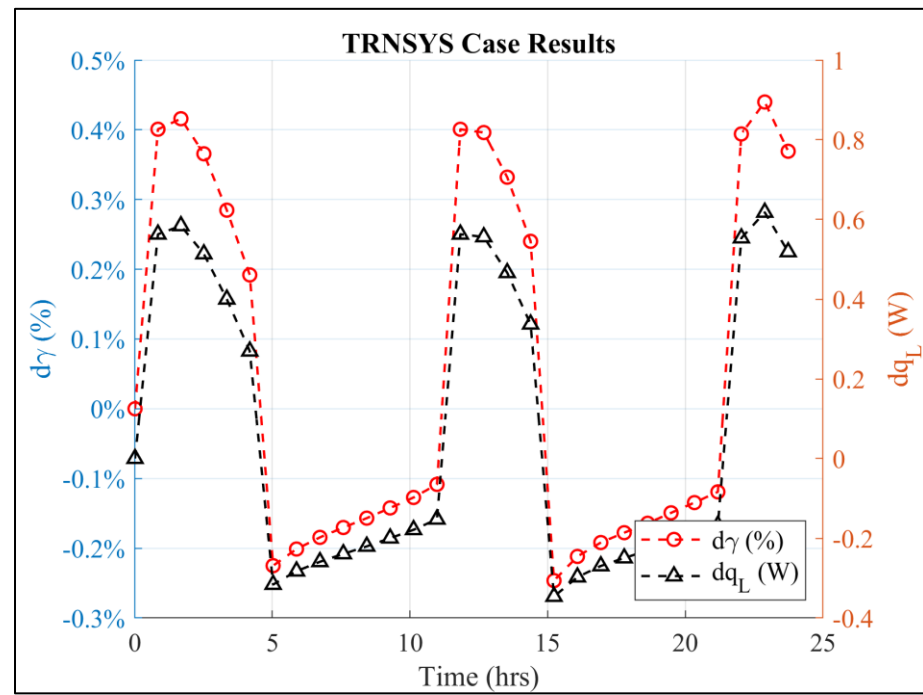


Figure 45: Change in Melt Fraction ‘ $d\gamma$ (%)’ and Change in Latent Energy Storage Rate ‘ dq_L (W)’

Thus, the parameters for estimating the performance of this storage device are the total energy stored ‘Q (Wh or BTU)’ and the Energy Storage Density ‘ Q_p ($\frac{\text{kWh}}{\text{m}^3}$ or $\frac{\text{BTU}}{\text{ft}^3}$)’, as given in Table 13 below.

Table 13: Results for estimating performance of LTES Device

Parameter	Value	Unit
Q	246	Wh
	839	BTU
Q_p	245.08	$\frac{\text{kWh}}{\text{m}^3}$
	23,672	$\frac{\text{BTU}}{\text{ft}^3}$

6.4.2 Results with real-time data

The UMass Power Plant produces low pressure steam from which heat can be extracted. This thermal energy can be stored using multiple LTES devices with performance as given in [section 6.4.1](#). Real time data for heat released during steam production for a day was utilized to estimate the total amount (volume) of storage required to store and release the thermal energy available. The thermal energy available for a period of 24 hours can be seen in [Figure 46](#) below.

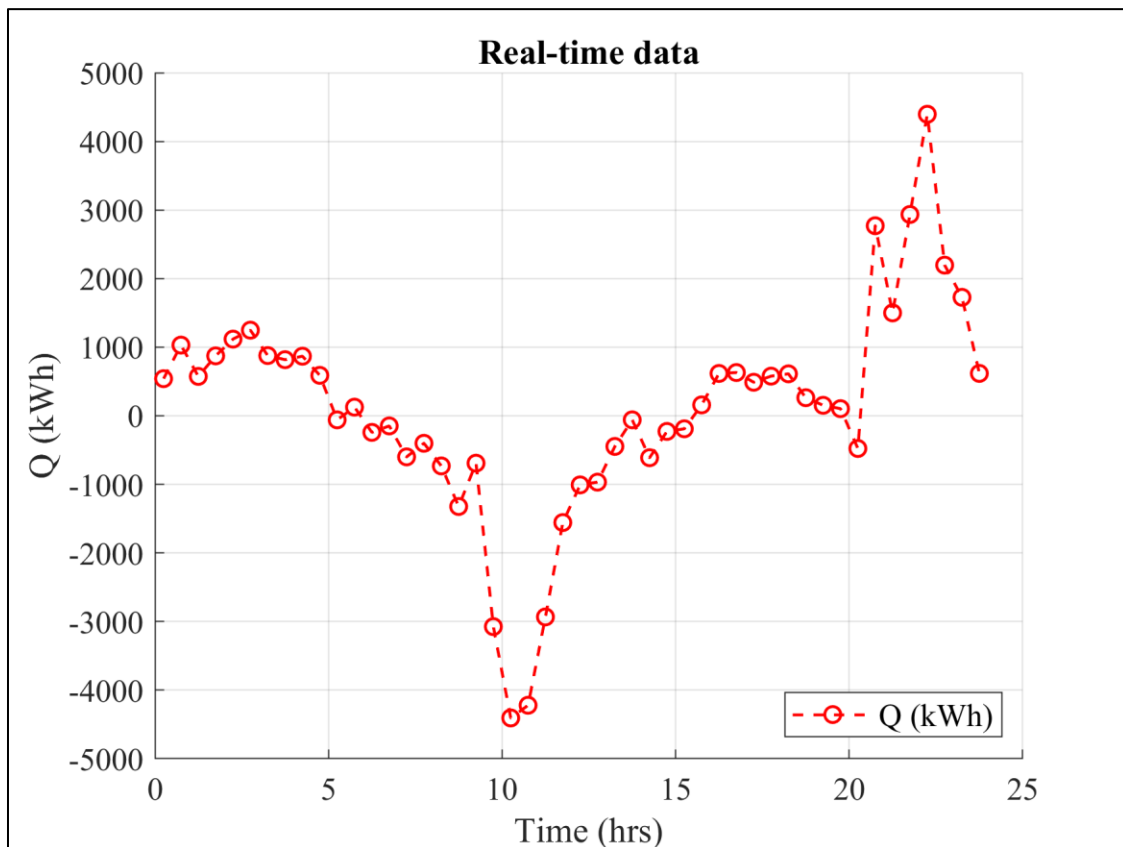


Figure 46: Real-time data for 24 hrs

For storing the thermal energy available as shown in Figure 46, LTES devices with performance as described in [section 6.4.1](#) can be utilized. Initially the thermal energy is stored for a period of approximately 6 hours, after which the discharging or

solidification cycle progresses for approximately 10 hours. Subsequent charging and discharging cycles are also considered after considering the data as shown in [Figure 46](#). To optimize the volume of storage required for the system, increments of 5 m^3 were considered from (125 to 165 m^3). The comparison for the Melt Fraction with different volume sizes can be seen below in Figure 47.

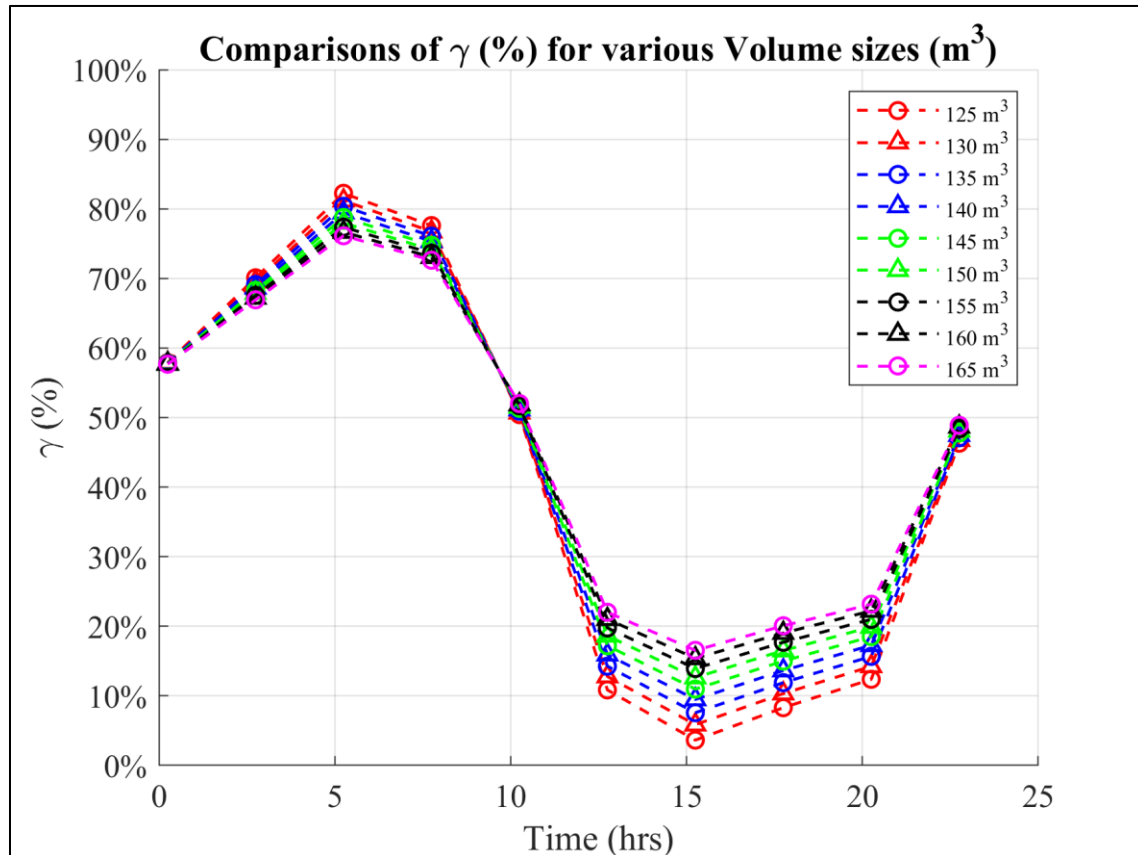


Figure 47: Comparisons of Melt Fraction ‘ γ (%)’ for various Volume Sizes (m^3)

An optimized total volume of storage is determined to be 145 m^3 or $5,120.63\text{ ft}^3$ for the LTES system. The results for performance of LTES devices have been displayed below in Figures 48 and 49.

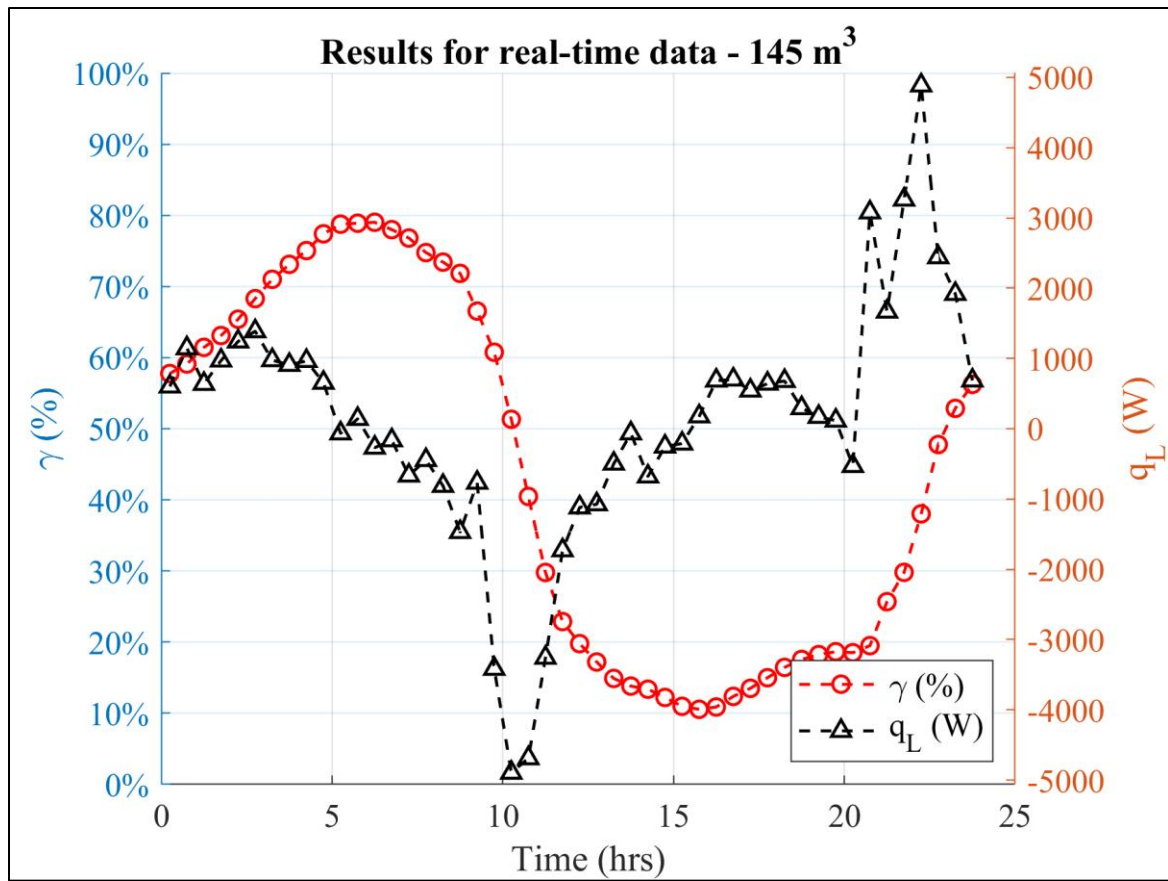


Figure 48: Performance of LTES devices with real time data – 145 m³

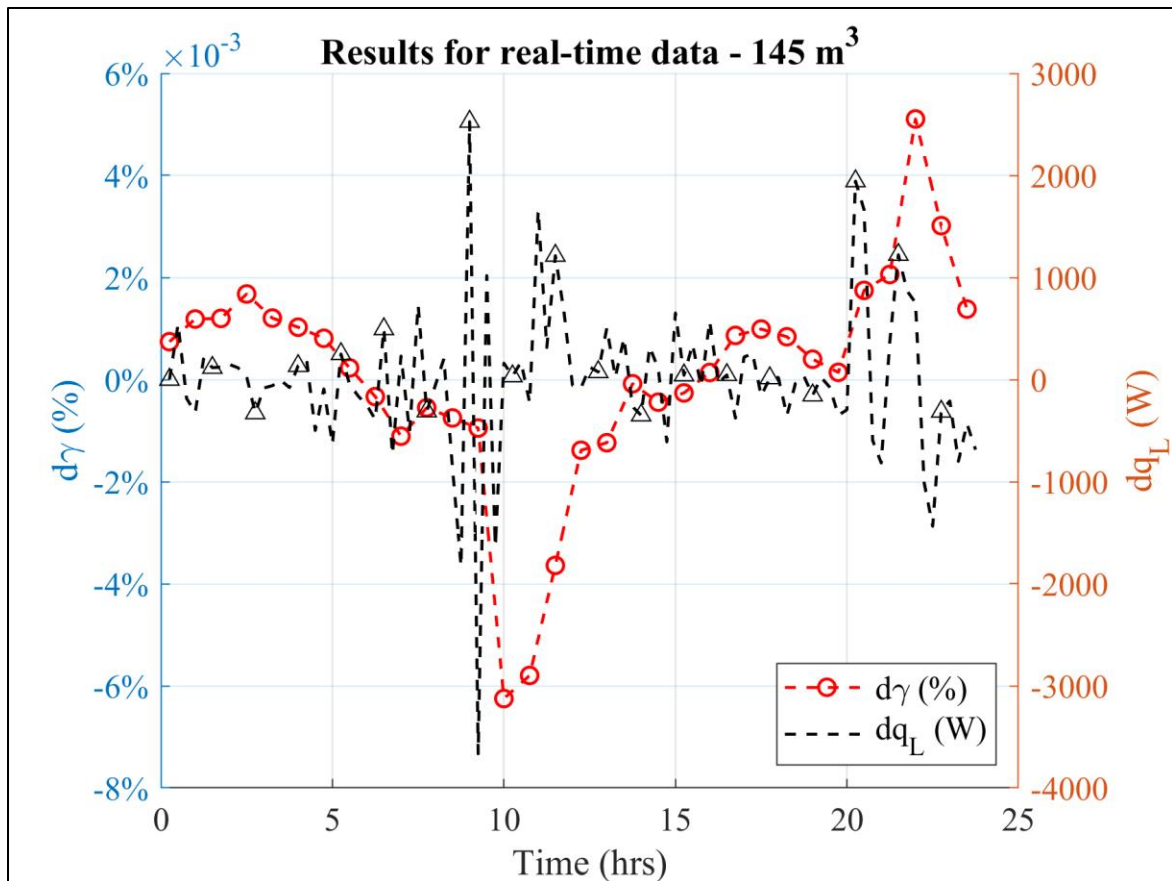


Figure 49: Change in Melt Fraction ‘ $d\gamma$ (%)’ and Change in Latent Energy Storage Rate ‘ dq_L (W)’ for real time data – 145 m^3

The storage system size required can be summarized with parameters like Number of storage devices required, denoted as ‘ N_{LTES} ’, and total Volume of storage required, denoted as ‘ V_{LTES} (in m^3 or ft^3)’, as can be seen in Table 14 below for our analysis.

Table 14: Size of LTES system

Parameter	Value	Unit
N_{LTES}	160	-
V_{LTES}	145	m^3
	5,120.63	ft^3

Note: It is assumed that the heat available from steam production is consistent, which ensures adequate availability of thermal energy during discharging cycle as can be seen in Figure 47, for a duration of approximately 10 hours (6 to 16 hrs).

CHAPTER 7

FUTURE WORK

7.1 Parameters for correlation analysis

The parameters for which simulations are carried out over the defined range of laminar natural convection and laminar heat transfer fluid flow, are restricted to '(D_o)_{pcm}', ' T_i ', and ' V_i '. The other properties of the material were kept constant to have a conclusive analysis of melting/solidification with regards to current parameters. These properties like the thermal conductivity and latent heat capacity, along with the inner tube diameter, length of device, injection of the HTF, and others, can be considered to further analyze their respective effects on the Latent energy storage.

Along with this, a correlation can also be developed considering multiple PCMs to further understand the phenomena involved in melting/solidification.

7.2 Comparison with real time data/cases

The cases considered in the TRNSYS model, are for existing dataset. These can be further compared with real experiments, considering the specific parameters, by modifications to the model to determine the accuracy of prediction. This analysis proves effective to schedule usage of the LTES devices.

With real time data from the in house power plant at UMass, the usage of such devices can be modeled much more effectively, for which the following details should be considered,

- Data available from the plant should be analyzed, to determine schedule for charging/discharging, keeping in mind the campus heating requirements.

- Along with this, more components would be required to setup the storage system like pumps, intermediate heat exchangers, piping and valves which can be added to the existing TRNSYS model to have an in-depth analysis of the system.
- Heat losses are a major factor in determining the efficiency of the storage system which will also need to be evaluated further with a complete model.
- TRNSYS provides a transient simulation environment which has components to evaluate these factors, and thus can be utilized to further improve the existing model.
- For determining the potential savings and implementation costs, tariffs and rates should be analyzed carefully, along with standard estimates for the cost of LTES device systems.

APPENDIX A

LINEAR REGRESSION SCRIPT FILE WITH NON-DIMENSIONAL NUMBERS

```
% % --- Linear Regression with Non-Dimensional Numbers-----%%%%%
% % -----%%%%%
clc
clear all
close all

%Read the data with non-dimensional numbers
%Grashof Number
Gr = xlsread('LinReg.xlsx','gr','R73:R135'); %Gr = C1*D^3*dT

%Reynold's Number
Re = [1020; 1530; 2040]; %Inlet Re

%Volumetric Ratio
Vr = [2.857143, 9.285714, 18.28571]; %V*

%Reshape matrices
Re1 = repmat(Re,21,1);

Vr0 = reshape(repmat(Vr,3,1),9,1);

Vr1 = repmat(Vr0,7,1);

LGr = log10(Gr);

LRe = log10(Re1);

LVr = log10(Vr1);

%Regression
X = [ones(63,1), LGr, LRe, LVr];

tm = xlsread('LinReg.xlsx','Sheet2','G2:G64');

Y = log10(tm);

%Regression Matrix Formation - Y = [phi]*[X]
phi = inv(X'*X)*X'*Y

ltm = X*phi;

tmp = 10.^ (ltm);

%Residuals
yresid = tmp - tm;
```

```

SSresid = sum(yresid.^2);
SStot = (length(tmp)-1) * var(tmp);
rsq = 1 - (SSresid/SStot)

%Scatter Plot
figure(1)
markerSize = 100;
scatter3(Gr,Vr1,tm,markerSize,Rel,'o')
xlabel('Gr')
ylabel('V*')
zlabel('tm')
colorbar
hold on
markerSize = 100;
scatter3(Gr,Vr1,tmp,markerSize,Rel,'^','filled')
colorbar
hold all
legend('tm','tmp')
title('Melting Time (hrs)')

%Response Plot
figure(2)
t1 = tmp';
fitpoly2 = fit(tmp,tm,'poly2');
scatter(t1,tm,'bo','filled')
xlim([0,8])
ylim([0,8])
hold on
plot(fitpoly2,'k','predobs')
hold off
title('Prediction Plot - Power Law')
xlabel('Melting Time (hrs)')
ylabel('Predicted Melting Time (hrs)')
grid on
legend('tm-pred','location','southeast')
set(gca,'fontname','times','fontsize',12)
print(figure(2),'PLdim.png','-dpng','-r300');

%tmp V parameters
figure(3)
markerSize = 100;
scatter(Gr,tm,'ro','filled')
xlabel('Gr')
ylabel('tm')
hold on
scatter(Gr,tmp,'b^','filled')
xlabel('Gr')
ylabel('Melting Time (hrs)')
hold all
legend('tm','tm-pred','location','southeast')
grid on

```

```

title('Melting Time (hrs) Vs Gr')
set(gca,'fontname','times','fontsize',12)
print(figure(3), 'Grtmpred.png','-dpng','-r300');

%tmp V parameters
figure(4)
markerSize = 100;
scatter(Re1,tm,'ro','filled')
xlabel('Gr')
ylabel('tm')
hold on
scatter(Re1,tmp,'b^','filled')
xlabel('Re')
ylabel('Melting Time (hrs)')
hold all
legend('tm','tm-pred','location','southeast')
grid on
title('Melting Time (hrs) Vs Re')
set(gca,'fontname','times','fontsize',12)
print(figure(4), 'Retmpred.png','-dpng','-r300');

%tmp V parameters
figure(5)
markerSize = 100;
scatter(Vr1,tm,'ro','filled')
xlabel('Gr')
ylabel('tm')
hold on
scatter(Vr1,tmp,'b^','filled')
xlabel('V*')
ylabel('Melting Time (hrs)')
hold all
legend('tm','tm-pred','location','southeast')
grid on
title('Melting Time (hrs) Vs V*')
set(gca,'fontname','times','fontsize',12)
print(figure(5), 'Vrtmpred.png','-dpng','-r300');

```

APPENDIX B

INTERPOLATION SCRIPT FILE WITH PARAMETERS

```
% % --- Linear Interpolation Model with parameter query points -----%%%%%
% % -----
Dq = 55; %mm Diameter query point
Tiq = 425.15; %K Inlet Temperature query point
Vq = 15; %m/s Inlet Velocity query point
tq = 0.017; %hrs
Tmelt = 390.85; %K Mean Melting Temperature of PCM

%Read variables (all files in C:\Trnsys17\MyProjects\RD_Trnsys\
if (Tiq > Tmelt)
ds = xlsread('Data.xlsx','3','A1:RC64');
else if (Tiq < Tmelt)
ds = xlsread('Data.xlsx','4','A1:AFE28');
end
end

%Variables
D = ds(2:end,1);
T = ds(2:end,2);
tm = ds(1,4:end);
V = ds(2:end,3);
M = ds(2:end,4:end);

if (Tiq > Tmelt)

%All in dataset
if (ismember(Dq,D) & ismember(Tiq,T) & ismember(Vq,V))
%Linear interpolation
indal = find(D==Dq);
T1=find(T==Tiq);
indta = intersect(T1,indal);
V1 = find(V==Vq); s = intersect(V1,indta);
Mfva = 100.*M(s,1:end);
int1 = interp1(tm,1:length(tm),tq,'nearest');
x = Mfva(int1);
MF = Mfva(1,int1:end);
tf = tm(int1:end);
mqb = find(100==MF);
mb1 = mqb(1);
Mb = round(MF(1,1:mb1),2);
tqf = tf(1,1:mb1); tqf(1) = tq;
treq = tqf(1,mb1);
end

%None in dataset
```

```

if (~ismember(Dq,D) & ~ismember(Tiq,T) & ~ismember(Vq,V))
    diff = D - Dq; a = diff(diff<0); i1 = a(max(find(a<0)));
    inda1 = find(a==i1);
    inda2 = inda1 + 21;
%Dial - Temp and vel interp
dtf1 = T(inda1,1)-Tiq;
b = dtf1(dtf1<0);
i2 = b(max(find(b<0)));
indta1 = inda1(find(b==i2));
indta2 = indta1 + 3;
Mfva = 100.*M(indta1,1:end);
Mfvb = 100.*M(indta2,1:end);
MFval = interp1(V(indta1),Mfva,Vq,'linear');
MFvbl = interp1(V(indta2),Mfvb,Vq,'linear');
MFv1 = [MFval;MFvbl];
Ta1 = unique(T(indta1)); Ta2 = unique(T(indta2)); Ta = [Ta1;Ta2];
Mft1 = interp1(Ta, MFv1, Tiq, 'linear');

%Dia2 - Temp and vel interp
indtb1 = indta1+21; indtb2 = indtb1 + 3;
Mfvc = 100.*M(indtb1,1:end); Mfvd = 100.*M(indtb2,1:end);
MFvc1 = interp1(V(indtb1),Mfvc,Vq,'linear');
MFvd1 = interp1(V(indtb2),Mfvd,Vq,'linear');
MFv2 = [MFvc1;MFvd1];
Tb1 = unique(T(indtb1)); Tb2 = unique(T(indtb2)); Tb = [Tb1;Tb2];
Mft2 = interp1(Tb, MFv2, Tiq, 'linear');
MF1 = [Mft1;Mft2];
D1 = unique(D(inda1)); D2 = unique(D(inda2)); Dia = [D1;D2];
MFd = round(interp1(Dia, MF1, Dq, 'linear'),1);
int1 = interp1(tm,1:length(tm),tq,'nearest');
x = interp1(tm(1,int1:end),MFd(1,int1:end),tq,'linear');
MF = MFd(1,int1:end);
MF(1) = x;
tf = tm(int1:end);
mqb = find(100==MF);
mb1 = mqb(1);
Mb = round(MF(1,1:mb1),2);
tqf = tf(1,1:mb1); tqf(1) = tq;
treq = tqf(1,mb1);
end

% 2 in dataset
%Temp and vel
if (~ismember(Dq,D) & ismember(Tiq,T) & ismember(Vq,V))
    diff = D - Dq; a = diff(diff<0); i1 = a(max(find(a<0)));
    inda1 = find(a==i1);
    inda2 = inda1 + 21;
%Dial - Temp and vel interp
Tl = find(T==Tiq);
indta1 = intersect(Tl,inda1);
Mfva = 100.*M(indta1,1:end);
MFval = interp1(V(indta1),Mfva,Vq,'linear');

```

```

%Dia2 - Temp and vel interp
indtb1 = indta1+21; Mfvc = 100.*M(indtb1,1:end);
MFvc1 = interp1(V(indtb1),Mfvc,Vq, 'linear');
MF1 = [MFval;MFvc1];
D1 = unique(D(inda1)); D2 = unique(D(inda2)); Dia = [D1;D2];
MFd = round(interp1(Dia, MF1, Dq, 'linear'),1);
int1 = interp1(tm,1:length(tm),tq, 'nearest');
x = interp1(tm(1,int1:end),MFd(1,int1:end),tq, 'linear');
MF = MFd(1,int1:end);
MF(1) = x; tf = tm(int1:end);
mqb = find(100==MF);
mb1 = mqb(1);
Mb = round(MF(1,1:mb1),2);
tqf = tf(1,1:mb1); tqf(1) = tq;
treq = tqf(1,mb1);
end

%Dia and Temp
if (ismember(Dq,D) & ismember(Tiq,T) & ~ismember(Vq,V))
    inda1 = find(Dq == D);
    T1 = find(T == Tiq);
    indta1 = intersect(T1,inda1);
    Mfva = 100.*M(indta1,1:end);
    MFval = interp1(V(indta1),Mfva,Vq, 'linear');
    MF1 = [MFval];
    int1 = interp1(tm,1:length(tm),tq, 'nearest');
    x = interp1(tm(1,int1:end),MF1(1,int1:end),tq, 'linear');
    MF = MF1(1,int1:end);
    MF(1) = x;
    tf = tm(int1:end);
    mqb = find(100==MF);
    mb1 = mqb(1);
    Mb = round(MF(1,1:mb1),2);
    tqf = tf(1,1:mb1); tqf(1) = tq;
    treq = tqf(1,mb1);
end

%Dia and Vel
if (ismember(Dq,D) & ~ismember(Tiq,T) & ismember(Vq,V))
    inda1 = find(Dq == D);
    v1 = find(V == Vq);
    iv1 = intersect(v1,inda1);
    dtf1 = T(inda1,1)-Tiq; b = dtf1(dtf1<0);
    it1 = b(max(find(b<0)));
    ita1 = inda1(find(b==it1)); ita2 = ita1 + 3; it2 = [ita1;ita2];
    indta1 = intersect(iv1,it2);
    Mfva = 100.*M(indta1,1:end);
    MFval = interp1(T(indta1),Mfva,Tiq, 'linear');
    MF1 = [MFval];
    int1 = interp1(tm,1:length(tm),tq, 'nearest');
    x = interp1(tm(1,int1:end),MF1(1,int1:end),tq, 'linear');

```

```

MF = MFl(1,int1:end);
MF(1) = x;
tf = tm(int1:end);
mqb = find(100==MF);
mb1 = mqb(1);
Mb = round(MF(1,1:mb1),2);
tqf = tf(1,1:mb1); tqf(1) = tq;
treq = tqf(1,mb1);
end

% 1 in dataset
% Dia in
if (ismember(Dq,D) & ~ismember(Tiq,T) & ~ismember(Vq,V))
    inda1 = find(Dq == D);
    dtf1 = T(inda1,1)-Tiq; b = dtf1(dtf1<0);
    i2 = b(max(find(b<0)));
    indta1 = inda1(find(b==i2));
    indta2 = indta1 + 3;
    Mfva = 100.*M(indta1,1:end); Mfvb = 100.*M(indta2,1:end);
    MFval = interp1(V(indta1),Mfva,Vq,'linear');
    MFvb1 = interp1(V(indta2),Mfvb,Vq,'linear');
    MFv1 = [MFval;MFvb1];
    MFl = [MFv1];
    int1 = interp1(tm,1:length(tm),tq,'nearest');
    x = interp1(tm(1,int1:end),MFl(1,int1:end),tq,'linear');
    MF = MFl(1,int1:end);
    MF(1) = x;
    tf = tm(int1:end);
    mqb = find(100==MF);
    mb1 = mqb(1);
    Mb = round(MF(1,1:mb1),2);
    tqf = tf(1,1:mb1); tqf(1) = tq;
    treq = tqf(1,mb1);
end

%V in dataset
if (~ismember(Dq,D) & ~ismember(Tiq,T) & ismember(Vq,V))
    diff = D - Dq; a = diff(diff<0); il = a(max(find(a<0)));
    inda1 = find(il==a);
    inda2 = inda1 + 21;
%Dia 1
    dtf1 = T(inda1,1)-Tiq; b = dtf1(dtf1<0);
    i2 = b(max(find(b<0)));
    indta1 = inda1(find(b==i2));
    indta2 = indta1 + 3;
    Mfval = 100.*M(indta1,1:end); Mfva2 = 100.*M(indta2,1:end);
    Mv1 = interp1(V(indta1),Mfval,Vq,'linear');
    Mv2 = interp1(V(indta2),Mfva2,Vq,'linear');
    MFv1 = [Mv1;Mv2];
    Ta1 = unique(T(indta1)); Ta2 = unique(T(indta2)); Ta = [Ta1;Ta2];
    Mft1 = interp1(Ta, MFv1, Tiq, 'linear');

```

```

%Dia 2
dtf2 = T(inda2,1)-Tiq; c = dtf2(dtf2<0);
i3 = c(max(find(c<0)));
indtb1 = inda2(find(c==i2));
indtb2 = indtb1 + 3;
Mfvb1 = 100.*M(indtb1,1:end); Mfvb2 = 100.*M(indtb2,1:end);
Mb1 = interp1(V(indtb1),Mfvb1,Vq,'linear');
Mb2 = interp1(V(indtb2),Mfvb2,Vq,'linear');
MFv2 = [Mb1;Mb2];
Tb1 = unique(T(indtb1)); Tb2 = unique(T(indtb2)); Tb = [Tb1;Tb2];
Mft2 = interp1(Tb, MFv2, Tiq, 'linear');
Mfl = [Mft1;Mft2];
D1 = unique(D(inda1)); D2 = unique(D(inda2)); Dia = [D1;D2];
MFd = round(interp1(Dia, Mfl, Dq, 'linear'),1);
int1 = interp1(tm,1:length(tm),tq,'nearest');
x = interp1(tm(1,int1:end),MFd(1,int1:end),tq,'linear');
MF = MFd(1,int1:end);
MF(1) = x;
tf = tm(int1:end);
mqb = find(100==MF);
mb1 = mqb(1);
Mb = round(MF(1,1:mb1),2);
tqf = tf(1,1:mb1); tqf(1) = tq;
treq = tqf(1,mb1);
end

%T in dataset
if (~ismember(Dq,D) & ismember(Tiq,T) & ~ismember(Vq,V))
    diff = D - Dq; a = diff(diff<0); il = a(max(find(a<0)));
    inda1 = find(il==a);
    inda2 = inda1 + 21;
%Dia 1
    dtf1 = T(inda1,1)-Tiq; b = dtf1(dtf1<0);
    i2 = b(max(find(b<0)));
    indta1 = inda1(find(b==i2));
    indta2 = indta1 + 3;
    Mfva1 = 100.*M(indta1,1:end); Mfva2 = 100.*M(indta2,1:end);
    Mv1 = interp1(V(indta1),Mfva1,Vq,'linear');
    Mv2 = interp1(V(indta2),Mfva2,Vq,'linear');
    MFv1 = [Mv1;Mv2];
    Ta1 = unique(T(indta1)); Ta2 = unique(T(indta2)); Ta = [Ta1;Ta2];
    Mft1 = interp1(Ta, MFv1, Tiq, 'linear');
%Dia 2
    dtf2 = T(inda2,1)-Tiq; c = dtf2(dtf2<0);
    i3 = c(max(find(c<0)));
    indtb1 = inda2(find(c==i3));
    indtb2 = indtb1 + 3;
    Mfvb1 = 100.*M(indtb1,1:end); Mfvb2 = 100.*M(indtb2,1:end);
    Mb1 = interp1(V(indtb1),Mfvb1,Vq,'linear');
    Mb2 = interp1(V(indtb2),Mfvb2,Vq,'linear');
    MFv2 = [Mb1;Mb2];

```

```

Tb1 = unique(T(indtb1)); Tb2 = unique(T(indtb2)); Tb = [Tb1;Tb2];
Mft2 = interp1(Tb, MFv2, Tiq, 'linear');
Mf1 = [Mft1;Mft2];
D1 = unique(D(inda1)); D2 = unique(D(inda2)); Dia = [D1;D2];
MFd = round(interp1(Dia, Mf1, Dq, 'linear'),1);
int1 = interp1(tm,1:length(tm),tq,'nearest');
x = interp1(tm(1,int1:end),MFd(1,int1:end),tq,'linear');
MF = MFd(1,int1:end);
MF(1) = x;
tf = tm(int1:end);
mqb = find(100==MF);
mb1 = mqb(1);
Mb = round(MF(1,1:mb1),2);
tqf = tf(1,1:mb1); tqf(1) = tq;
treq = tqf(1,mb1);
end
end

if (Tiq < Tmelt)
%All in dataset
if (ismember(Dq,D) & ismember(Tiq,T) & ismember(Vq,V))
%Linear interpolation
inda1 = find(D==Dq);
T1=find(T==Tiq);
indta = intersect(T1,inda1);
V1 = find(V==Vq); s = intersect(V1,indta);
Mfva = 100.*M(s,1:end);
int1 = interp1(tm,1:length(tm),tq,'nearest');
x = Mfva(int1);
MF = Mfva(1,int1:end);
tf = tm(int1:end);
mqb = find(0==MF);
mb1 = mqb(1);
Mb = round(MF(1,1:mb1),2);
tqf = tf(1,1:mb1); tqf(1) = tq;
treq = tqf(1,mb1);
end

%None in dataset
if (~ismember(Dq,D) & ~ismember(Tiq,T) & ~ismember(Vq,V))
diff = D - Dq; a = diff(diff<0); i1 = a(max(find(a<0)));
inda1 = find(a==i1);
inda2 = inda1 + 9;
%Dial - Temp and vel interp
dtf1 = T(inda1,1)-Tiq;
b = dtf1(dtf1<0);
i2 = b(max(find(b<0)));
indta1 = inda1(find(b==i2));
inda2 = indta1 + 3;
Mfva = 100.*M(indta1,1:end);
Mfvb = 100.*M(indta2,1:end);

```

```

MFval = interp1(V(indta1),Mfva,Vq,'linear');
MFvb1 = interp1(V(indta2),Mfvb,Vq,'linear');
MFv1 = [MFval;MFvb1];
Ta1 = unique(T(indta1)); Ta2 = unique(T(indta2)); Ta = [Ta1;Ta2];
Mft1 = interp1(Ta, MFv1,Tiq,'linear');
%Dia2 - Temp and vel interp
indtb1 = indta1+9; indtb2 = indtb1 + 3;
Mfvc = 100.*M(indtb1,1:end); Mfvd = 100.*M(indtb2,1:end);
MFvc1 = interp1(V(indtb1),Mfvc,Vq,'linear');
MFvd1 = interp1(V(indtb2),Mfvd,Vq,'linear');
MFv2 = [MFvc1;MFvd1];
Tb1 = unique(T(indtb1)); Tb2 = unique(T(indtb2)); Tb = [Tb1;Tb2];
Mft2 = interp1(Tb, MFv2,Tiq,'linear');
Mfl = [Mft1;Mft2];
D1 = unique(D(inda1)); D2 = unique(D(inda2)); Dia = [D1;D2];
MFd = round(interp1(Dia, Mfl, Dq, 'linear'),1);
int1 = interp1(tm,1:length(tm),tq,'nearest');
x = interp1(tm(1,int1:end),MFd(1,int1:end),tq,'linear');
MF = MFd(1,int1:end);
MF(1) = x;
tf = tm(int1:end);
mqb = find(0==MF);
mb1 = mqb(1);
Mb = round(MF(1,1:mb1),2);
tqf = tf(1,1:mb1); tqf(1) = tq;
treq = tqf(1,mb1);
end

% 2 in dataset
%Temp and vel
if (~ismember(Dq,D) & ismember(Tiq,T) & ismember(Vq,V))
    diff = D - Dq; a = diff(diff<0); i1 = a(max(find(a<0)));
    inda1 = find(a==i1);
    inda2 = inda1 + 9;
%Dial - Temp and vel interp
Tl = find(T==Tiq);
indta1 = intersect(Tl,inda1);
Mfva = 100.*M(indta1,1:end);
MFval = interp1(V(indta1),Mfva,Vq,'linear');
%Dia2 - Temp and vel interp
indtb1 = indta1+9; Mfvc = 100.*M(indtb1,1:end);
MFvc1 = interp1(V(indtb1),Mfvc,Vq,'linear');
Mfl = [MFval;MFvc1];
D1 = unique(D(inda1)); D2 = unique(D(inda2)); Dia = [D1;D2];
MFd = round(interp1(Dia, Mfl, Dq, 'linear'),1);
int1 = interp1(tm,1:length(tm),tq,'nearest');
x = interp1(tm(1,int1:end),MFd(1,int1:end),tq,'linear');
MF = MFd(1,int1:end);
MF(1) = x; tf = tm(int1:end);
mqb = find(0==MF);
mb1 = mqb(1);

```

```

Mb = round(MF(1,1:mb1),2);
tqf = tf(1,1:mb1); tqf(1) = tq;
treq = tqf(1,mb1);
end

%Dia and Temp
if (ismember(Dq,D) & ismember(Tiq,T) & ~ismember(Vq,V))
    inda1 = find(Dq == D);
    T1 = find(T == Tiq);
    indta1 = intersect(T1,inda1);
    Mfva = 100.*M(indta1,1:end);
    MFval = interp1(V(indta1),Mfva,Vq,'linear');
    MF1 = [MFval];
    int1 = interp1(tm,1:length(tm),tq,'nearest');
    x = interp1(tm(1,int1:end),MF1(1,int1:end),tq,'linear');
    MF = MF1(1,int1:end);
    MF(1) = x;
    tf = tm(int1:end);
    mqb = find(0==MF);
    mb1 = mqb(1);
    Mb = round(MF(1,1:mb1),2);
    tqf = tf(1,1:mb1); tqf(1) = tq;
    treq = tqf(1,mb1);
end

%Dia and Vel
if (ismember(Dq,D) & ~ismember(Tiq,T) & ismember(Vq,V))
    inda1 = find(Dq == D);
    v1 = find(V == Vq);
    iv1 = intersect(v1,inda1);
    dtf1 = T(inda1,1)-Tiq; b = dtf1(dtf1<0);
    it1 = b(max(find(b<0)));
    ita1 = inda1(find(b==it1)); ita2 = ita1 + 3; it2 = [ita1;ita2];
    indta1 = intersect(iv1,it2);
    Mfva = 100.*M(indta1,1:end);
    MFval = interp1(T(indta1),Mfva,Tiq,'linear');
    MF1 = [MFval];
    int1 = interp1(tm,1:length(tm),tq,'nearest');
    x = interp1(tm(1,int1:end),MF1(1,int1:end),tq,'linear');
    MF = MF1(1,int1:end);
    MF(1) = x;
    tf = tm(int1:end);
    mqb = find(0==MF);
    mb1 = mqb(1);
    Mb = round(MF(1,1:mb1),2);
    tqf = tf(1,1:mb1); tqf(1) = tq;
    treq = tqf(1,mb1);
end

% 1 in dataset
% Dia in

```

```

if (ismember(Dq,D) & ~ismember(Tiq,T) & ~ismember(Vq,V))
    inda1 = find(Dq == D);
    dtf1 = T(inda1,1)-Tiq; b = dtf1(dtf1<0);
    i2 = b(max(find(b<0)));
    indta1 = inda1(find(b==i2));
    indta2 = indta1 + 3;
    Mfva = 100.*M(indta1,1:end); Mfvb = 100.*M(indta2,1:end);
    MFval = interp1(V(indta1),Mfva,Vq,'linear');
    MFvb1 = interp1(V(indta2),Mfvb,Vq,'linear');
    MFv1 = [MFval;MFvb1];
    MF1 = [MFv1];
    int1 = interp1(tm,1:length(tm),tq,'nearest');
    x = interp1(tm(1,int1:end),MF1(1,int1:end),tq,'linear');
    MF = MF1(1,int1:end);
    MF(1) = x;
    tf = tm(int1:end);
    mqb = find(0==MF);
    mbl = mqb(1);
    Mb = round(MF(1,1:mbl),2);
    tqf = tf(1,1:mbl); tqf(1) = tq;
    treq = tqf(1,mbl);
end

%V in dataset
if (~ismember(Dq,D) & ~ismember(Tiq,T) & ismember(Vq,V))
    diff = D - Dq; a = diff(diff<0); il = a(max(find(a<0)));
    inda1 = find(il==a);
    inda2 = inda1 + 9;
%Dia 1
    dtf1 = T(inda1,1)-Tiq; b = dtf1(dtf1<0);
    i2 = b(max(find(b<0)));
    indta1 = inda1(find(b==i2));
    indta2 = indta1 + 3;
    Mfval = 100.*M(indta1,1:end); Mfva2 = 100.*M(indta2,1:end);
    Mv1 = interp1(V(indta1),Mfval,Vq,'linear');
    Mv2 = interp1(V(indta2),Mfva2,Vq,'linear');
    MFv1 = [Mv1;Mv2];
    Ta1 = unique(T(indta1)); Ta2 = unique(T(indta2)); Ta = [Ta1;Ta2];
    Mft1 = interp1(Ta,MFv1,Tiq,'linear');
%Dia 2
    dtf2 = T(inda2,1)-Tiq; c = dtf2(dtf2<0);
    i3 = c(max(find(c<0)));
    indtb1 = inda2(find(c==i3));
    indtb2 = indtb1 + 3;
    Mfvb1 = 100.*M(indtb1,1:end); Mfvb2 = 100.*M(indtb2,1:end);
    Mb1 = interp1(V(indtb1),Mfvb1,Vq,'linear');
    Mb2 = interp1(V(indtb2),Mfvb2,Vq,'linear');
    MFv2 = [Mb1;Mb2];
    Tb1 = unique(T(indtb1)); Tb2 = unique(T(indtb2)); Tb = [Tb1;Tb2];
    Mft2 = interp1(Tb,MFv2,Tiq,'linear');
    MF1 = [Mft1;Mft2];

```

```

D1 = unique(D(inda1)); D2 = unique(D(inda2)); Dia = [D1;D2];
MFd = round(interp1(Dia, MFl, Dq, 'linear'),1);
int1 = interp1(tm,1:length(tm),tq,'nearest');
x = interp1(tm(1,int1:end),MFd(1,int1:end),tq,'linear');
MF = MFd(1,int1:end);
MF(1) = x;
tf = tm(int1:end);
mqb = find(0==MF);
mb1 = mqb(1);
Mb = round(MF(1,1:mb1),2);
tqf = tf(1,1:mb1); tqf(1) = tq;
treq = tqf(1,mb1);
end

%T in dataset
if (~ismember(Dq,D) & ismember(Tiq,T) & ~ismember(Vq,V))
    diff = D - Dq; a = diff(diff<0); i1 = a(max(find(a<0)));
    inda1 = find(i1==a);
    inda2 = inda1 + 9;
%Dia 1
    dtf1 = T(inda1,1)-Tiq; b = dtf1(dtf1<0);
    i2 = b(max(find(b<0)));
    indta1 = inda1(find(b==i2));
    indta2 = indta1 + 3;
    Mfval = 100.*M(indta1,1:end); Mfva2 = 100.*M(indta2,1:end);
    Mv1 = interp1(V(indta1),Mfval,Vq,'linear');
    Mv2 = interp1(V(indta2),Mfva2,Vq,'linear');
    MFv1 = [Mv1;Mv2];
    Ta1 = unique(T(indta1)); Ta2 = unique(T(indta2)); Ta = [Ta1;Ta2];
    Mft1 = interp1(Ta, MFv1, Tiq, 'linear');
%Dia 2
    dtf2 = T(inda2,1)-Tiq; c = dtf2(dtf2<0);
    i3 = c(max(find(c<0)));
    indtb1 = inda2(find(c==i2));
    indtb2 = indtb1 + 3;
    Mfvb1 = 100.*M(indtb1,1:end); Mfvb2 = 100.*M(indtb2,1:end);
    Mb1 = interp1(V(indtb1),Mfvb1,Vq,'linear');
    Mb2 = interp1(V(indtb2),Mfvb2,Vq,'linear');
    MFv2 = [Mb1;Mb2];
    Tb1 = unique(T(indtb1)); Tb2 = unique(T(indtb2)); Tb = [Tb1;Tb2];
    Mft2 = interp1(Tb, MFv2, Tiq, 'linear');
    Mfl = [Mft1;Mft2];
    D1 = unique(D(inda1)); D2 = unique(D(inda2)); Dia = [D1;D2];
    MFd = round(interp1(Dia, Mfl, Dq, 'linear'),1);
    int1 = interp1(tm,1:length(tm),tq,'nearest');
    x = interp1(tm(1,int1:end),MFd(1,int1:end),tq,'linear');
    MF = MFd(1,int1:end);
    MF(1) = x;
    tf = tm(int1:end);
    mqb = find(0==MF);
    mb1 = mqb(1);

```

```

Mb = round(MF(1,1:mb1),2);
tqf = tf(1,1:mb1); tqf(1) = tq;
treq = tqf(1,mb1);
end
end

figure(1)
plot(tqf(1,1:mb1),Mb(1:mb1), 'b-',tqf(1:mb1),Mb(1:mb1),...
'ro','LineWidth',1.1)
title('Melt Fraction (%) Vs Time (hrs)', 'fontname','times','fontsize',12)
grid on
ytickformat('percentage')
xlabel('Time (hrs)')
ylabel('Melt Fraction (%)')
set(gca,'fontname','times','fontsize',12)

```

BIBLIOGRAPHY

- [1] “The Basics of Combined Heat and Power,” pp. 1–3, Oct. 2019.
- [2] I. Dincer and M. A. Rosen, “Thermal energy storage,” *Building Services Engineering Research & Technology*, 2011.
- [3] A. De Gracia and L. F. Cabeza, “Phase change materials and thermal energy storage for buildings,” *Energy Build.*, vol. 103, pp. 414–419, Jun. 2015.
- [4] A. Sørensen and T. Schmidt, “Monitoring Results from Large Scale Heat Storages for District Heating in Denmark,” Apr. 2018.
- [5] T. Schmidt and H. Müller-Steinhagen, “The Central Solar Heating Plant with Aquifer Thermal Energy Store in Rostock -Results after four years of operation System description,” pp. 20–23, Jun. 2004.
- [6] M. Reuss, W. Beuth, M. Schmidt, and W. Schoelkopf, “Solar district heating with seasonal storage in Attenkirchen,” *Proc. IEA Conf. ECOSTOCK, Richard Stock. Coll. Pomona, New Jersey, USA*, 2006.
- [7] B. en Zalba, J. M. Marin, L. F. Cabeza, and H. Mehling, “Review on thermal energy storage with phase change: materials, heat transfer analysis and applications”, Oct. 2002.
- [8] S. Höhlein, A. König-Haagen, and D. Brüggemann, “Thermophysical characterization of MgCl₂·6H₂O, xylitol and erythritol as phase change materials (PCM) for latent heat thermal energy storage (LHTES),” *Materials (Basel)*., vol. 10, no. 4, Apr. 2017.
- [9] A. J. Parry, P. C. Eames, and F. B. Agyenim, “Modeling of thermal energy storage shell-and-tube heat exchanger,” *Heat Transf. Eng.*, vol. 35, no. 1, pp. 1–14, 2014.
- [10] D. V Hale, M. J. Hoover, and M. J. O’neill, “NASA CONTRACTOR REPORT NASA CR-51363 PHASE CH,_NGE MATERIALS HANDBOOK,” 1971.
- [11] G. John, A. König-Haagen, C. K. King’ondu, D. Brüggemann, and L. Nkhonjera, “Galactitol as phase change material for latent heat storage of solar cookers: Investigating thermal behavior in bulk cycling,” *Sol. Energy*, 2015.
- [12] J. Buschle, W.-D. Steinmann, and R. Tamme, “Latent heat storage for process heat applications,” *Conf. Proc.*, no. LiCl, 2006.
- [13] S. D. Sharma and K. Sagara, “Latent Heat Storage Materials and Systems: A

- Review,” *Int. J. Green Energy*, vol. 2, no. 1, pp. 1–56, 2005.
- [14] D. H, PERRY , ROBERT W, GREEN, “Perry S Chemical Engineers,”, p. 360, 1999.
 - [15] A. Fallahi, G. Guldentops, M. Tao, S. Granados-Focil, and S. Van Dessel, “Review on solid-solid phase change materials for thermal energy storage: Molecular structure and thermal properties,” *Appl. Therm. Eng.*, vol. 127, pp. 1427–1441, 2017.
 - [16] O. J. Almeida and B. G. Dixon, “Lamellar Metallo-Alkylphosphonates as Solid-State Phase-Change Materials,” *Chem. Mater.*, vol. 7, no. 11, pp. 2039–2044, 1995.
 - [17] M. Tirumala *et al.*, “Continuous solid-state phase transitions in energy storage materials with orientational disorder – Computational and experimental approach,” *Energy*, vol. 91, pp. 334–349, Jul. 2015.
 - [18] H. Shmueli, G. Ziskind, and R. Letan, “Melting in a vertical cylindrical tube: Numerical investigation and comparison with experiments,” *Int. J. Heat Mass Transf.*, vol. 53, no. 19–20, pp. 4082–4091, May 2010.
 - [19] ANSYS, “ANSYS Fluent User’s Guide,” vol. 15317, Nov. 2013.
 - [20] M. Longeon, A. Soupart, J. F. Fourmigué, A. Bruch, and P. Marty, “Experimental and numerical study of annular PCM storage in the presence of natural convection,” *Appl. Energy*, vol. 112, pp. 175–184, Jun. 2013.
 - [21] C. Moler, “Numerical Computation with MATLAB”, 2004.